MINISTRY OF AVIATION

AERONAUTICAL RESEARCH COUNCIL

CURRENT PAPERS

Supersonic Wind Tunnel Measurements of the Loads and Internal Pressure Distributions on Ducts at Incidence

by

P. H. Cook

SUPERSONIC WIND TUNNEL MEASUREMENTS OF THE LOADS AND
INTERNAL PRESSURE DISTRIBUTIONS ON DUCTS AT INCIDENCE

by

P. H. Cook

SUMMARY

An attempt has been made to find a method of estimating the external lift
of full scale engine nacelles and the internal lift of rectangular cross section
ducts used to represent engine nacelles on wind tunnel models.

The results for the total lift curve slope of circular cross section ducts
look promising in that an adequate collapse of the experimental data has been
achieved. For the rectangular ducts, the internal lift at low incidence may be
predictable if the internal flow Mach number is known, and the available results
for total lift suggest a similar collapse to that achieved for the circular
ducts. The experimental data for the rectangular ducts are limited and will be
supplemented later by a further series of models.

<u>CONTENTS</u>

<u>TABLES</u>

ILLUSTRATIONS

1   INTRODUCTION

In a configuration where the engine nacelles represent a large proportion of the total frontal area, the lift contribution from the engines may be a large proportion of the whole, and the trim and stability characteristics may be greatly influenced by the centre of action of this engine lift contribution. In particular the internally generated lift of the duct inclined to the incident flow appears to have received little attention in the past so that neither its full scale contribution nor the correction for the wind tunnel representation could be properly assessed.

The present investigation was undertaken to examine the lift and pitching moment from circular ducts and rectangular ducts of various cross sectional aspect ratios, over a range of length/span ratios. Internal and external loads have been separated in the case of rectangular ducts by internal wall pressure surveys, and subsequent integrations.

One example of an integrated duct/wing configuration has been tested, the triangular wing panels being placed symmetrically about a rectangular cross section duct.

2   MODELS

Details of the models are given in Figs.1 to 4 and Table 1.

The winged duct is shown in Fig.1. The wing is a flat plate 1/16 in. thick chamfered 0.1 in. from the leading edge only. The net wing area is 4.5 in.^{2}, the net aspect ratio 0.5 and the leading edge sweepback is 83°. The thickness of the duct wall is tapered out at the nose equally on the inner and outer surfaces to a nose radius of 0.001 in. giving a semi-wedge angle of about 2.3°.

With the wings removed, and by means of detachable noses the models shown in Fig.2 can be obtained with nose droop angles of 0, 5° and 10°.

The straight rectangular cross section ducts 2, 4 and 6 in. long and 1^1/16 or 11/16 in. internal depth are shown in Fig.3(a). The width and one of the depths of these ducts are common to the winged duct, as are the wall thickness and nose dimensions.

The circular cross section ducts, 1^3/8 in. internal diameter have the same lengths and nose dimensions as the rectangular ducts and are shown in Fig.3(b).

The pressure plotting model shown in Fig.4 is a 6 in. long duct 1^7/16 in. wide by 1^1/16 in. deep with 0.014 in. diameter pressure holes at 0.2 in. pitch on the centre line of the inner surface starting 0.8 in. aft of the nose. A 2 in. long pressure plotting model has been tested. It is similar to the first 2 in. of the 6 in. long duct, but with the first pressure hole 0.4 in. aft of the nose.

3   DETAILS OF TEST

The tests were made in the R.A.E. No.19 supersonic wind tunnel which has a working section 18 in. square and is continuous in operation. The stagnation

pressure had to be restricted to 15 in. Hg. absolute by the strength of the attachment of the model to the sting. This attachment was weak since it had to be designed not to interfere with the internal flow through the duct, and to have the minimum effect on the external flow. The Reynolds number per inch corresponding to the test Mach numbers are given below:-

M	2.19	2.02	1.58
$Re/10^5$ per in.	1.45	1.55	1.80

All the tests were made with free boundary layer transition.

Photographs of a model mounted in the working section are shown in Fig.5.

The models were mounted on a twin boom sting shown in Fig.6. Normal force, pitching moment and axial force can be measured by balances housed within the windshield. The normal force and pitching moment bridges have two strain gauges wired in series in each arm of the bridge, the two gauges being mounted in identical positions on the two booms. The drag unit has four strain gauge stations, two operated by each boom. The output from these balances was measured on self-balancing servos.

A thermistor was mounted on the sting for temperature correction of the balance readings.

No correction has been made for the effect of the sting on the model base pressure.

In the examination of the internal flow the pressures were measured on self-balancing capsule manometers with a vacuum datum.

The model incidence was measured optically.

The rectangular cross section ducts were tested at Mach numbers of 2.19 and 2.02, the former being the highest Mach number available in the tunnel, and the latter the lowest available without causing choking of the model internal flow due to the internal contraction at the nose of the duct and the boundary layer growth. The circular ducts, however, would run supersonically at M = 1.58 but not at M = 1.4, as the contraction ratio of these ducts is smaller.

4   PRESENTATION OF RESULTS

The results for the rectangular ducts are given in terms of the duct overall length (ℓ), or depth at the nose (h) normalized with respect to the width of the duct inlet (b). The aerodynamic coefficients are based on the internal base area and the length of the duct, moments being measured about the nose.

4.1 Force measurements

The basic data, C_L, C_m and $C_D \sim \alpha$, followed by $C_m \sim C_L$ for each model and Mach number tested are presented in the following order.

(i) Straight ducts of rectangular cross section (Figs.7 to 13).

(ii) Straight ducts of circular cross section (Figs.14 to 18).

(iii) Drooped nose ducts (Figs.19 to 22).

(iv) Winged duct (Figs.23 to 25).

4.2 Pressure measurements

The basic pressure coefficients for the two Mach numbers are presented in Figs.26 and 27, followed by the derived changes in internal lift and pitching moment with duct length in Figs.32 and 33. The variation of internal lift and centre of pressure with duct length is compared with linear and slender body theories at small angles of incidence in Fig.35. Photographs of the internal flow by schlieren and oilflow visualisation are compared with the internal pressures in Fig.37.

5 THEORETICAL ESTIMATES

Both the force measurements of total lift and the internal lift obtained from pressure measurements have been compared with slender body and linear theories.

5.1 Rectangular ducts

5.1.1 Linear theory estimates

(i) $\ell/\beta h < 1$

The external lift was obtained by graphical integration of the pressure distribution for the corner solution given by Lagerstrom in Ref.1, and is given by

$$\frac{L}{qS} \simeq \frac{4\alpha}{\beta} \left(1 - \frac{0.384}{A\beta} \right)^* \qquad \text{for } A\beta > 1$$

where S = plan area

A = plan aspect ratio

$\beta^2 = M^2 - 1$

---

* The coefficient of $1/A\beta$ = f(h).As h $\rightarrow \infty$,f(h) $\rightarrow$ 0.384; whereas for a flat plate when h = 0, f(h) = 0.5.

or

$$C_{L_\alpha} = 4 \frac{\ell}{\beta h} \left(1 - 0.384 \frac{\ell}{\beta b}\right)$$

where C_L is based on the external base area and

h and b are the height and width respectively.

The internal lift is two dimensional:-

$$\frac{L}{qS} = \frac{4\alpha}{\beta}$$

where S is the plan area

or

$$C_{L_\alpha} = 4 \frac{\ell}{\beta h} \quad \text{based on base area} \quad .$$

The total linear lift estimate for the rectangular ducts is therefore given by:-

$$C_{L_\alpha} = 4 \frac{\ell}{\beta h} \left(2 - 0.384 \frac{\ell}{\beta b}\right)$$

for $\frac{\ell}{\beta h} < 1$ and $\frac{\ell}{\beta b} < 1$ $\left(\frac{\ell}{\beta b} < \frac{\ell}{\beta h} \text{ for all the models tested}\right)$.

(ii) $\underline{\ell/\beta h > 1}$

For the internal lift, first order linear theory predicts a succession of alternately reflected expansive and compressive Mach waves giving rise to a loading distribution along the duct which is in the form of a square wave of period 2 βh. This is illustrated in Fig.34 where β is the free stream value and h is the minimum internal height of the duct (h_I). On entering the duct the flow passes through either a compressive characteristic from the top lip of the duct or an expansive one from the bottom lip each with a turning angle equal to the incidence. After passing through both characteristics the flow is deflected through twice the incidence. From momentum considerations this results in twice the slender body theory value for internal normal force. The same result is of course obtained from linear theory following from the two dimensional value for surface pressure coefficient, $+\frac{2\alpha}{\beta}$ for the upper surface

and $-\frac{2\alpha}{\beta}$ for the lower surface.

- 8 -

At $\ell/\beta h_I = 2.0$ after passing through the reflected characteristics the flow at the exit is parallel to the free stream so that again from momentum considerations the total internal lift is zero. As before, this result follows from linear theory since the surface pressure which, for $1 < \ell/\beta h_I < 2$ is equal in magnitude, but opposite in sign, to that for $\ell/\beta h_I < 1$.

It is readily apparent that this shook/expansion pattern repeats throughout the duct length, which results in a surface pressure coefficient oscillating discontinuously between $\pm 2\alpha/\beta$ and 180° out of phase between the upper and lower surfaces. The resulting variation with duct length of normal force, pitching moment and centre of pressure are included in Fig.34.

This idealised flow cannot be expected to persist for any great distance along the duct as the influence of non-linear effects becomes more dominant in the character of the expansions and compressions, their reflections at the solid boundaries and their mutual interactions. At a finite incidence the width of expansion waves cannot be ignored, neither can the regular reflection of shook waves be realised after more than a few reflections. The internal flow is therefore likely to be of a highly complex form, with a high degree of rotation and large viscous effects. Nevertheless, after a sufficiently large number of reflections it is commonly assumed, although difficult to justify in general, that the velocity becomes sensibly uniform and parallel to the duct axis. It is further assumed that this velocity departs from the free stream value only to the first order in α, then from momentum considerations.

$$C_{L_\alpha} = 2 \text{ based on cross-section area of duct.}$$

This is, of course, identical with the slender theory results given in the next section.

5.1.2 Slender theory estimates

It can be shown that using slender body approximations and the cross flow potential derived in Durand[2] the external lift is given by:-

$$\frac{L}{8qb^2\alpha} = \frac{\pi\lambda^2}{b^2}(1 - k^2)^2 - \frac{h}{b}$$

where the quantities λ and k follow from the simultaneous solution of the following expressions:-

$$\frac{h}{2} = \lambda[E(k) - (1 - k^2)^2 K(k)]$$

$$\frac{b}{2} = \lambda[E(k') - k^2 K(k')]$$

where $k' = \sqrt{1 - k^2}$

and $K(k)$ and $E(k)$ are complete elliptic integrals of the first and second kind respectively.

The internal lift is obtained from the rate of change of vertical momentum i.e.

$$C_{L_\alpha} = 2 \text{ based on inlet area} \quad .$$

5.2 Circular ducts

5.2.1 Linear theory estimate

The total lift on a circular duct is given by Ward[3] as

$$C_{L_\alpha} = 8 \frac{\ell}{\beta D} \left\{ 1 - \frac{1}{12} \left(\frac{\ell}{\beta D} \right)^2 + \ldots \right\} \quad \text{for} \quad \frac{1}{\beta D} << 1 \quad .$$

where D is the duct diameter.

5.2.2 Slender theory estimate

Slender body theory estimates the external lift curve slope as 2, the inner and outer surfaces giving a total lift of

$$C_{L_\alpha} = 4$$

based on the base area of a duct with zero wall thickness.

5.3 Winged duct

The estimate of lift curve slope for the winged duct has been based on linear theory for flat plate wings and slender body theory for the lift from the internal duct flow.

The wing lift has been obtained from existing estimates for trapezoidal wings by Behrbohm[4] which are shown plotted in Fig.28 as t = 0.267 and t = 0.577, where t is the ratio of the tangents of the wing tip and Mach angles to the free stream direction. Indicated on the curves are the values of R, the ratio of L.E. and T.E. spans. Also shown in Fig.28 are the lift of rectangular (R = 1.0, t = 0) and delta (R = 0) wings given by Stanbrook[5]. The lift at constant values of R, upon which the estimate for the winged duct is based, are shown in Fig.28 as curves interpolated between t = 0.267 and t z 0.577 and drawn within the framework of the curves for the rectangular and delta wing. As the values of Aβ and R for the winged duct represent only a small extrapolation from the t = 0.267 curve the lift curve slope can be estimated with some confidence.

6   RESULTS

The measured values of initial lift curve slope of the rectangular and
circular cross section ducts are compared with the theoretical estimates in
Table 2.

6.1   Straight rectangular ducts

The lift curve slopes of the straight rectangular ducts are plotted
against $\ell/\beta h$ in Fig.29(a). The total lift is obtained directly from the force
measurements. For the internal lift, however, data for only two lengths of
duct are available, viz. 2 and 6 in., since this necessarily requires a know-
ledge of the internal pressure distribution, (section 6.5). When the pressures
measured on the 6 in. duct are integrated (Fig.29(b)) it transpires that the
peak lift curve slope occurs at length $\beta_E\, h_I$ from the entry, where β_E is the
value of β based on the measured exit Mach number instead of that for the free
stream and h_I is the minimum internal height of the duct.

The variation of internal lift curve slope with duct length shown in
Fig.29(b) is oscillatory, agrees well with linear theory for short lengths of
duct and damps to a slender body theory value for the longest.

The results for internal lift curve slope obtained in Fig.29(b) for the
6 in. long duct are transferred at the appropriate value of βh to Fig.29(a).
The internal lift for the 2 in. ducts obtained from the pressures measured on
a 2 in. duct are also shown and indicate the small error involved in assuming
that the first 2 in. of a 6 in. long duct can represent a 2 in. long duct. It
is implied that the Mach number within the duct can be considered constant and
is determined only by the effective area (i.e. less boundary layer thickness)
at the exit. This can be substantiated qualitatively in the case of the 6 in.
duct where the area ratio required to achieve the measured exit Mach number
demands a wall deflection of some 0.06 in. Approximately half of this is
accounted for by the internal wall taper at the nose, the remaining 0.03 in.
is not incompatible with the possible boundary layer displacement thickness
indicated by the few pitot measurements made in the boundary layer during the
measurement of exit Mach number, nor with that calculated for a turbulent
boundary layer.

The external lift curve slope shown in Fig.29(a) is obtained by differenc-
ing the total lift and the internal lift from the pressure measurements on a
6 in. duct.

6.2   Straight circular ducts

The experimental lift curve slopes for the circular cross section ducts
have been plotted against $\ell/\beta D$ in Fig.30 and compared with linear theory at low
values of $\ell/\beta D$ and slender theory at high values. Some correlation between the
experimental results themselves and with theory can be observed, the experimental
points matching well the linear theory estimates at low values of $\ell/\beta D$ and then
lying on a single fluctuating curve which tends to the slender theory value at
high $\ell/\beta D$. The dC_m/dC_L for the circular ducts, plotted in Fig.31 against $\ell/\beta D$,
show a similar oscillation; the position of the aerodynamic centre varying from
the nose to 0.5ℓ at low values of $\ell/\beta D$.

6.3 Drooped nose ducts

Drooping the nose of a rectangular duct does not appear to alter the lift curve slope (see Figs.19 and 20) but produces discontinuities in the drag (Fig.21) presumably due to separations from the intake lip.

6.4 Winged duct

The estimated linear theory lift curve slope of a flat plate wing of the same planform as the winged duct plus a slender body theory estimate of the internal lift resulting from the duct flow is compared with the experimental results in Fig.23. Close agreement between the estimated and measured lift in the range 0 to 7° incidence is obtained at both test Mach numbers.

6.5 Pressure measurements

The internal pressures on the top and bottom surfaces of rectangular ducts $h/b = 0.75$ have been measured on the centre line at 0.2 in. intervals starting 0.8 in. aft of the nose for the long duct ($\ell/b = 4.0$) and 0.4 in. aft for a shorter duct ($\ell/b = 1.33$). It was checked that the effect of the extra external pressure tubes at the nose in the latter case was negligible.

The pressures measured on the long and short ducts ($\ell/b = 4.0$ and 1.33) are shown in Figs.26 and 27. The curves for both the upper and lower surfaces of the shorter duct are similar in shape to those for the long duct but moved downstream.

By integrating the difference between the upper and lower surface pressure coefficients for the 6 in. long duct, assuming them constant across the width of the duct, the variation of internal normal force and pitching moment were obtained at M = 2.19 and 2.02. These results are shown in Figs.32 and 33 as the change in normal force and pitching moment aft of the first pressure hole. Extrapolating the pressure coefficients forward to the shock/expansion theory values at the nose of the duct and integrating gives curves for the internal lift and centre of pressure against duct length. These are compared in Fig.35 with the simple linear theory for the internal flow illustrated in Fig.34 and with the slender body theory.

The experimental results are similar to those predicted by linear theory for short ducts only and tend to the slender results at high $\ell/\beta h$. The pressure near the nose was higher and the peak lift further forward than the theoretical predictions based on the free stream Mach number, indicating an internal flow contraction due to the internal geometry, boundary layer growth and possibly separation from the walls. The measured exit Mach number of 1.87 at a free stream Mach number of 2.19, assumed constant throughout the duct (see section 6.1), is consistent with the peak pressure positions in Fig.35.

In Fig.36 the incremental pressure coefficients for 2° and 4° incidence are plotted against model length, showing that the load distribution along the duct is, for short models, similar to that described in Fig.34 by linear theory but with the Mach number appropriate to the exit instead of the free stream,

and the height that of the minimum internal height (section 6.1). There is a noticeable attenuation of lift as the number of internal shock/expansion reflections increases.

6.6 Flow visualisation

In order to examine the internal flow in detail a series of schlieren and oilflow pictures have been taken of a perspex model $h/b = 0.75$ and $\ell/b = 4.0$. These photographs, shown in Fig.37, were taken at $M = 2.19$ and $\alpha = 0$, 2°, 4° and 6°. The centre photographs are side views and the top and bottom pictures are plan views. Between the photographs are plotted the appropriate surface pressure coefficients. The schlieren shows the repeating internal shock pattern originating from the nose which is responsible for the fluctuating internal lift curves of Fig.35. The detail is poor, due to the bad optical properties of the model, but the intersection of the shocks with internal surfaces can be seen to correspond with the pressure peaks, and in most cases with lines in the oilflow pattern which are normal to the flow through the duct. The oilflow pattern is highly complex, with major disturbances being propagated from the sidewalls due, it is believed, to the internal contraction at the nose of the duct. It is thought that this internal contraction must make a considerable contribution to the difference between the measured surface pressures and those predicted by linear theory. Tests on a series of ducts which are parallel internally are therefore proposed before an attempt is made to describe the internal flow in detail. Nevertheless, despite the major differences found at zero incidence,the change in surface pressures with incidence is similar to that predicted.

7 CONCLUSIONS

The experimental evidence suggests that when engine nacelles on a wind tunnel model are represented by ducts similar to the type tested:-

(i) The lift may be predicted adequately by linear theory at $\ell/\beta h < 1$ and by slender theory at $\ell/\beta h > 4$.

(ii) For intermediate duct lengths $(1 < \ell/\beta h < 4)$ the lift is periodic with duct length, but not to the extent predicted by linearised theory for the internal lift, i.e. it does not drop to zero.

(iii) For intermediate duct lengths $(1 < \ell/\beta h < 4)$ the lift is periodic with duct length. The measured amplitude is less than that predicted by linear theory for the internal lift of a rectangular cross-section duct.

SYMBOLS

A   = plan aspect ratio

b   = width of duct at nose

C_D = drag coefficient

C_L = lift coefficient

C_m = pitching moment coefficient

C_{Z_I} = internal normal force coefficient

based on minimum internal cross section area of duct and duct length, with moments taken about the nose.

C_p = pressure coefficient = $\dfrac{\text{surface pressure - static pressure}}{q}$

$C.P._I$ = internal centre of pressure, x/ℓ aft of nose

C_{L_α} = initial lift curve slope, /radian

D   = nose diameter

h   = height of duct at nose

h_I = minimum internal height of duct

ℓ = length of duct

L   = lift

M   = free stream Mach number

M_E = exit Mach number

q   = $\frac{1}{2}\rho V^2$

S   = plan area

α = angle of incidence

β = $\sqrt{M^2 - 1}$

β_E = $\sqrt{M_E^2 - 1}$

REFERENCES

No.	Author	Title, etc
1	Lagerstrom, P.A. Van Dyke, M.D.	General considerations about planar and non-planar lifting systems. Douglas Aircraft Company. Rep. SM13432, P.32181.
2	Durand, W.F.	Aerodynamic theory, Vol.II, Division E, Chapter IV, Section 17.
3	Ward, G.N.	Linearised theory of steady high speed flow. Chapters 8.2 to 8.9. Cambridge University Press, 1955.
4	Behrbohm, H.	The lifting trapezoidal wing with small aspect ratio at supersonic speed. S.A.A.B. Technical Note No.10. 1952.
5	Stanbrook, A.	The lift curve slope and aerodynamic centre position of wings at subsonic and supersonic speeds. R.A.E. Technical Note No. Aero 2328, A.R.C. 17615. November, 1954.

TABLE 2

Initial lift curve slope

(C_L/RADIAN based on minimum cross section area of duct)

Model	h/b	ℓ/b	M = 2.19				M = 2.02				M = 1.58				
			ℓ/βh	Exp.	Theory		ℓ/βh	Exp.	Theory		ℓ/βh	Exp.	Theory		
					Slender	Linear			Slender	Linear			Slender	Linear	
Rectangular cross section	0.75	4.0	2.74	6.8	5.8		3.04	6.6	5.8						
		2.67	1.83	6.3			2.03	6.1							
		1.33	0.91	6.2		7.2	1.01	6.3		7.8					
	0.5	4.0	4.11	9.1	7.6		4.56	8.8	7.6						
		2.67	2.74	8.8			3.04	8.6							
		1.33	1.37	7.5		7.2	1.52	7.0		7.8					
Circular cross section		4.17	2.14	5.7	4.6		2.38	5.0	4.6		3.41	5.0	4.6		
		3.48	1.78	5.5			1.98	6.3			2.84	5.0			
		2.78	1.43	4.4			1.58	4.7			2.27	5.0			
		2.02	1.035	5.5											
		1.39	0.71	5.8		5.7	0.79	6.1		6.3	1.14	4.6		9.1	
Rectangular cross section with drooped nose	0.5	4.0		9.1				8.8							Nose droop = 0
				9.1				8.8							Nose droop = 5°
				9.1				8.8							Nose droop = 10°

N.B.   for circular cross section ducts, h = b = D
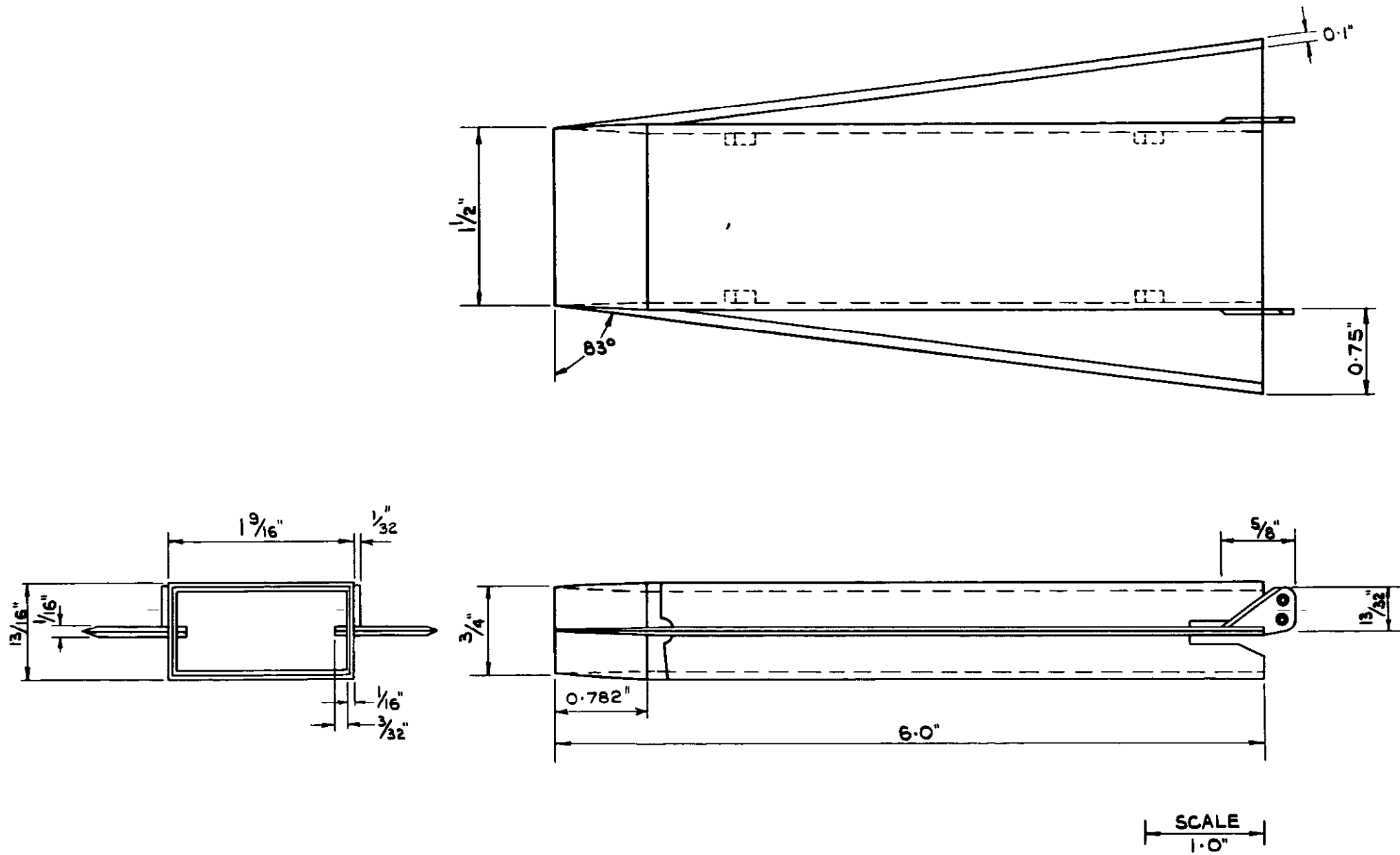
FIG I   SKETCH OF WINGED DUCT
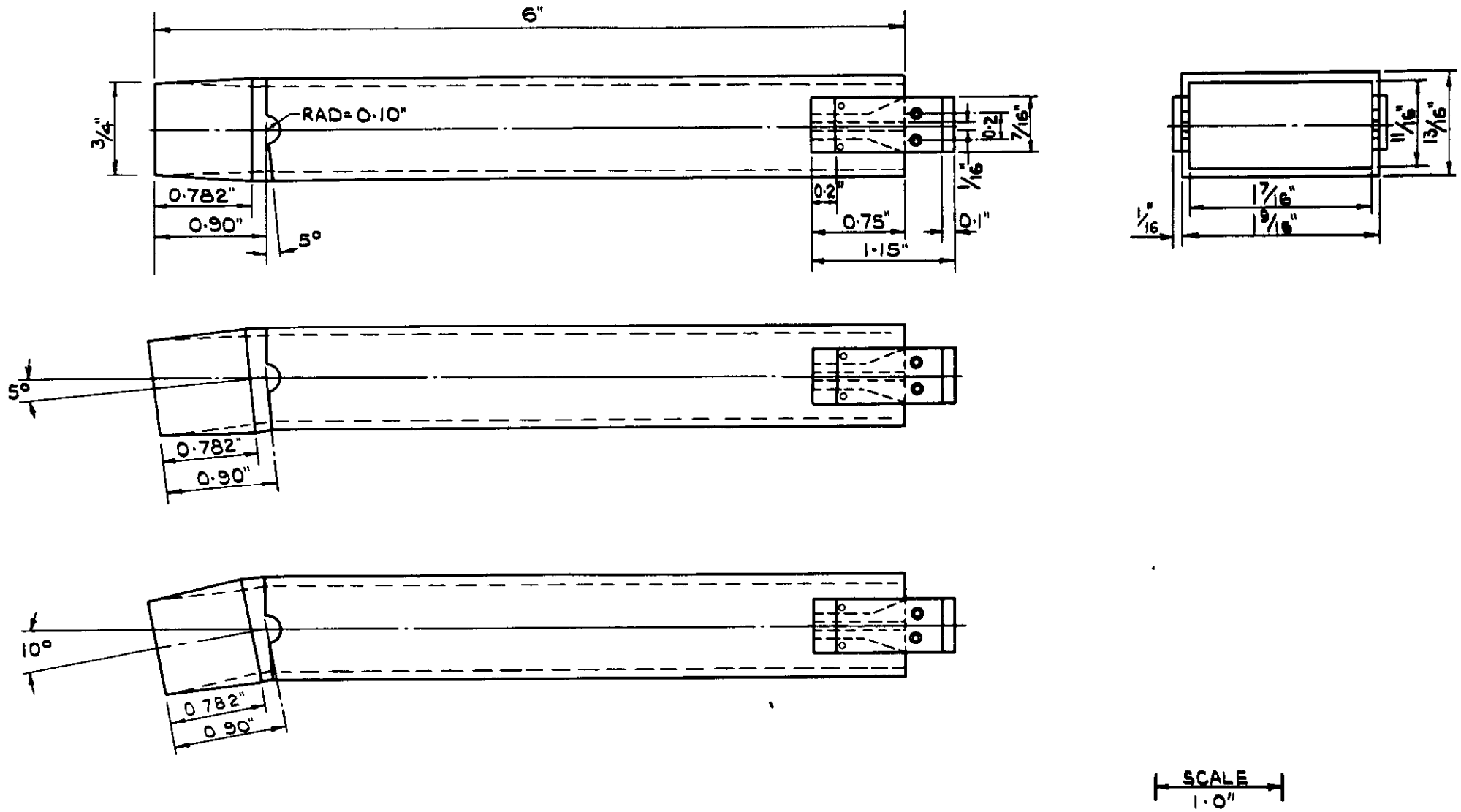
FIG.2 SKETCHES OF DROOPED NOSE DUCTS.

(a) RECTANGULAR CROSS SECTION.

ℓ = 2", 4" & 6"

h = 1⅛" & ¾"
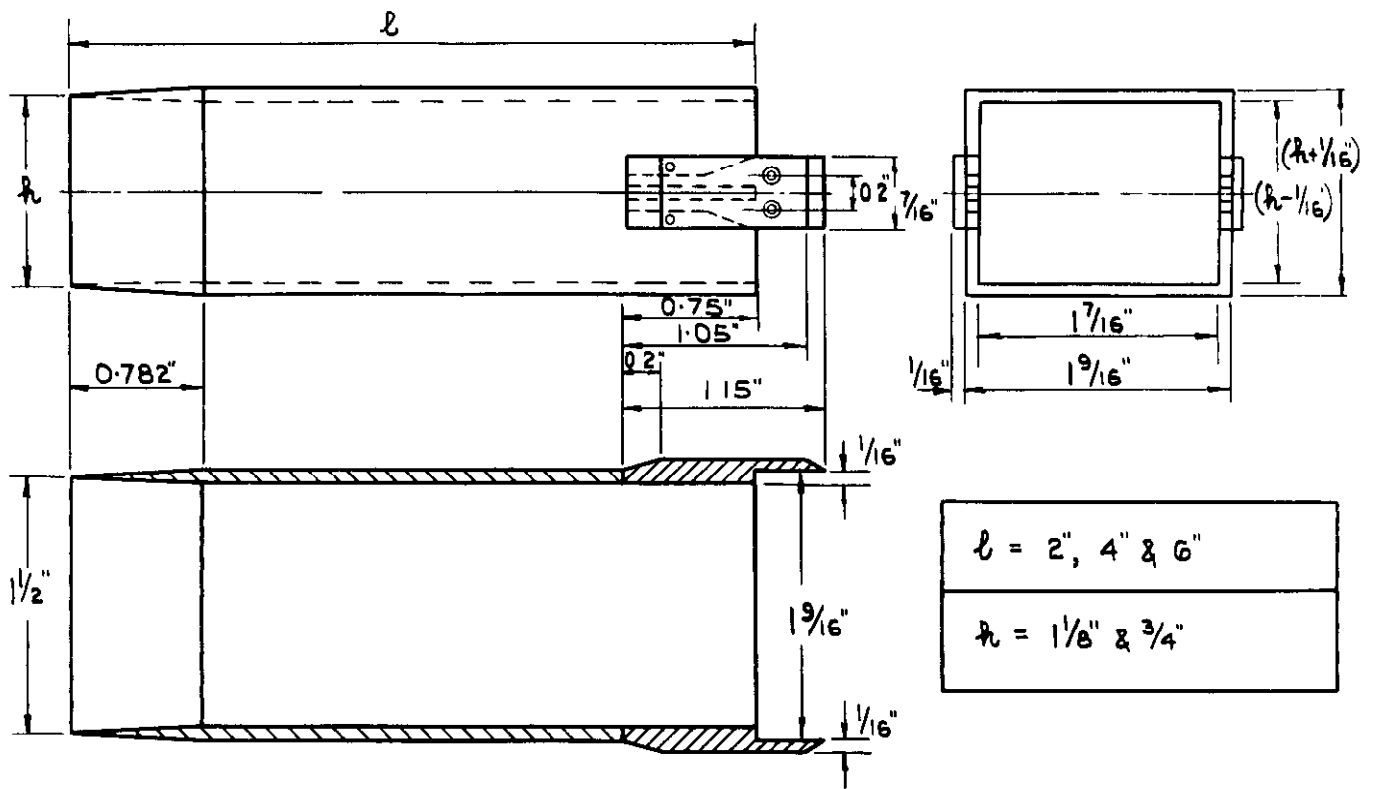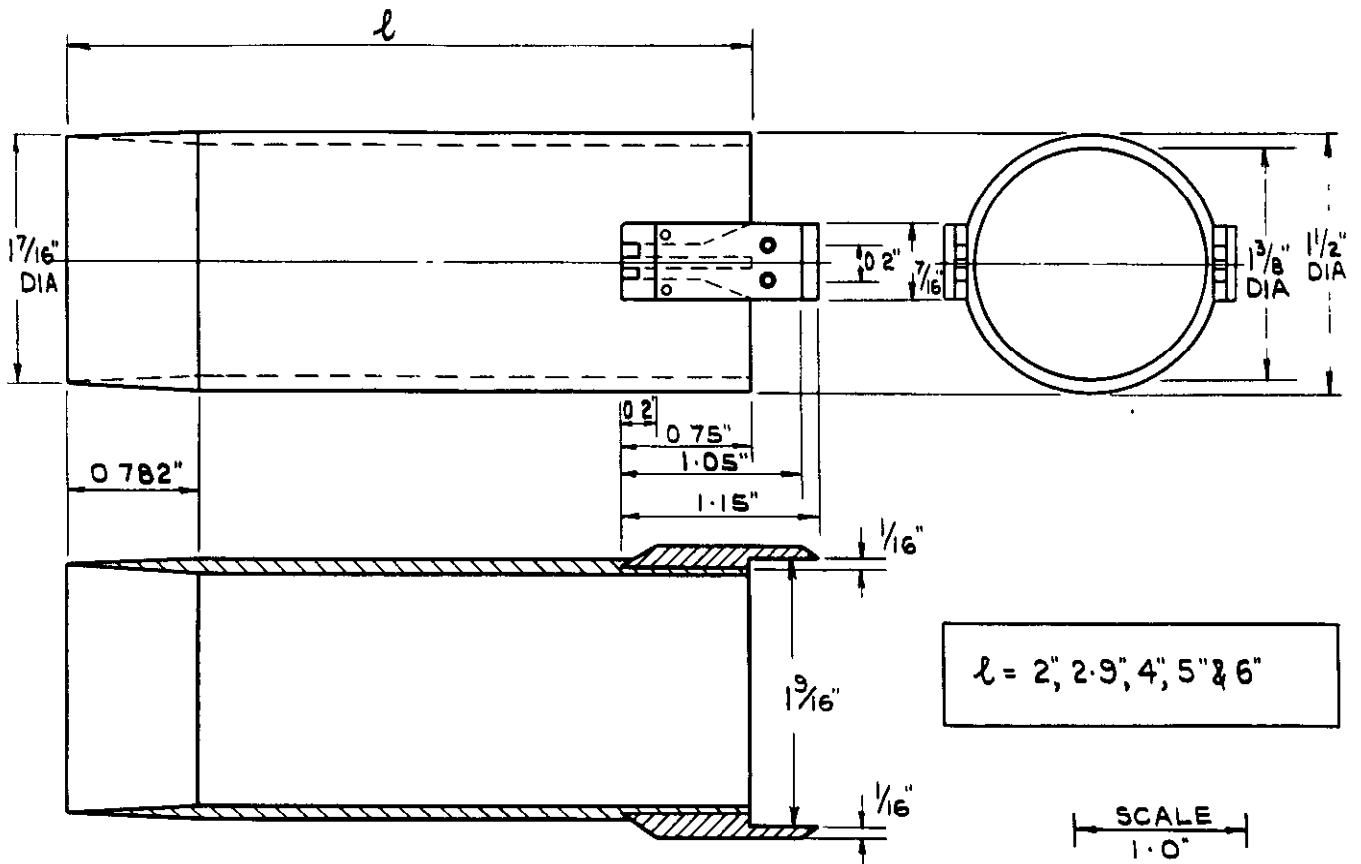
(b) CIRCULAR CROSS SECTION

ℓ = 2", 2·9", 4", 5" & 6"

SCALE
1·0"

FIG.3. SKETCHES OF STRAIGHT DUCTS.

0.8"   26 TUBES @ 0.2" PITCH   0.2" 0.75"

1½"

9/16"

0.782"

6"

1.15"

ARALDITE FAIRING

0.014" DIA. HOLE

1mm O.D. HYPODERMIC TUBE

1/16" 1/16"

FIRST TUBE 0.8" FROM NOSE

0.2"   0.2"

ENLARGED DETAIL

SCALE
0.25"

1⅛"

7/16"   13/16"

SCALE
1.0"
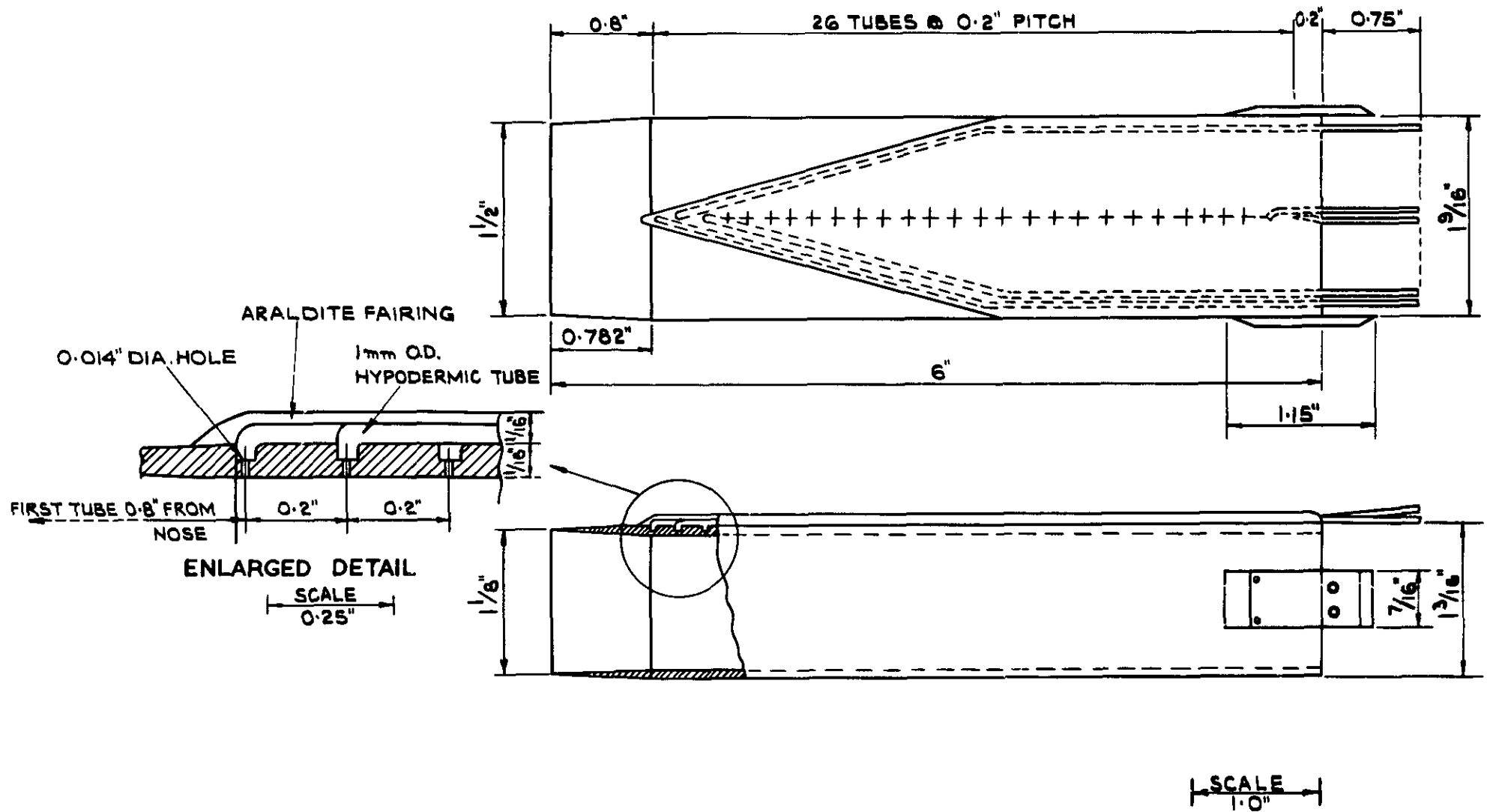
FIG 4   SKETCH OF PRESSURE-PLOTTING MODEL
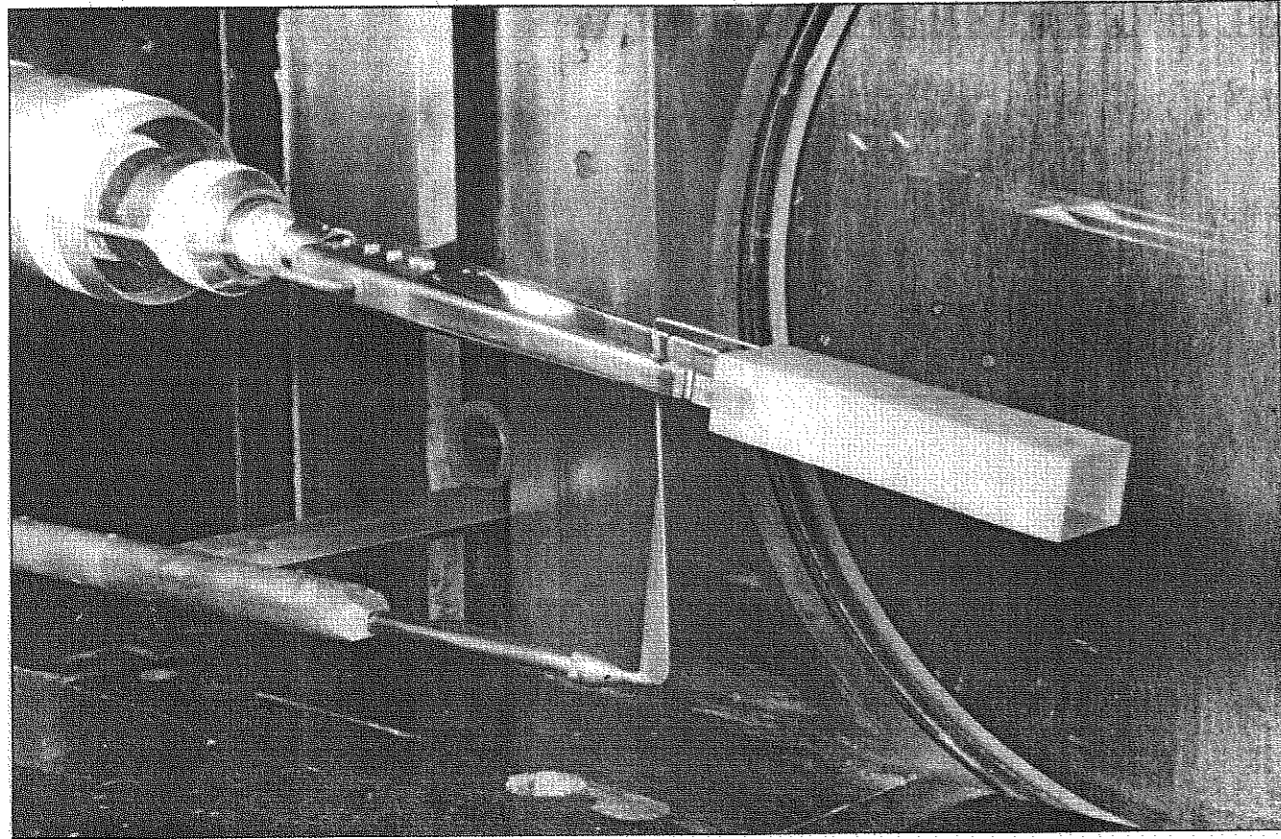
VIEWED FROM UPSTREAM
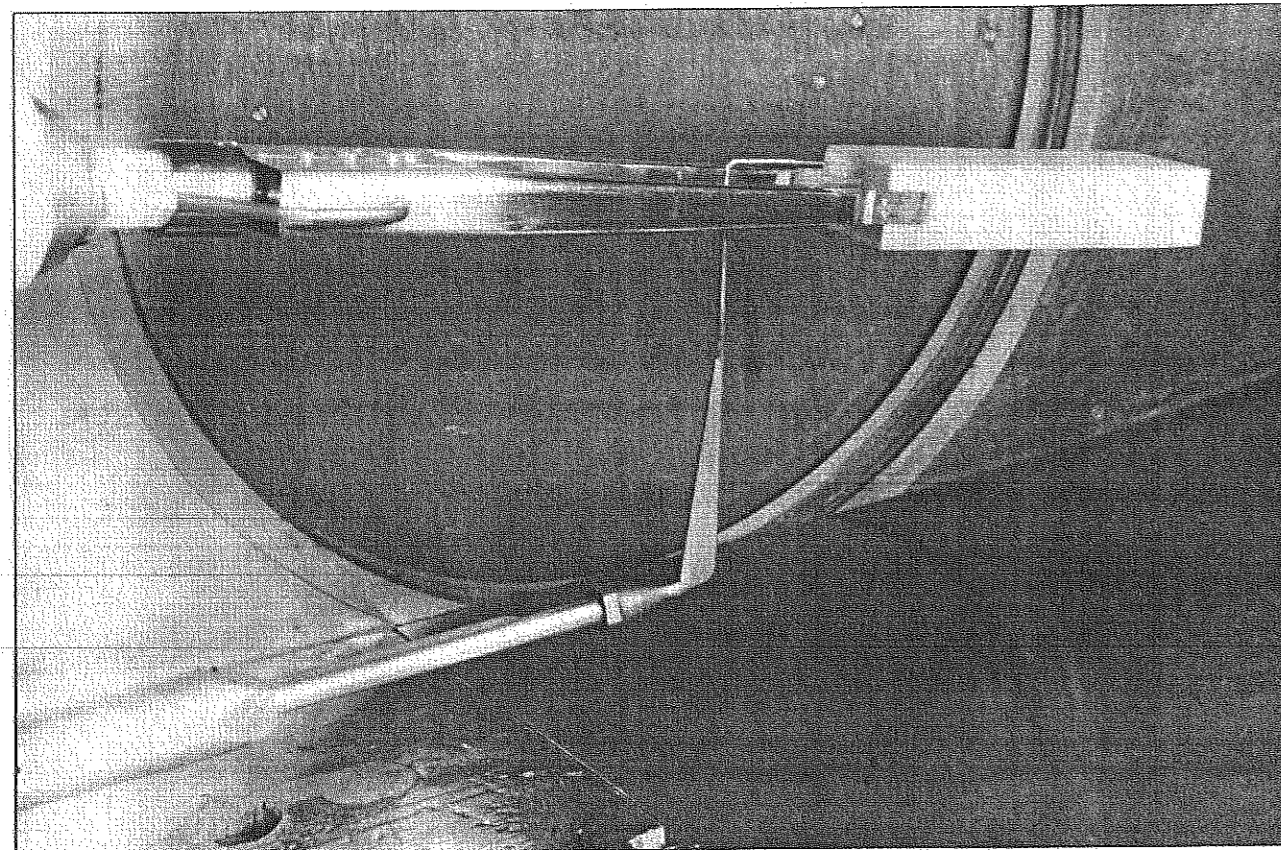
VIEWED FROM DOWNSTREAM

FIG.5. MODEL MOUNTED IN THE TUNNEL

0.5" 0.65"

1⅛"

2"

10.5"

9.0"

4.65"

15°

13/16"

2 3/16"

FRONT ELEVATION

0.782"

1.5" 1.85" 1⅛"

1/16"

SCALE
1.0"
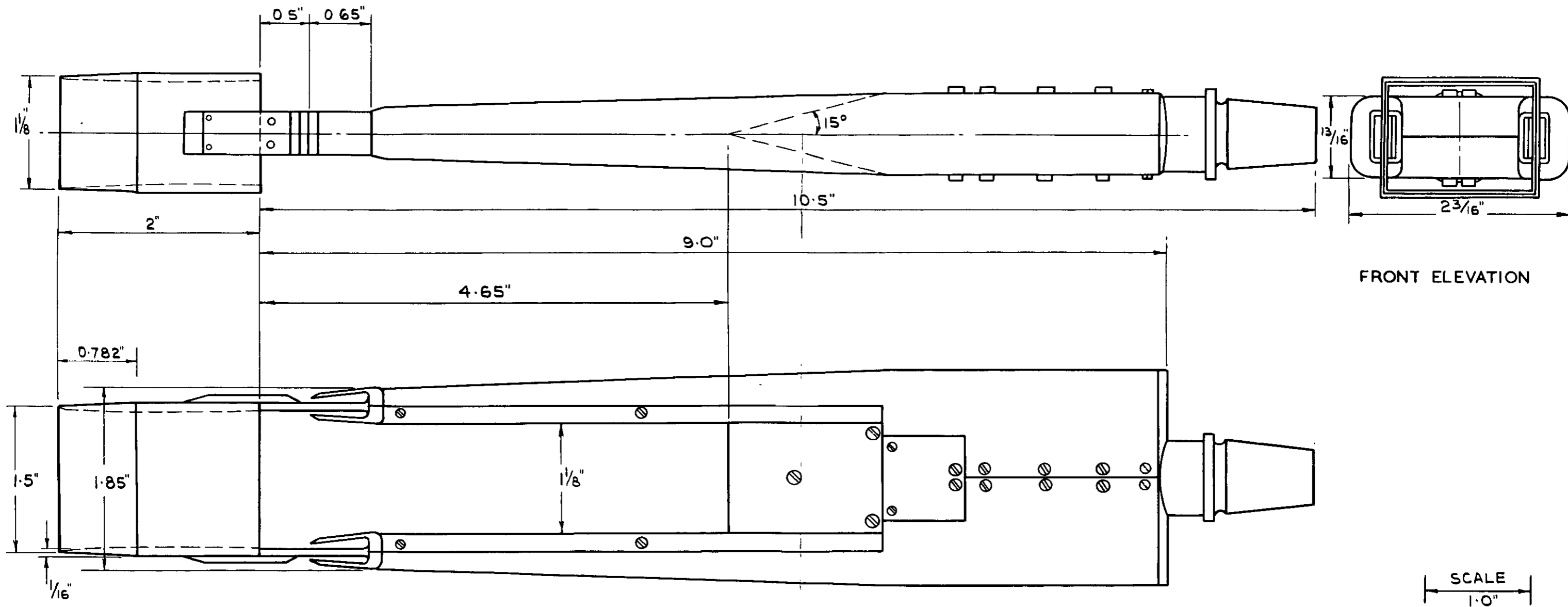
FIG 6 SKETCH OF TWIN BOOM STING.
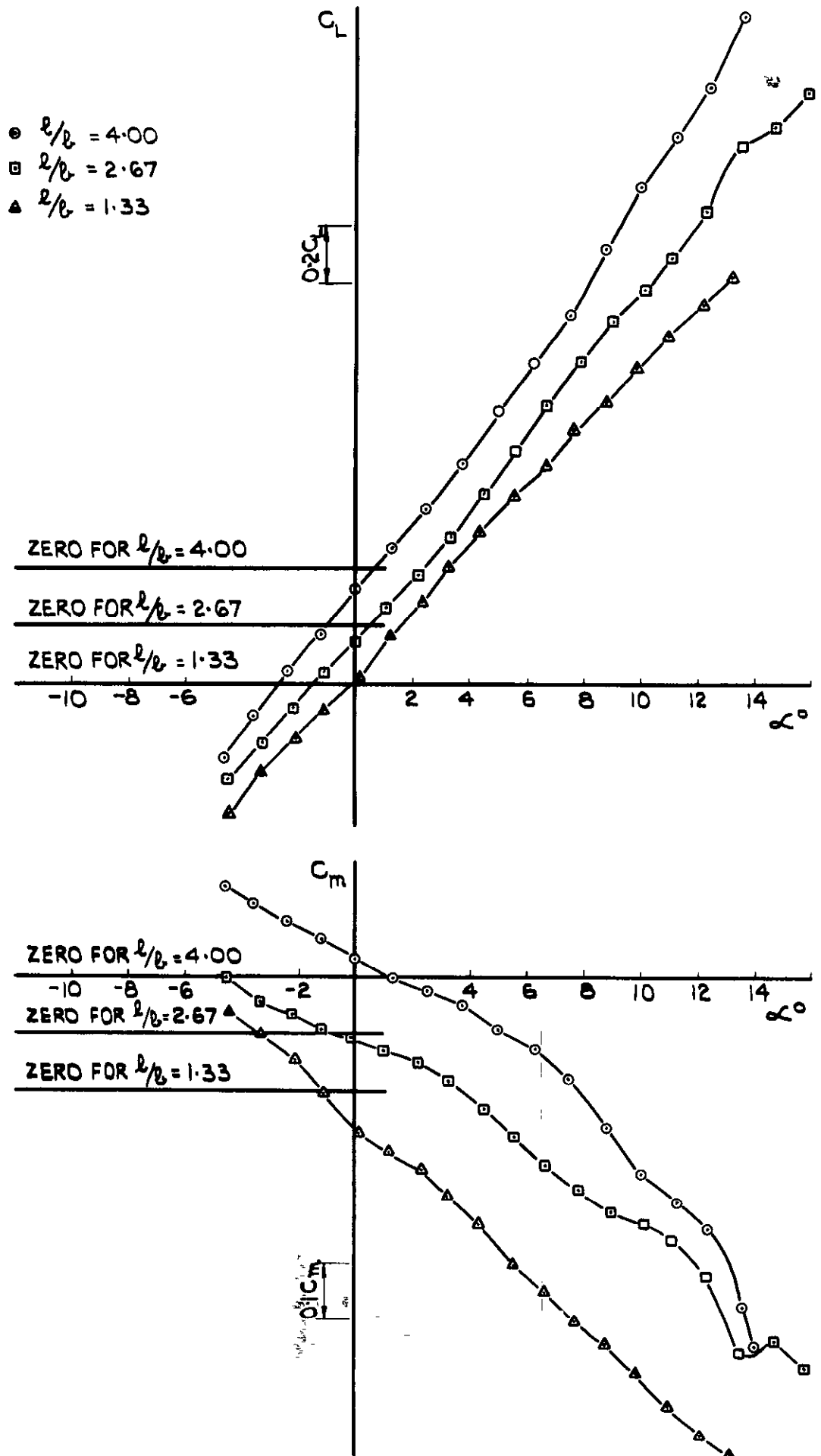
FIG.7. LIFT & PITCHING MOMENT AT M = 2·19 FOR RECTANGULAR DUCTS, h/b = 0·75.
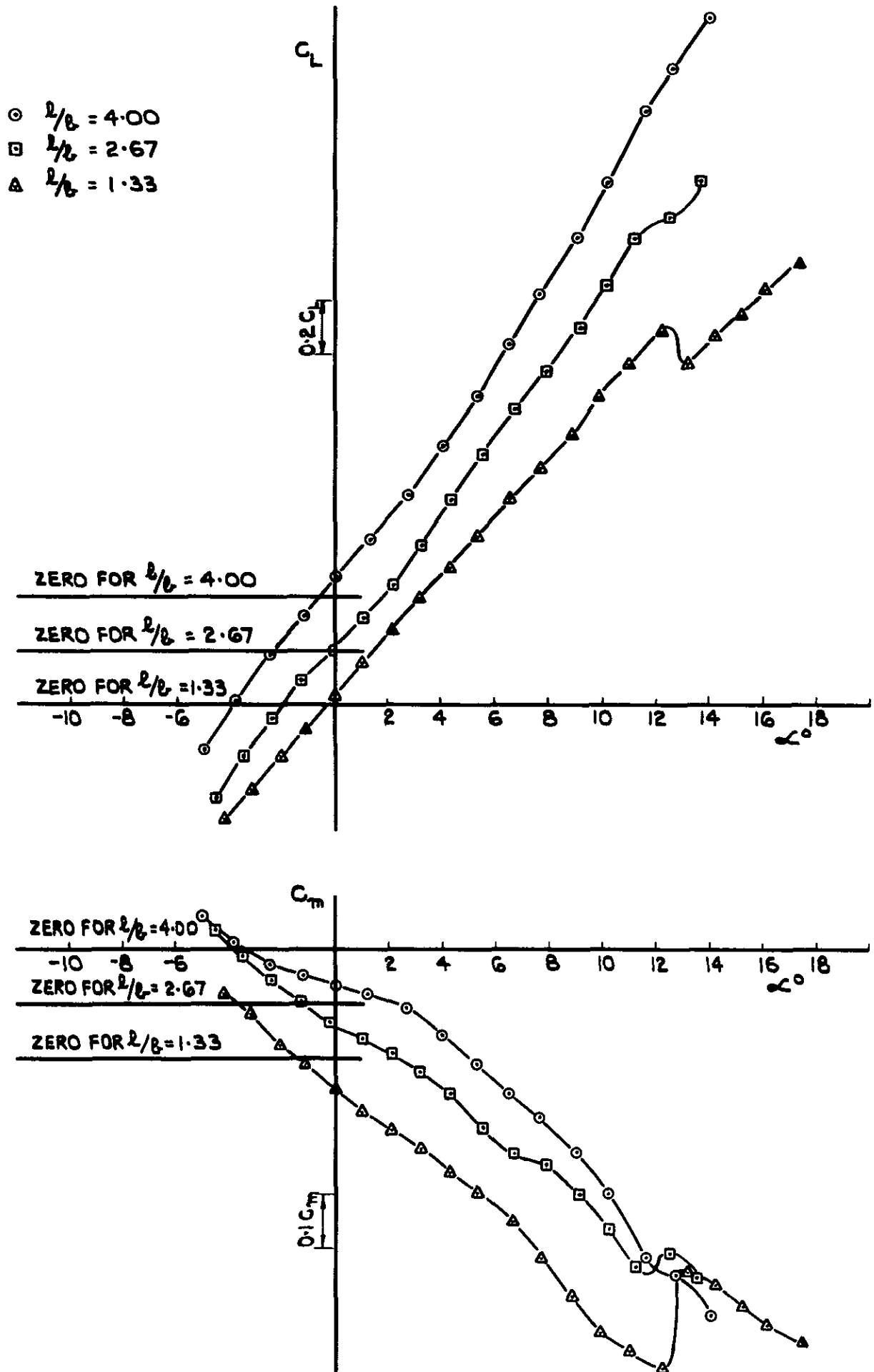
FIG.8. LIFT & PITCHING MOMENT AT M = 2·02 OF
RECTANGULAR DUCTS, $h/\ell = 0.75$.
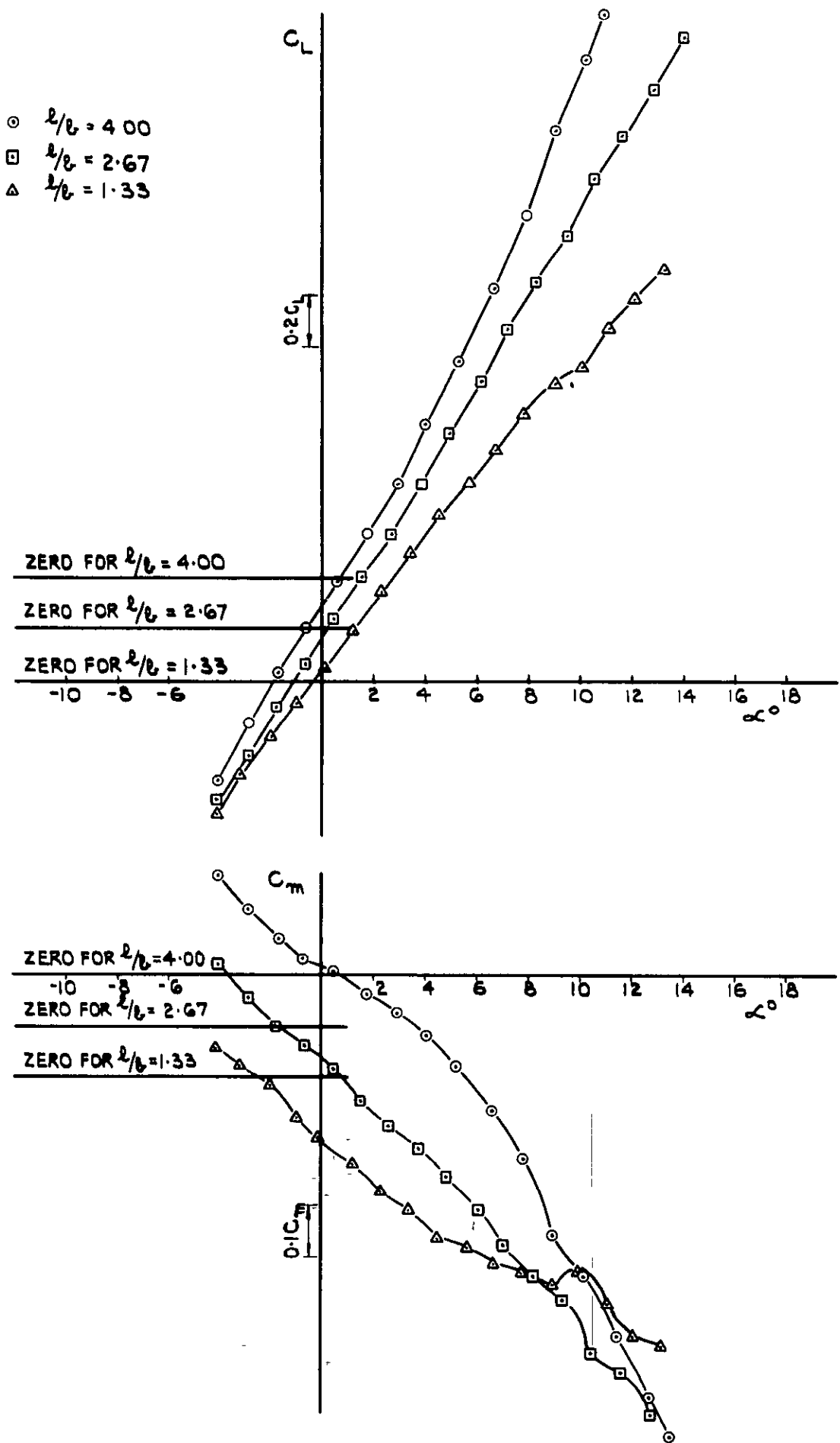
FIG.9. LIFT & PITCHING MOMENT AT M=2·19 FOR
RECTANGULAR DUCTS, h/ℓ=0·50.
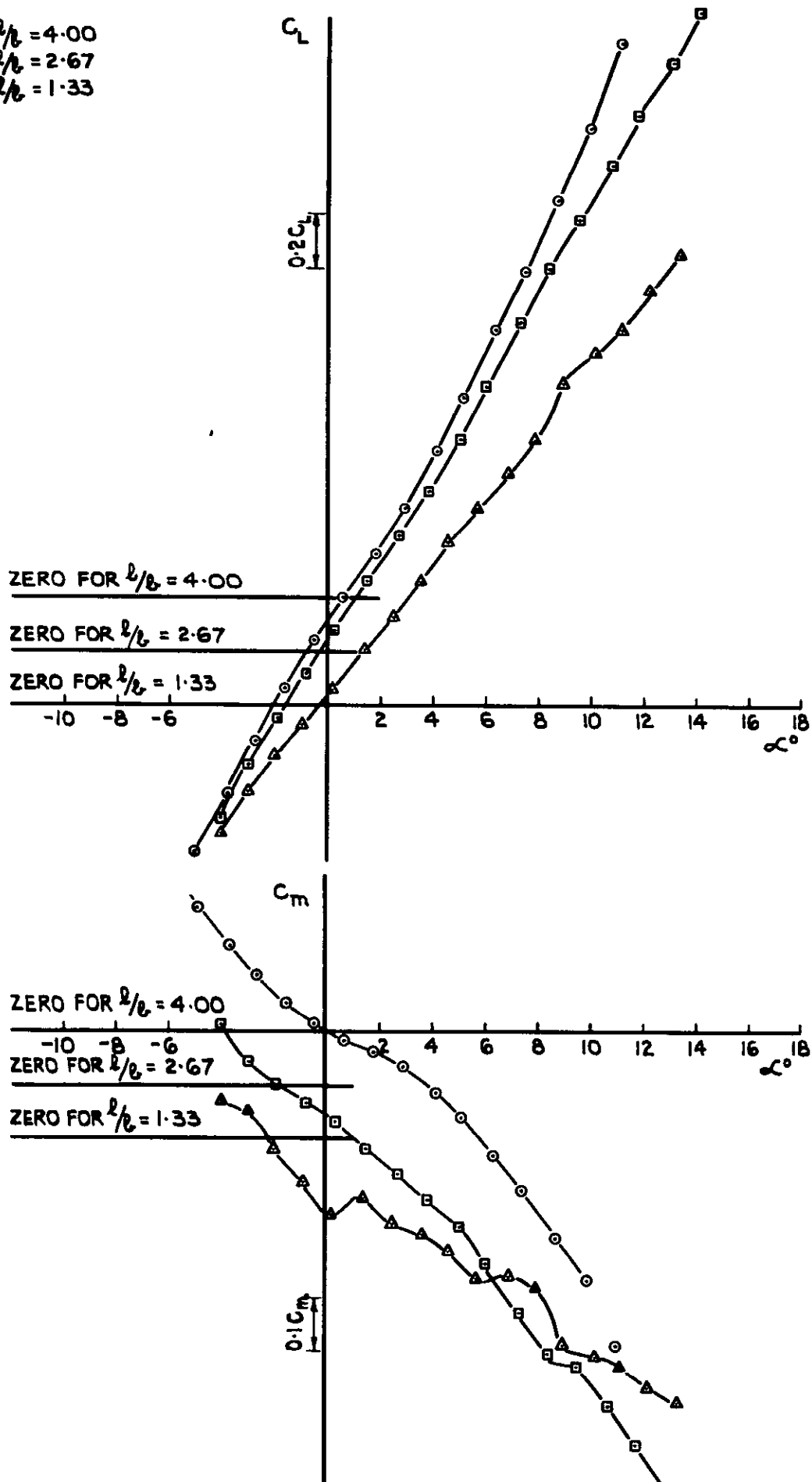
FIG.10. LIFT & PITCHING MOMENT AT M= 2·02 FOR RECTANGULAR DUCTS, h/ℓ = 0·50.
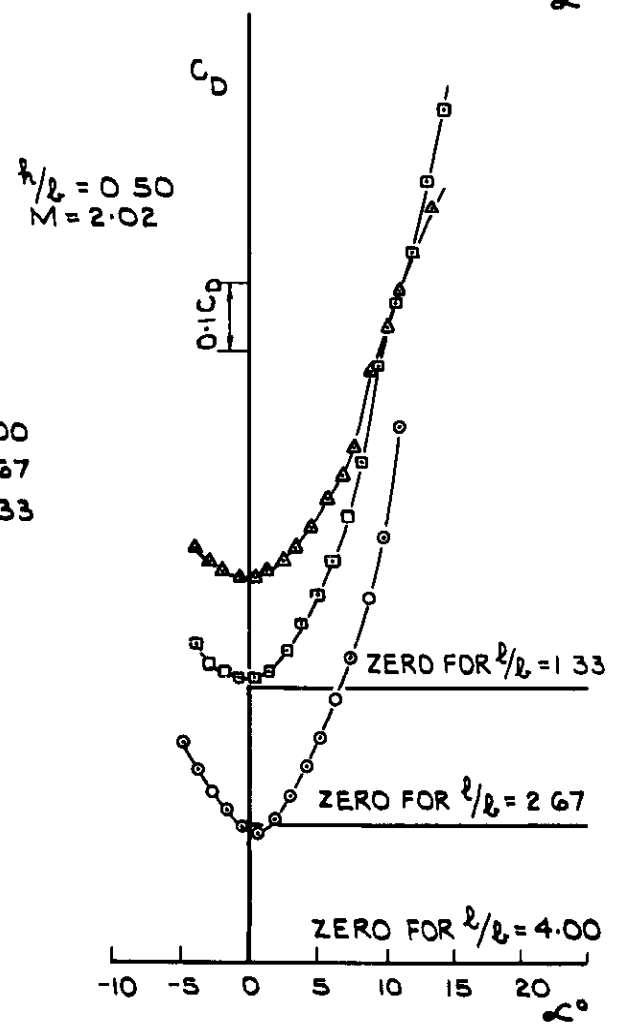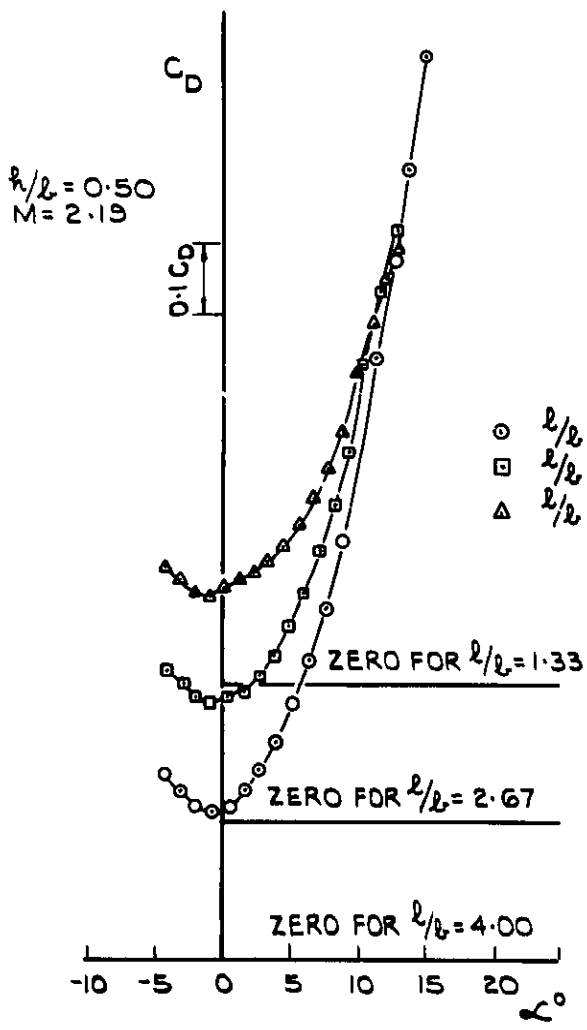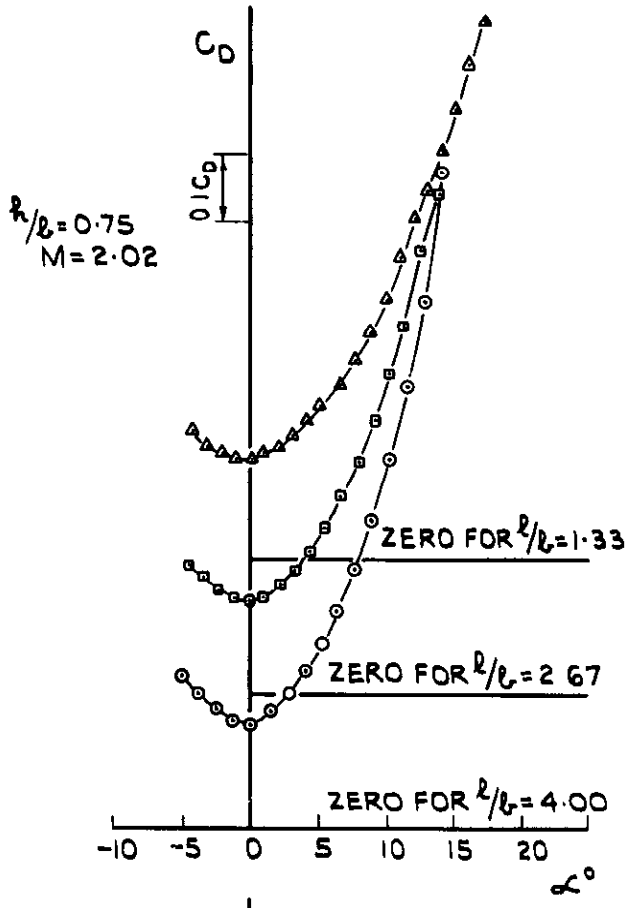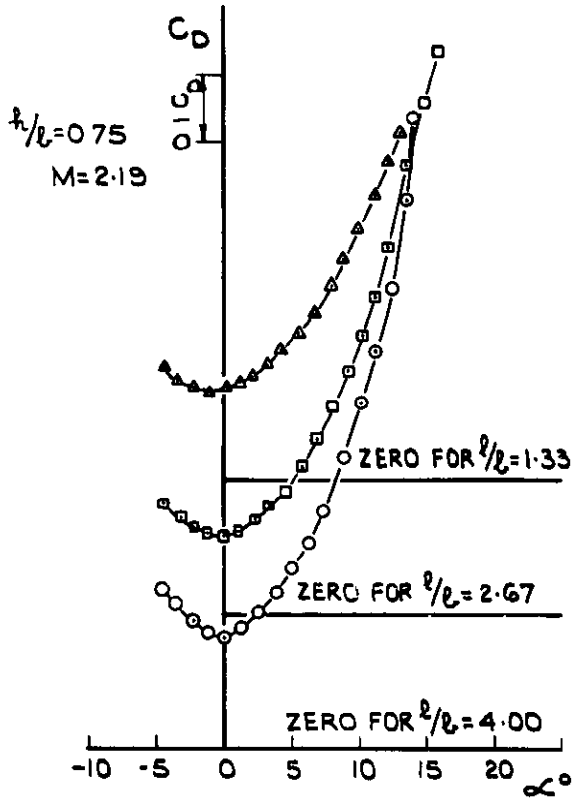
FIG. II. DRAG OF RECTANGULAR DUCTS.
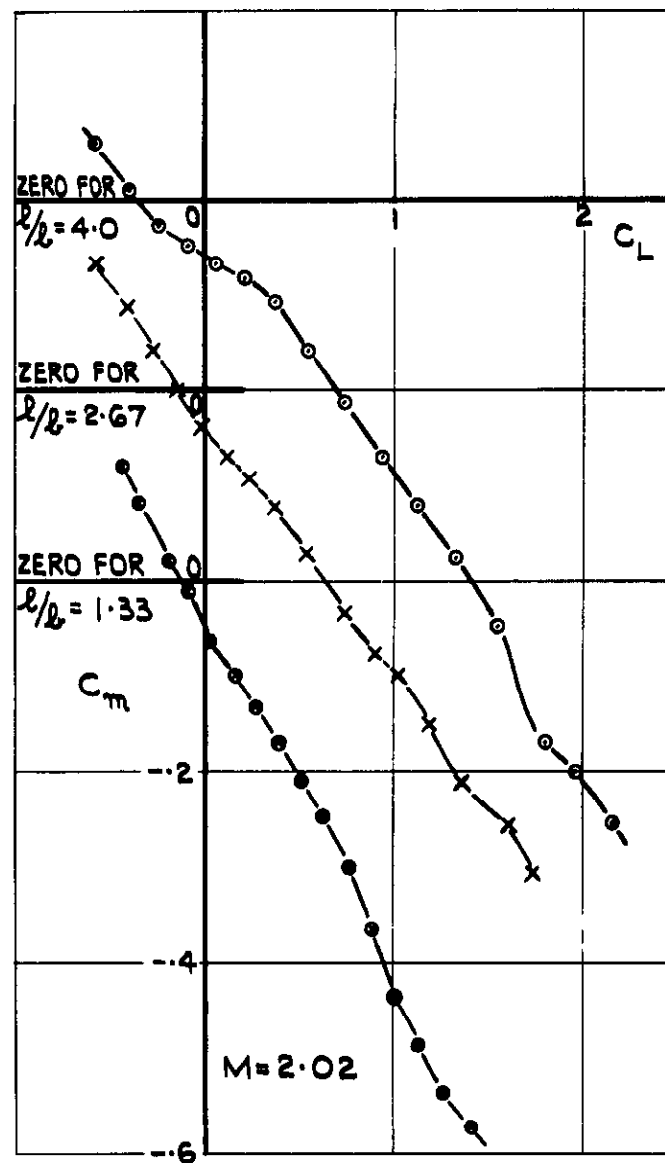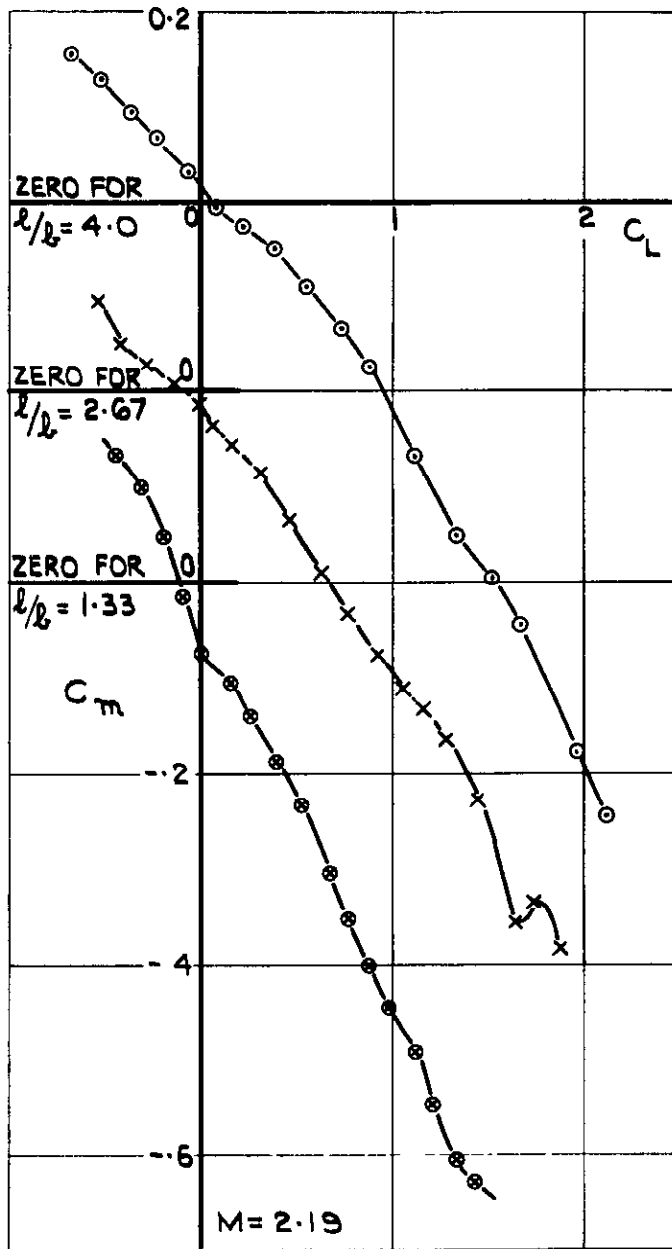
FIG 12. $C_m \sim C_L$ FOR RECTANGULAR DUCTS, $h/\ell = 0.75$.
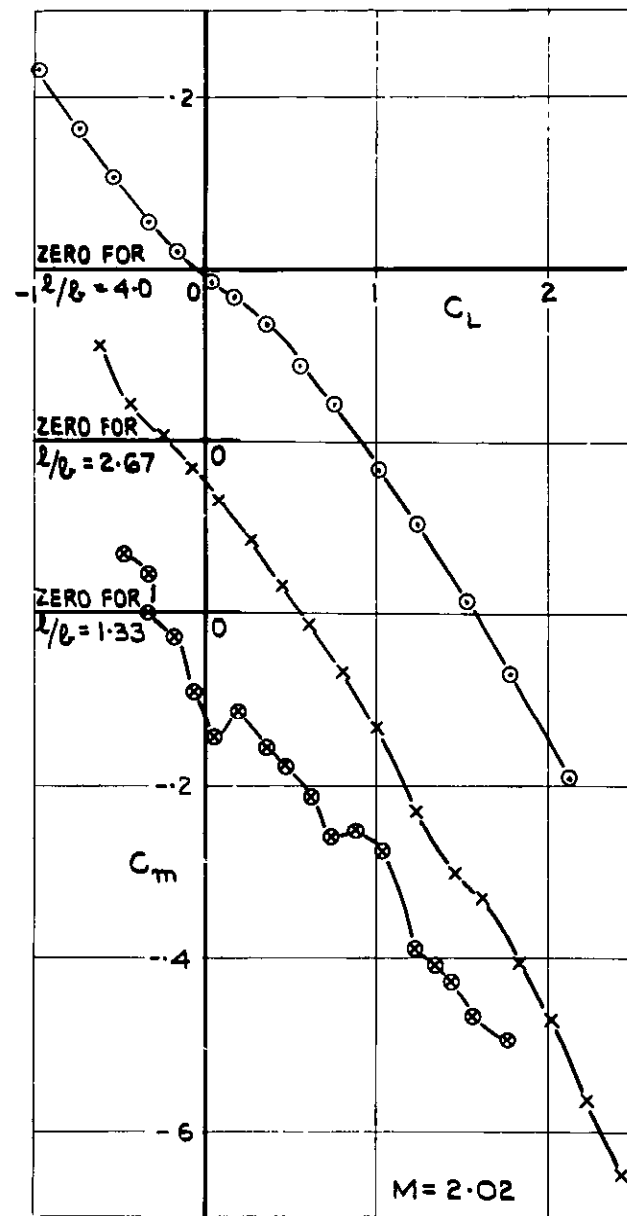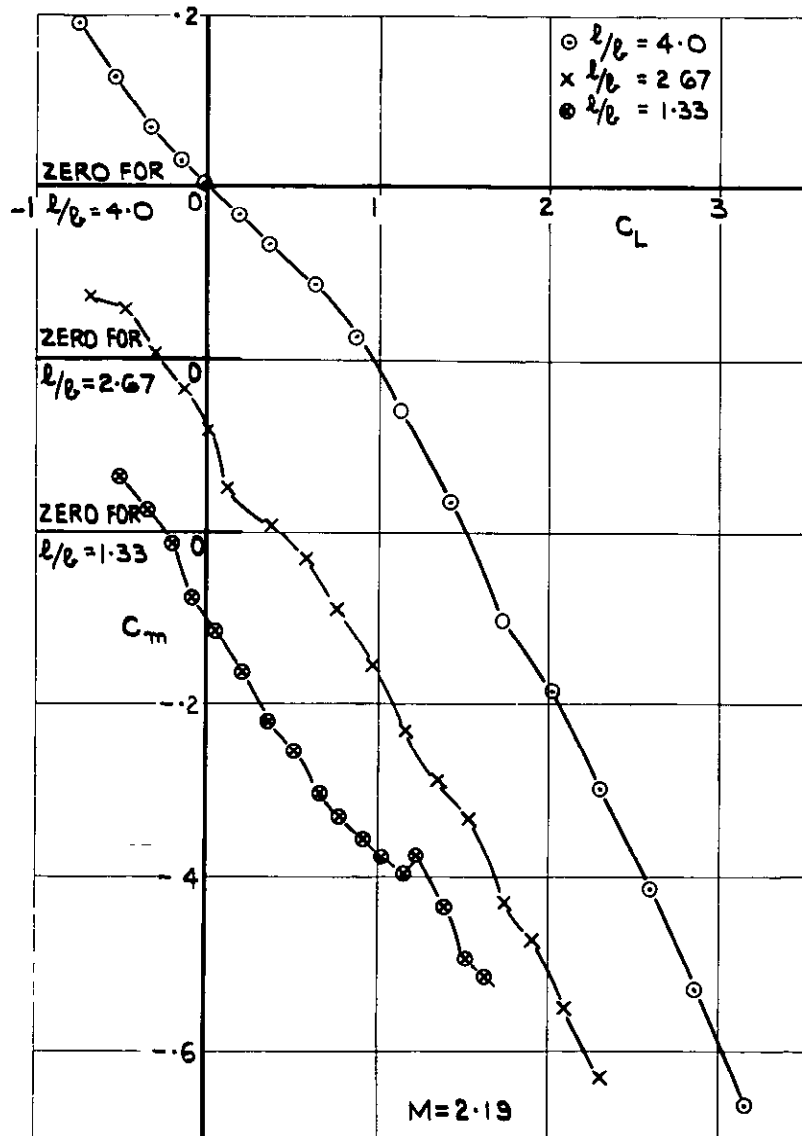
FIG.13 $C_m \sim C_L$ FOR RECTANGULAR DUCTS $h/\ell = 0.5$
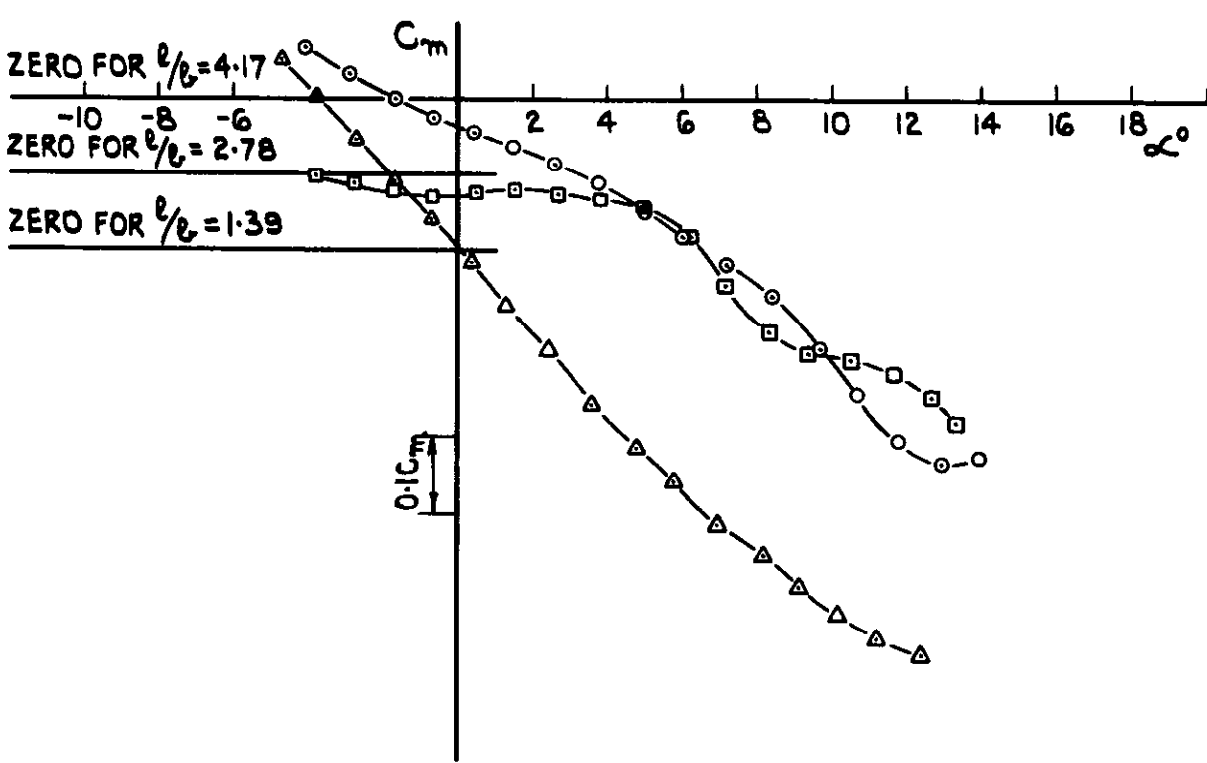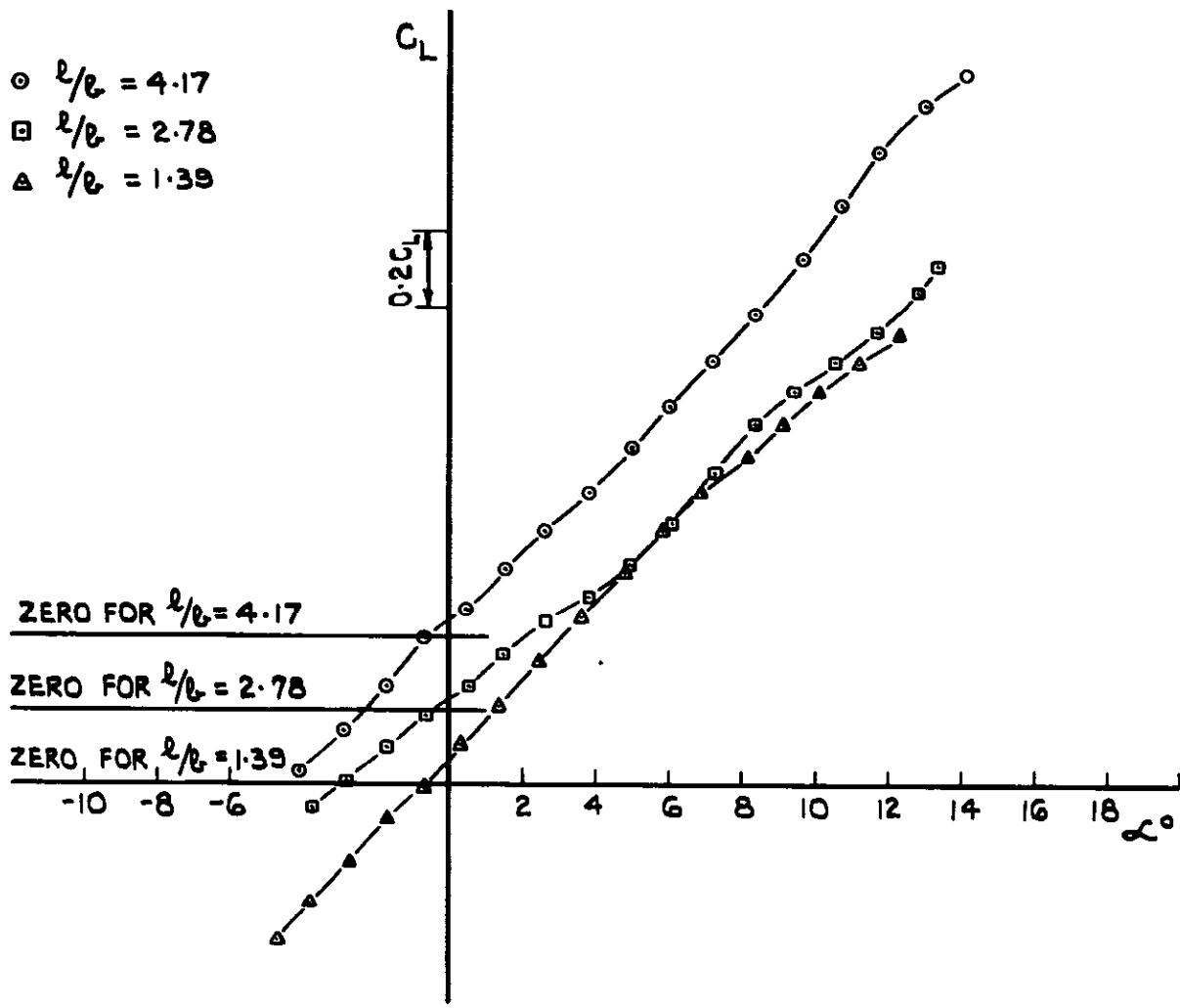
FIG.14. LIFT & PITCHING MOMENT AT M=2·19 FOR
CIRCULAR DUCTS.
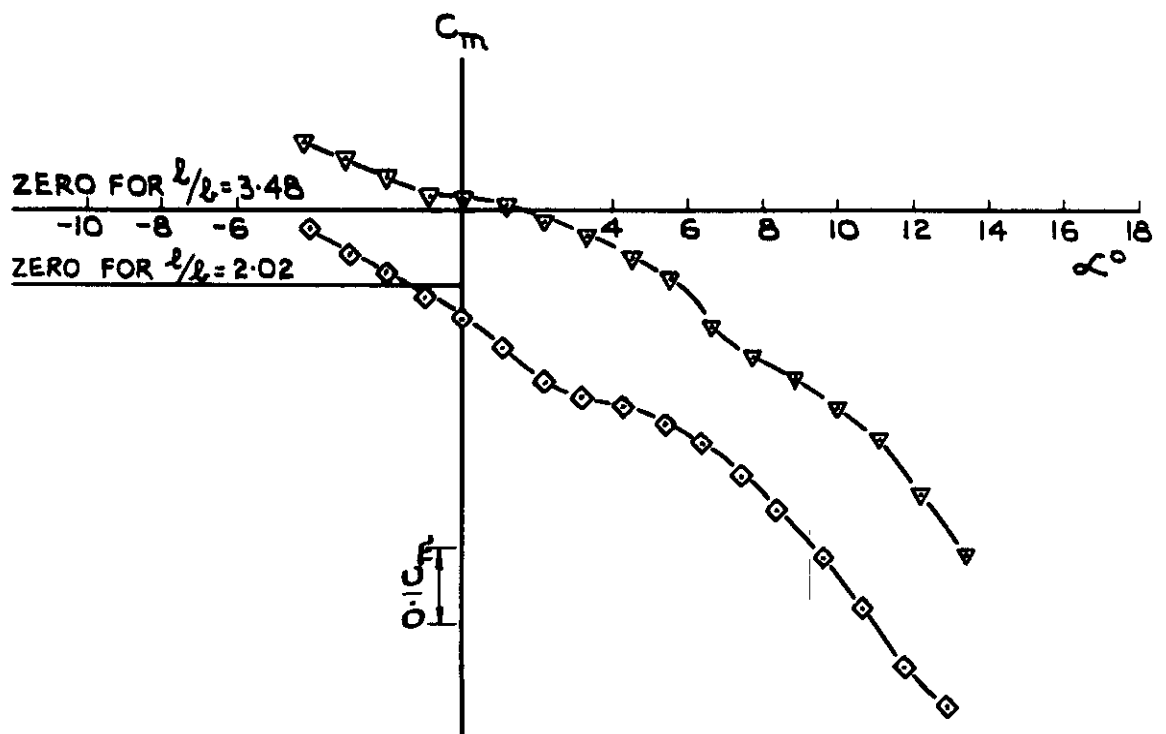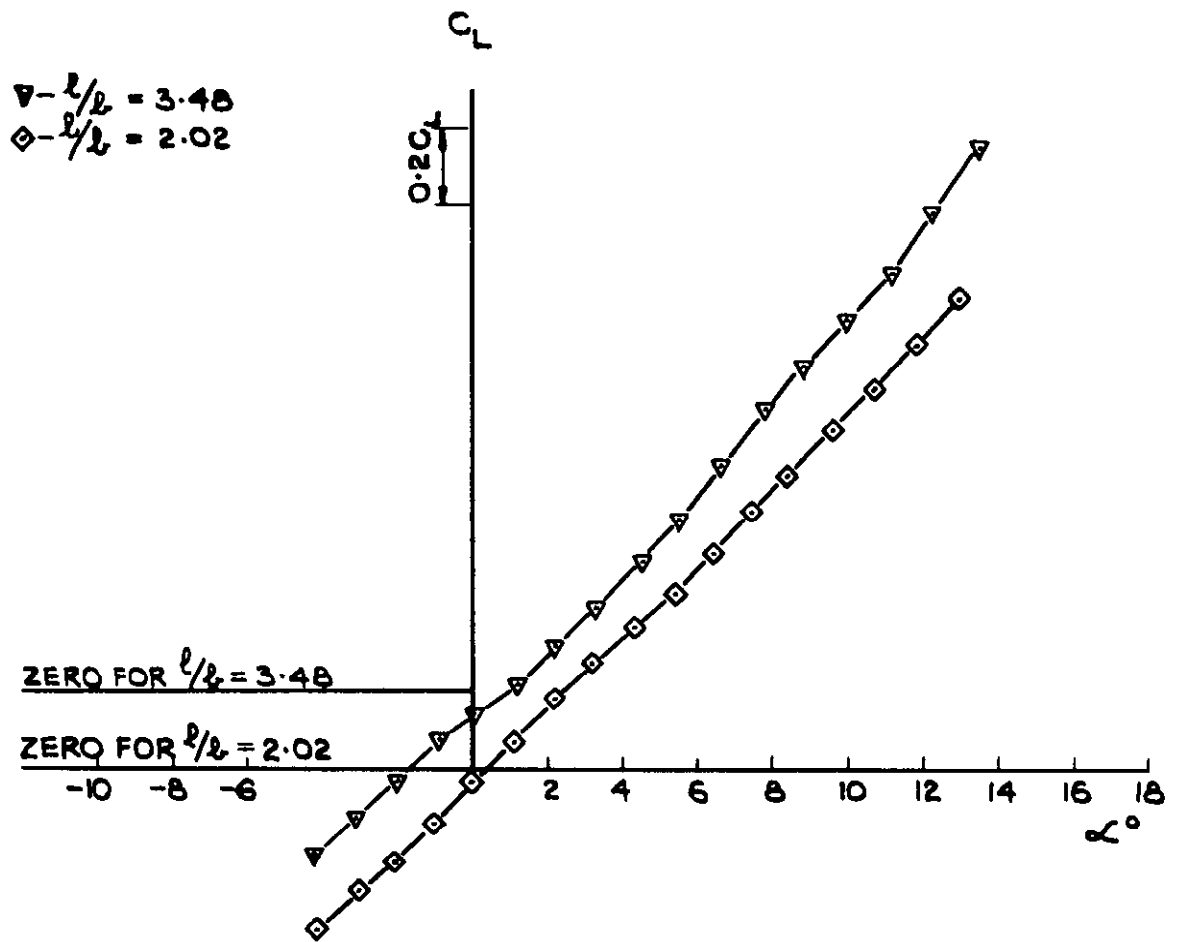
FIG. 14. (CONT'D) LIFT & PITCHING MOMENT AT M = 2·19 FOR CIRCULAR DUCTS.
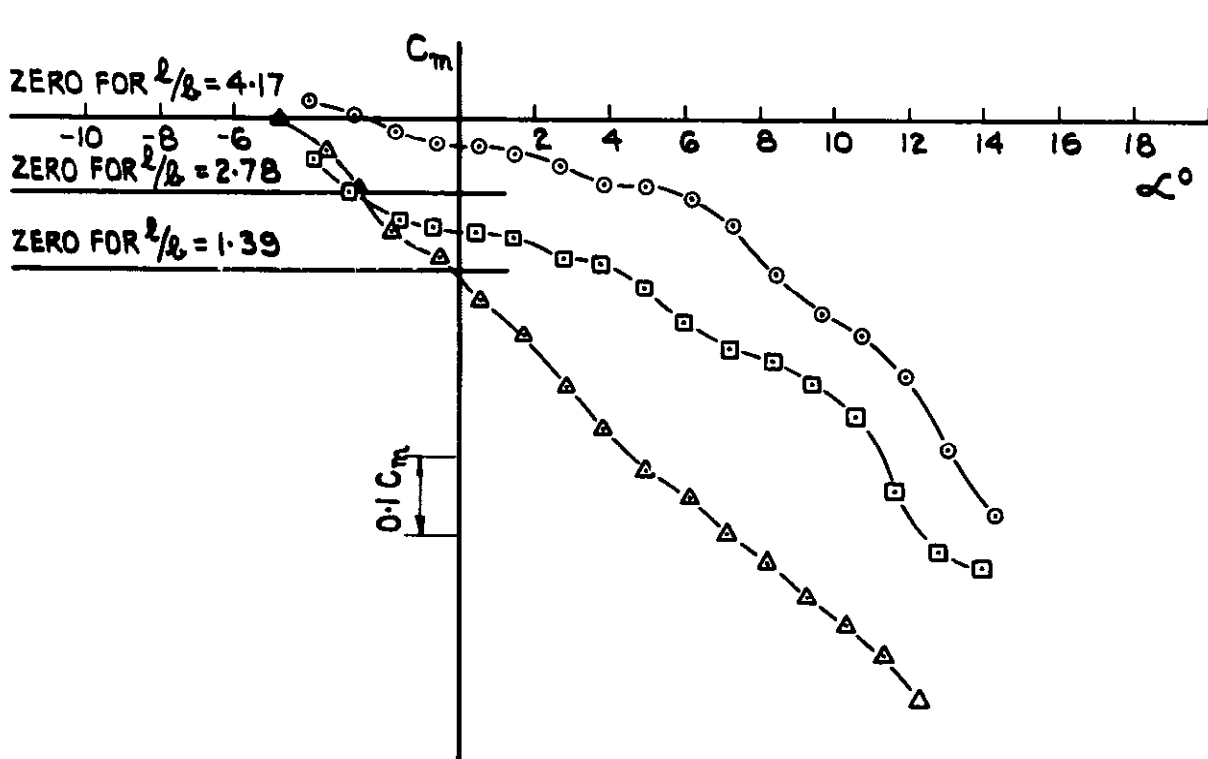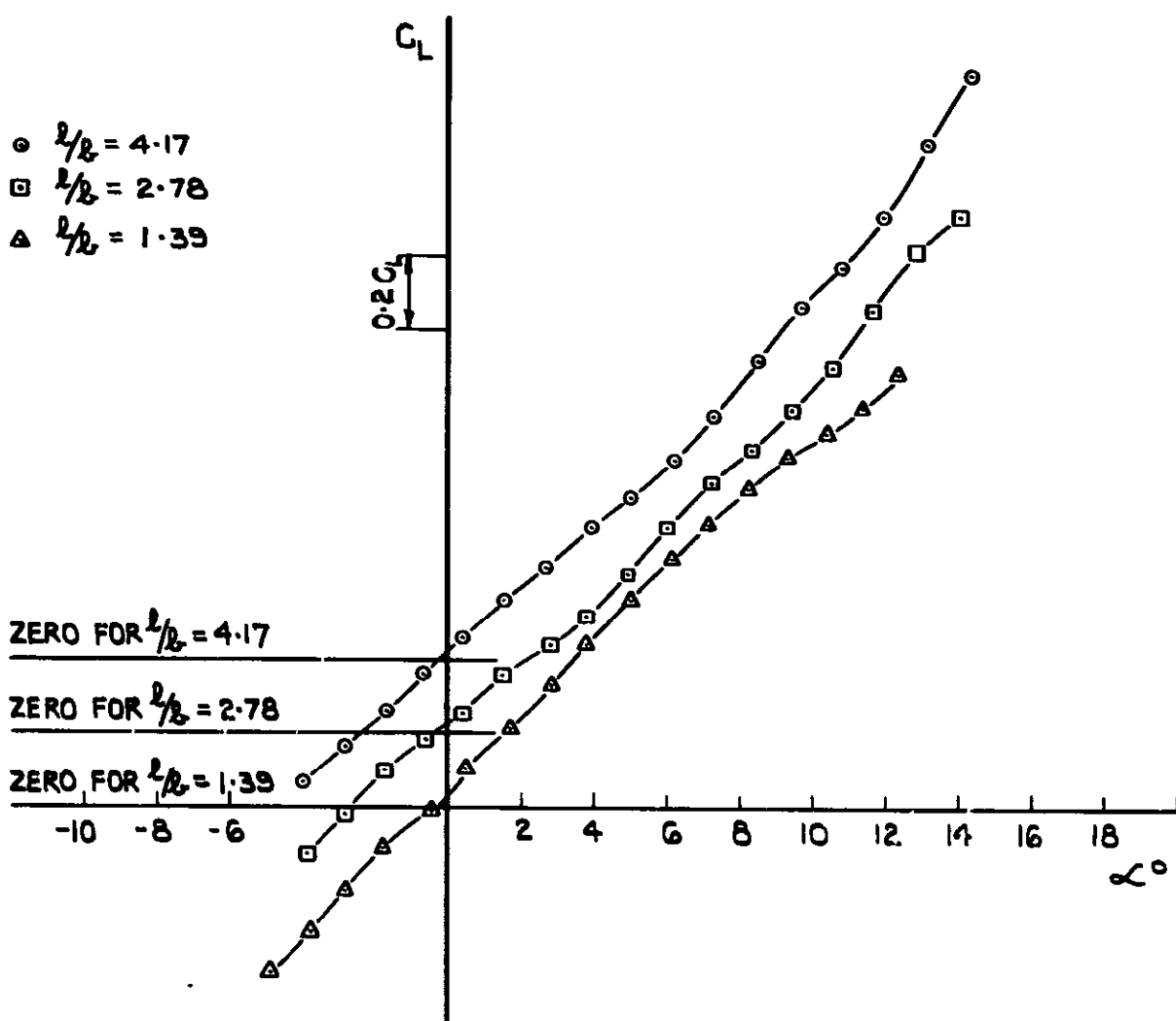
FIG.15. LIFT & PITCHING MOMENT AT M= 2·02 FOR CIRCULAR DUCTS
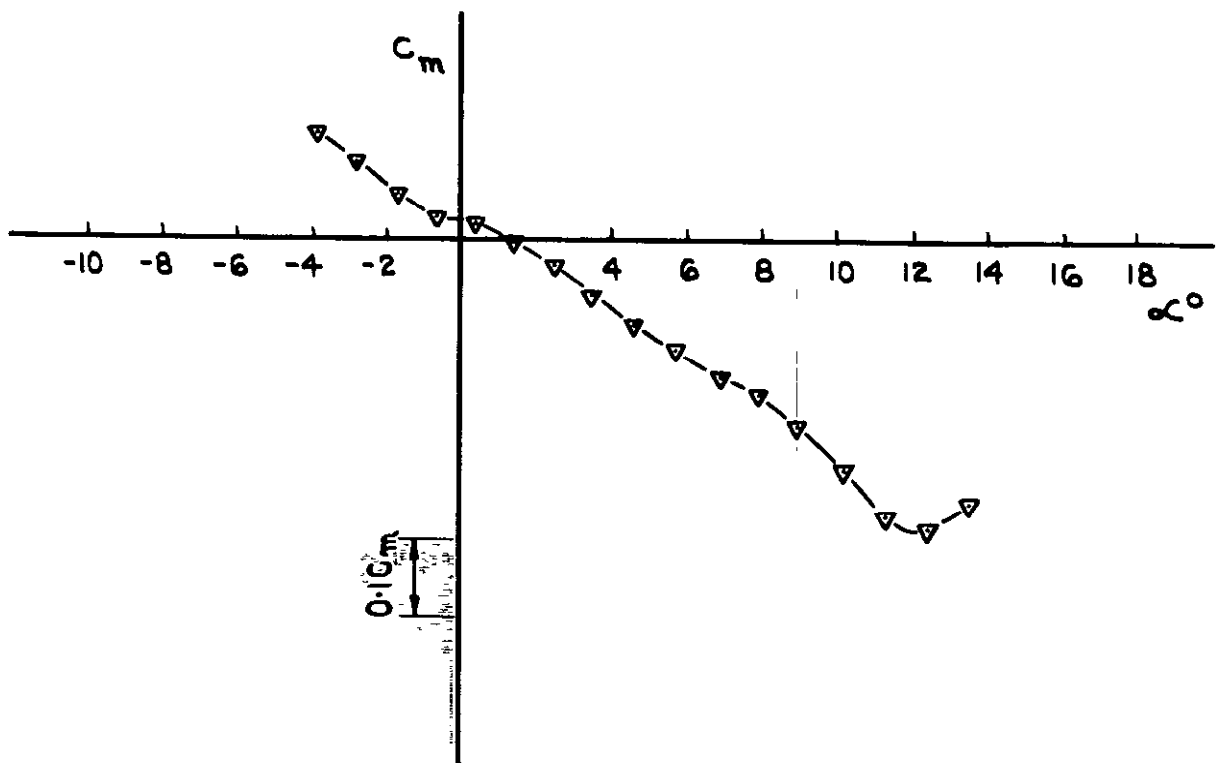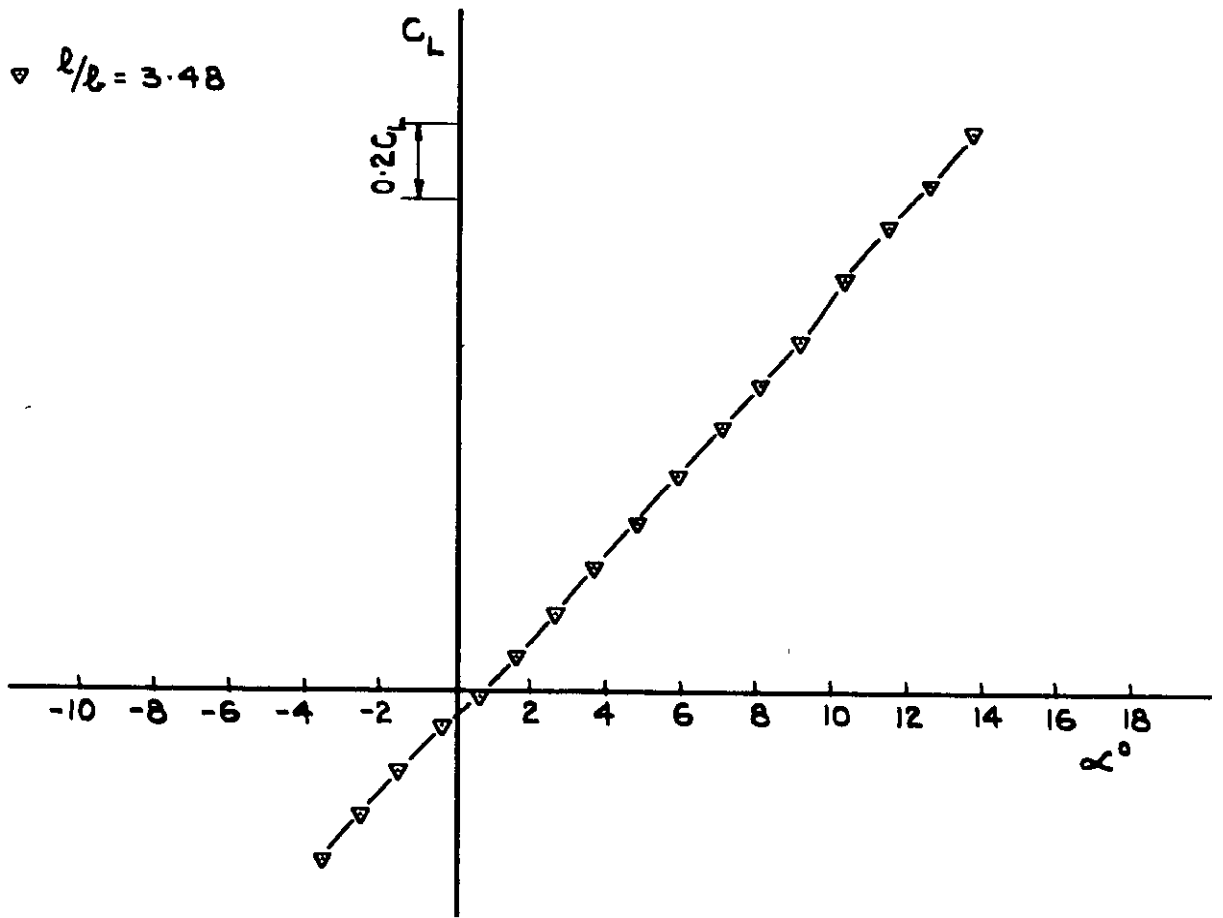
FIG.15.(CONTD) LIFT & PITCHING MOMENT AT M = 2·02 FOR CIRCULAR DUCTS.
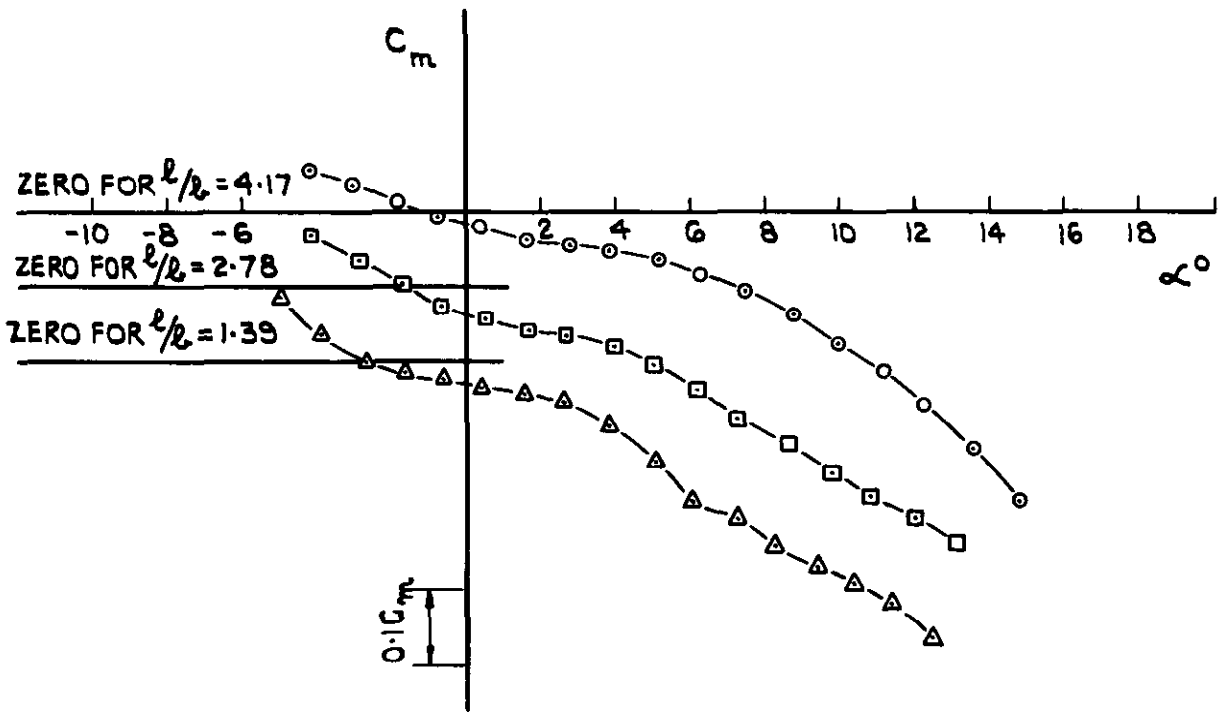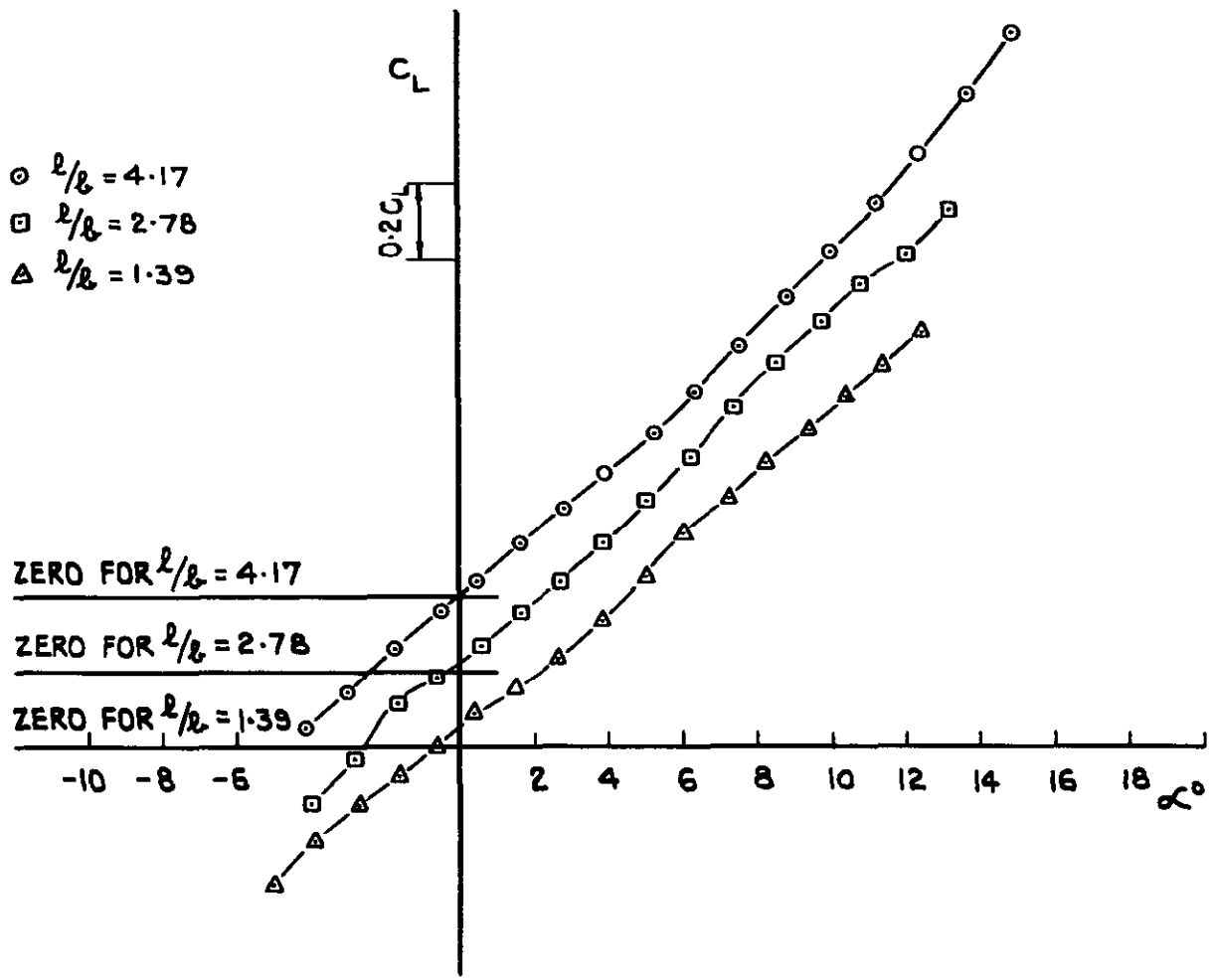
FIG.16. LIFT & PITCHING MOMENT AT M=1·58 FOR CIRCULAR DUCTS.

∇ − ℓ/ℓ = 3·48
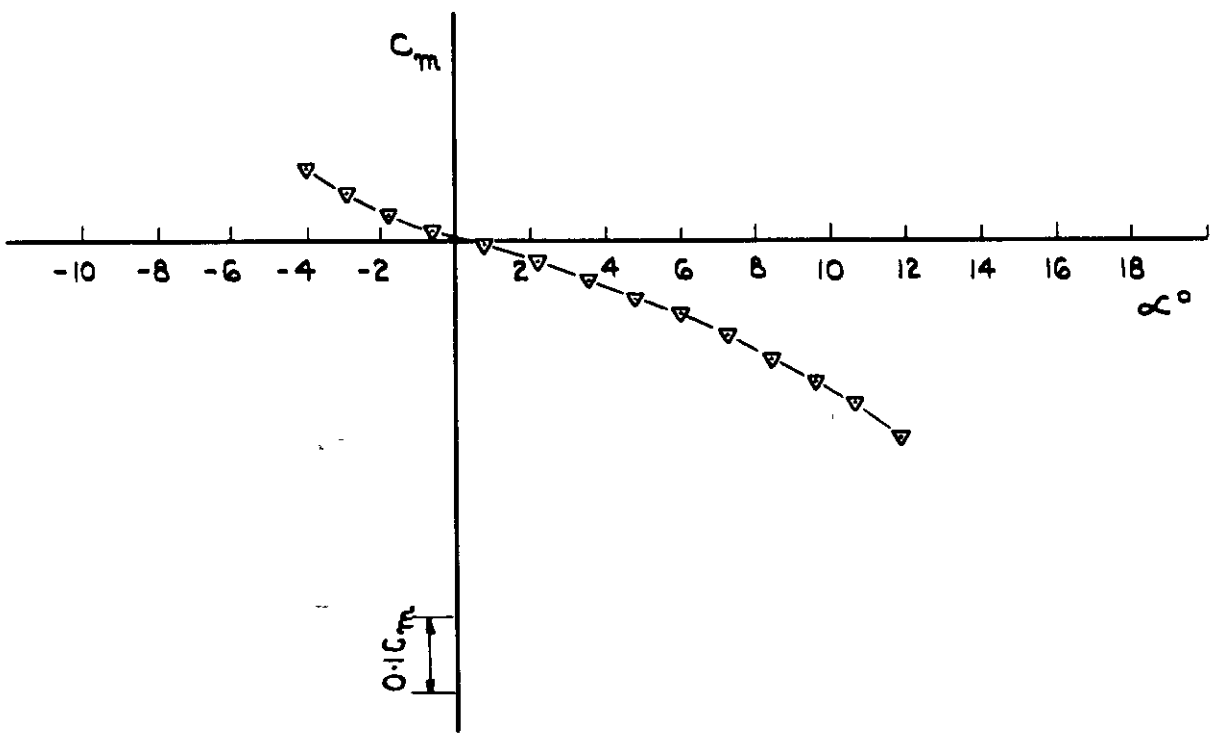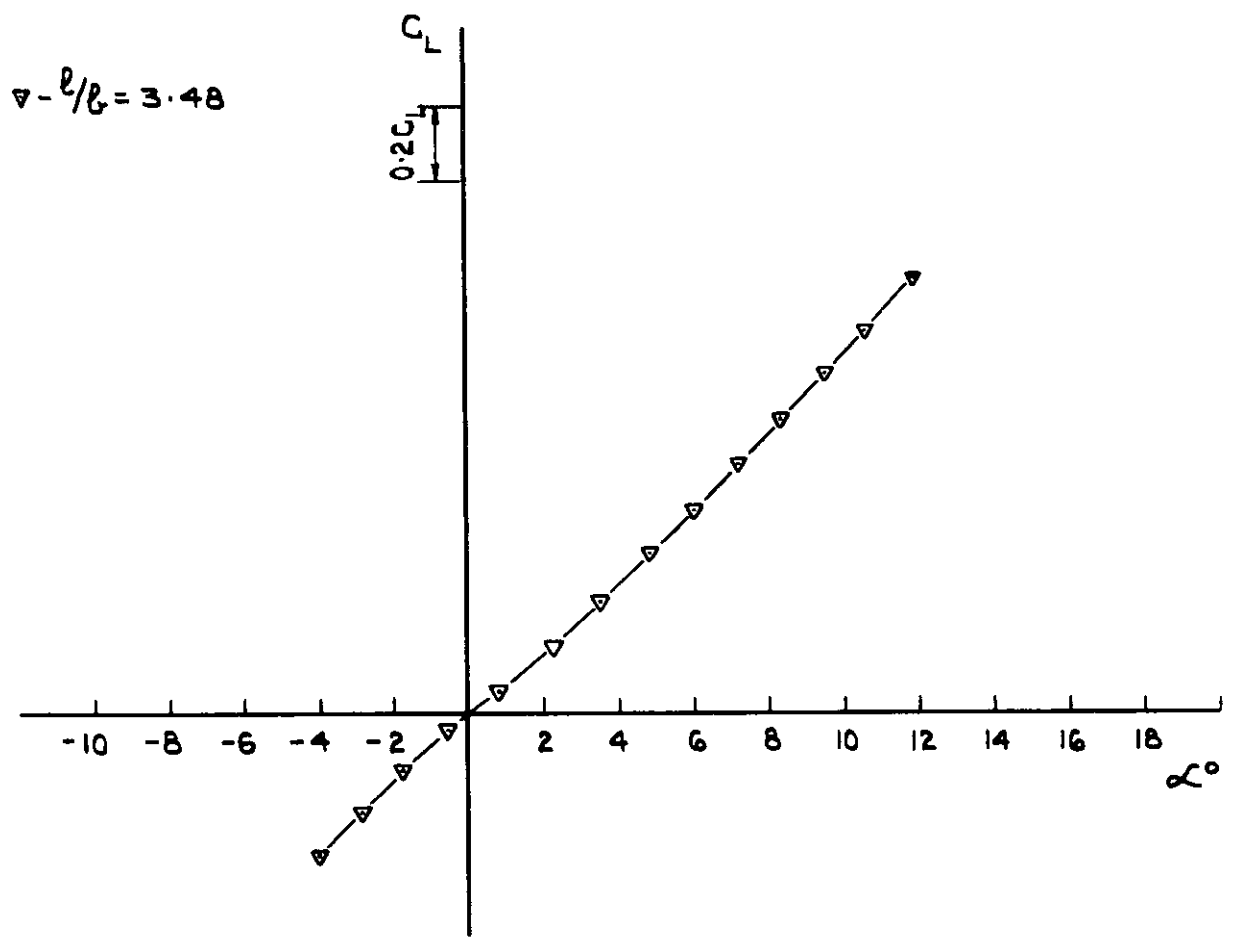
FIG 16.(CONTD.) LIFT & PITCHING MOMENT AT M=1·58 FOR
CIRCULAR DUCTS.
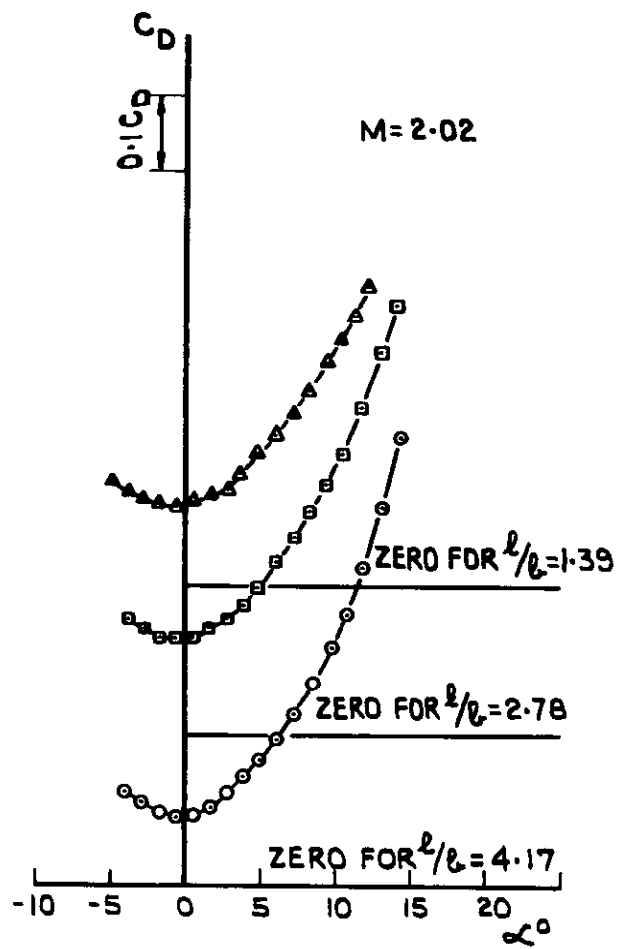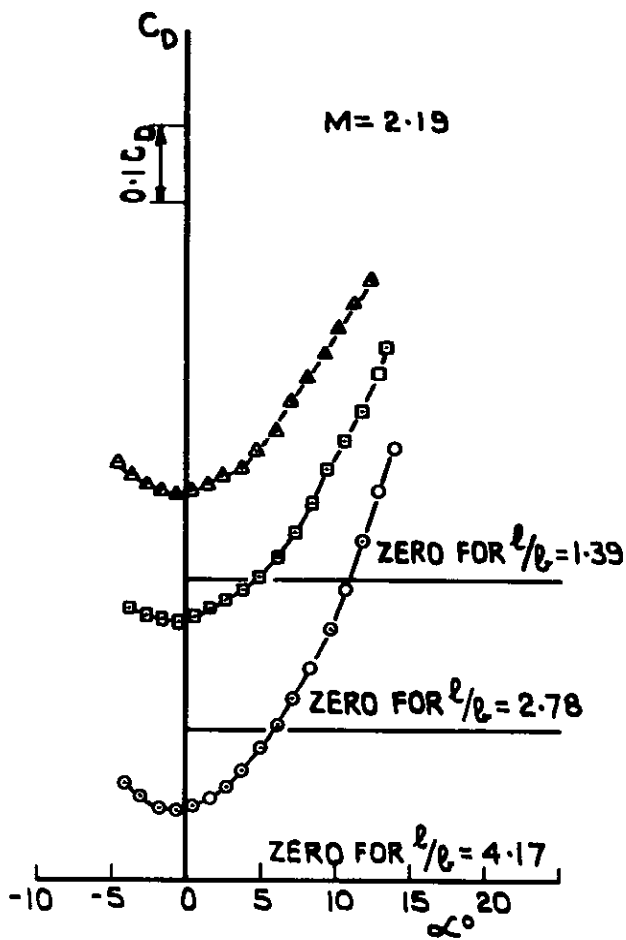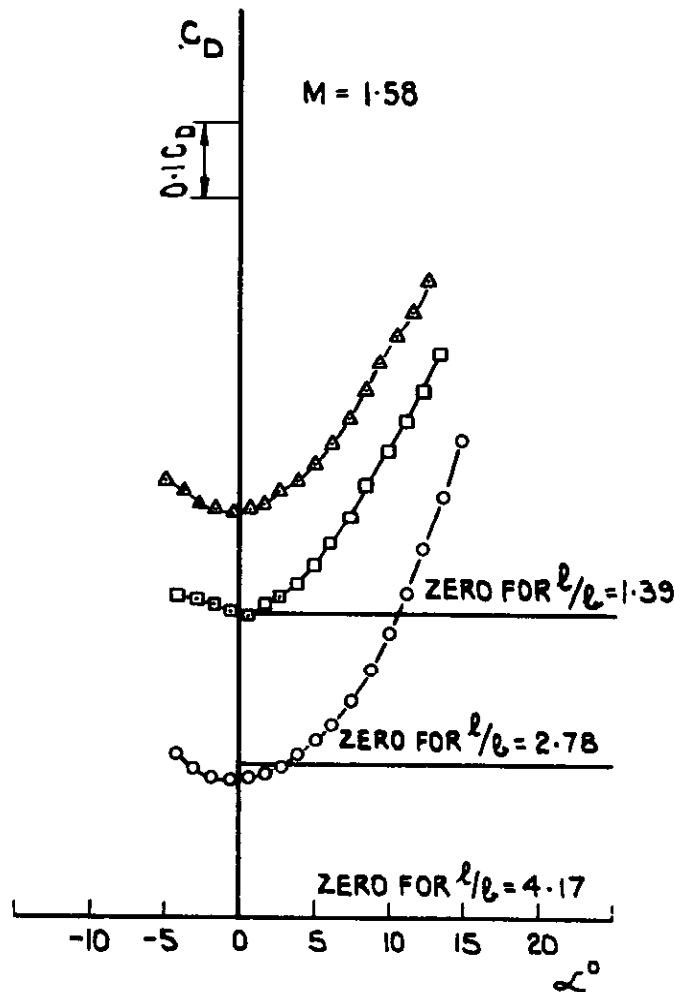
FIG.17. DRAG OF CIRCULAR DUCTS.
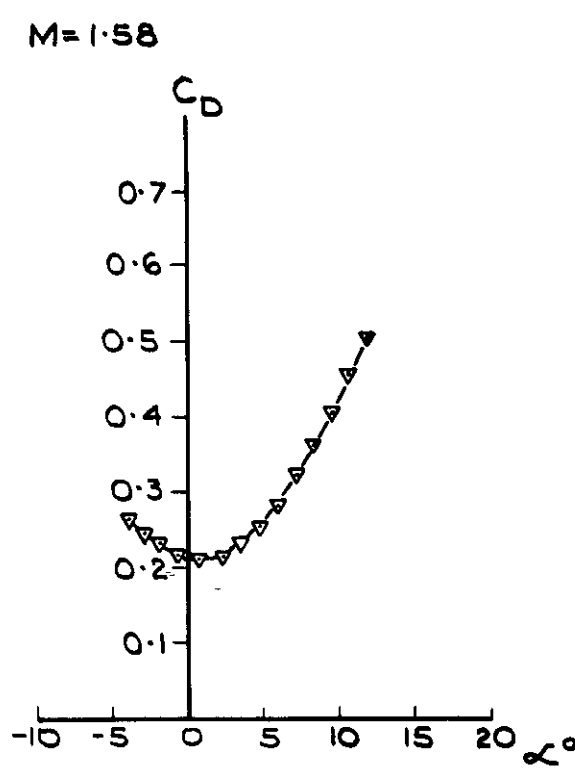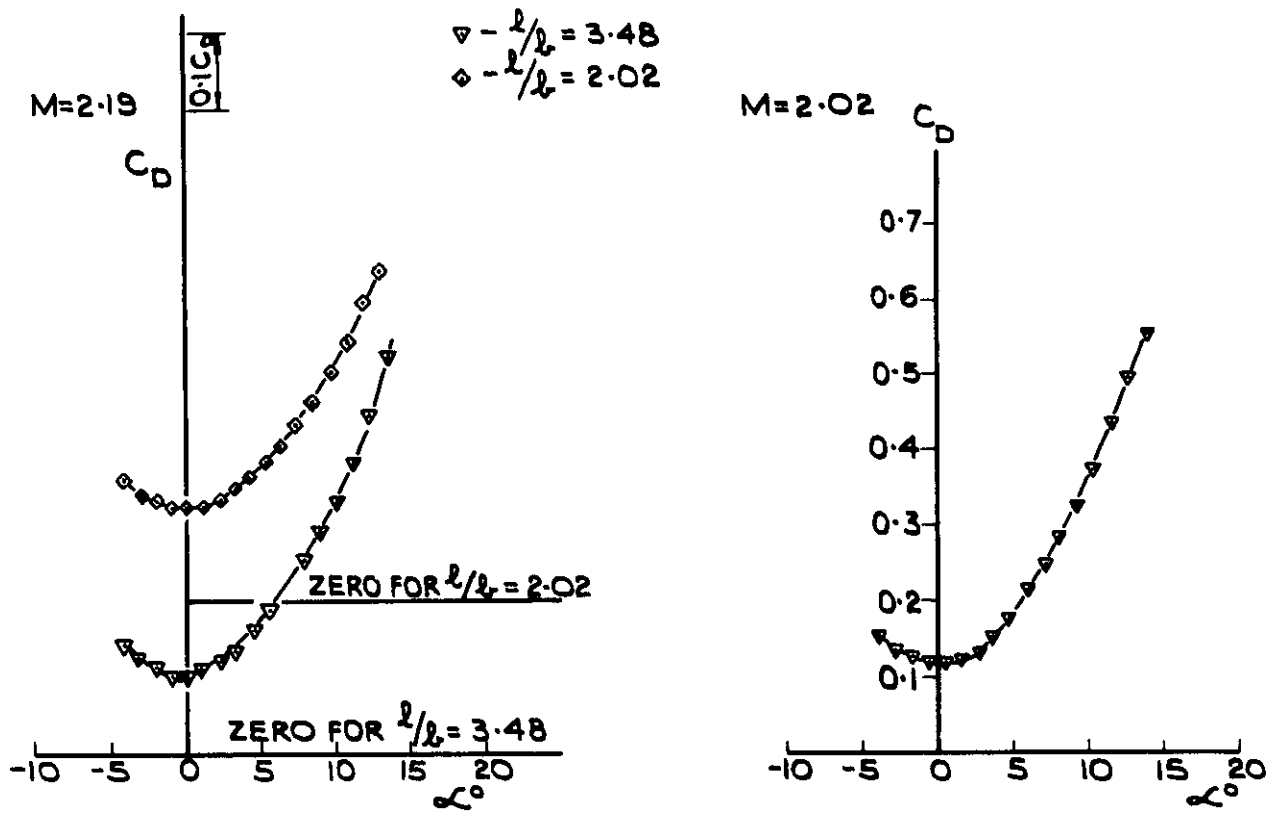
FIG 17. (CONTD)   DRAG OF CIRCULAR DUCTS
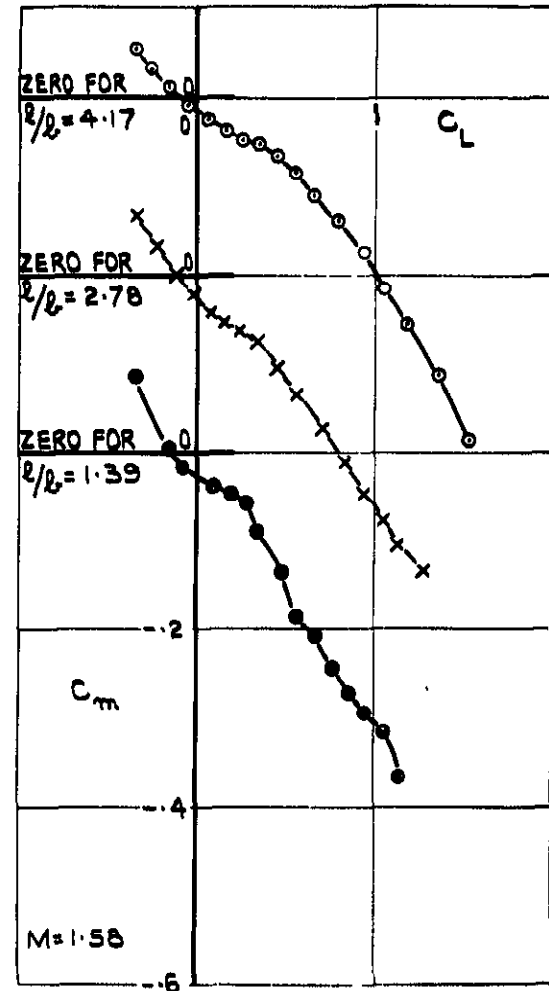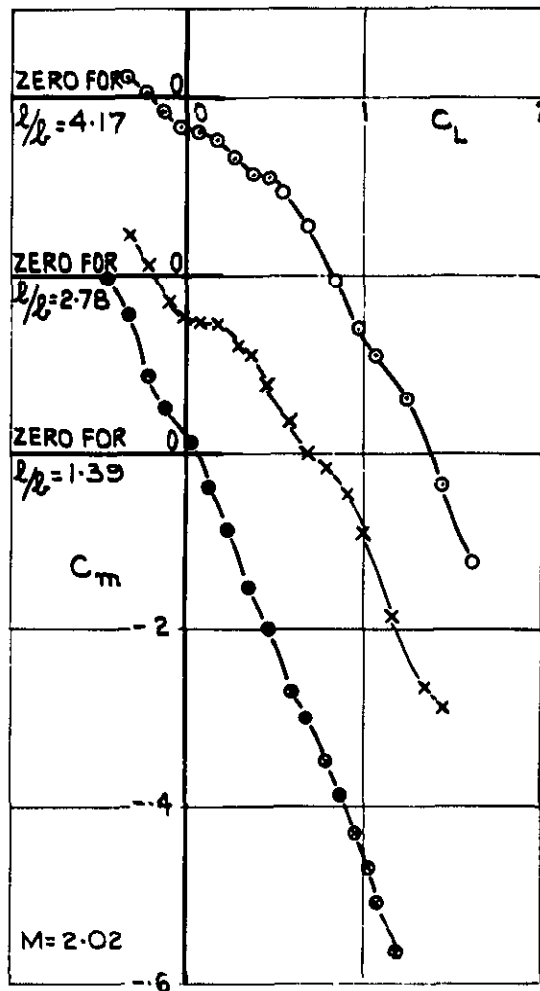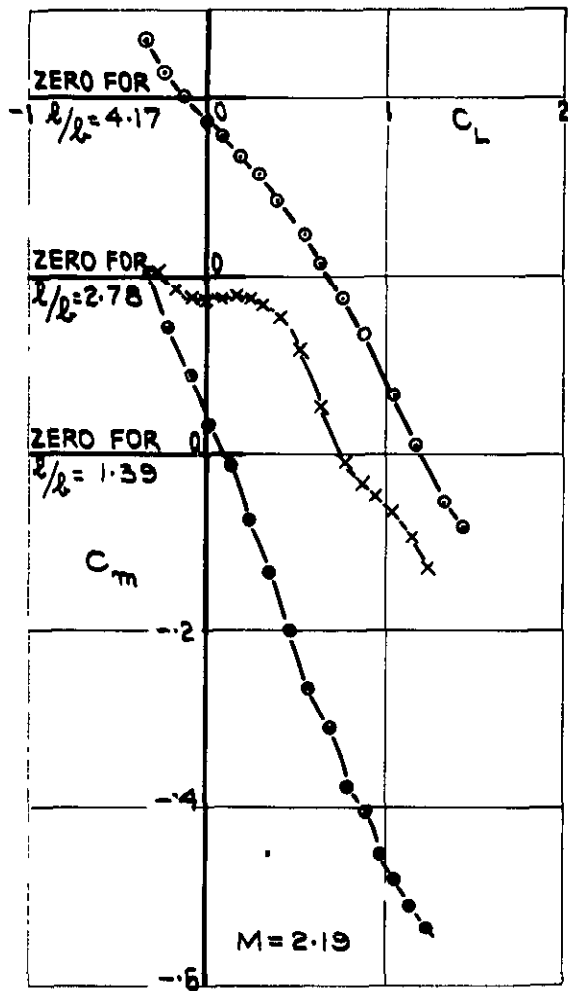
FIG. 18. $C_m \sim C_L$ FOR CIRCULAR DUCTS.
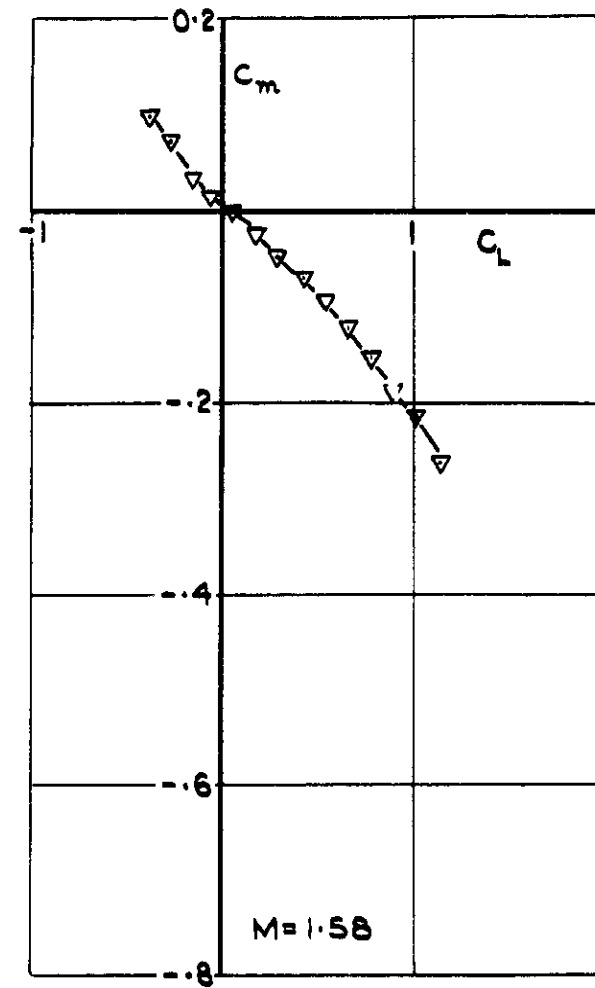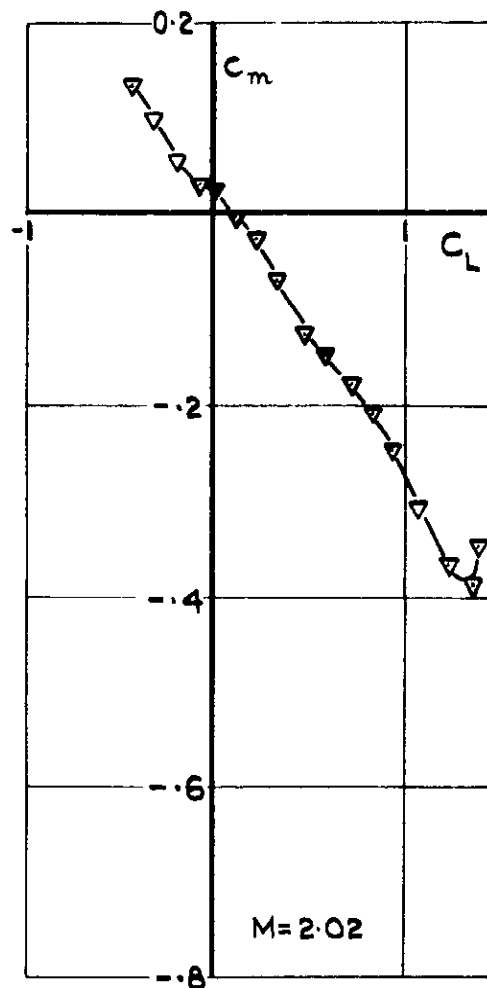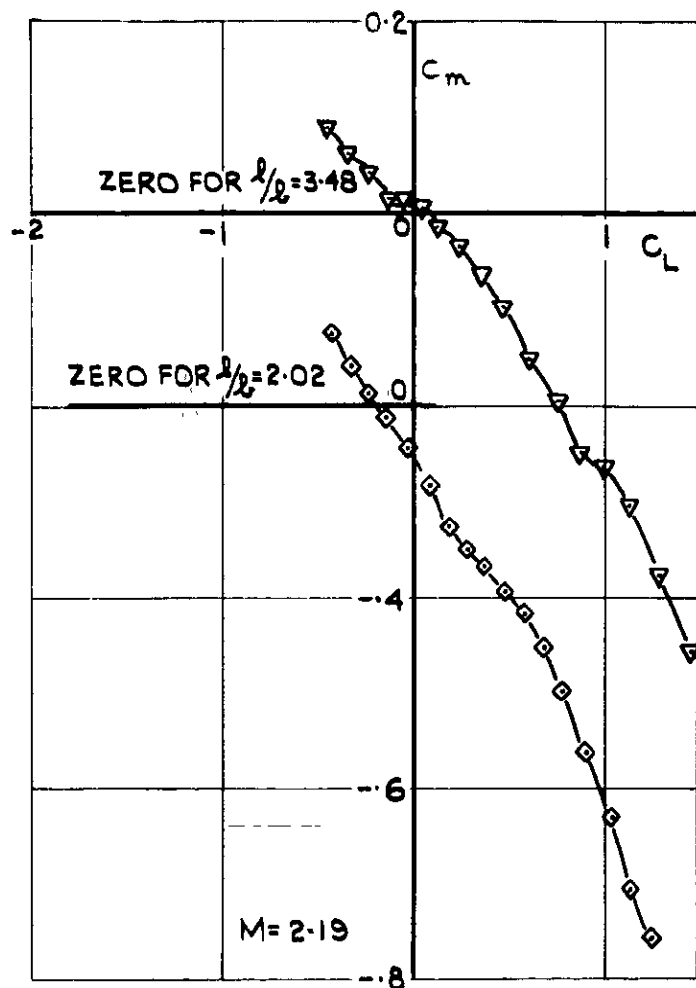
FIG.18 (CONT'D) $C_m \sim C_L$ FOR CIRCULAR DUCTS.
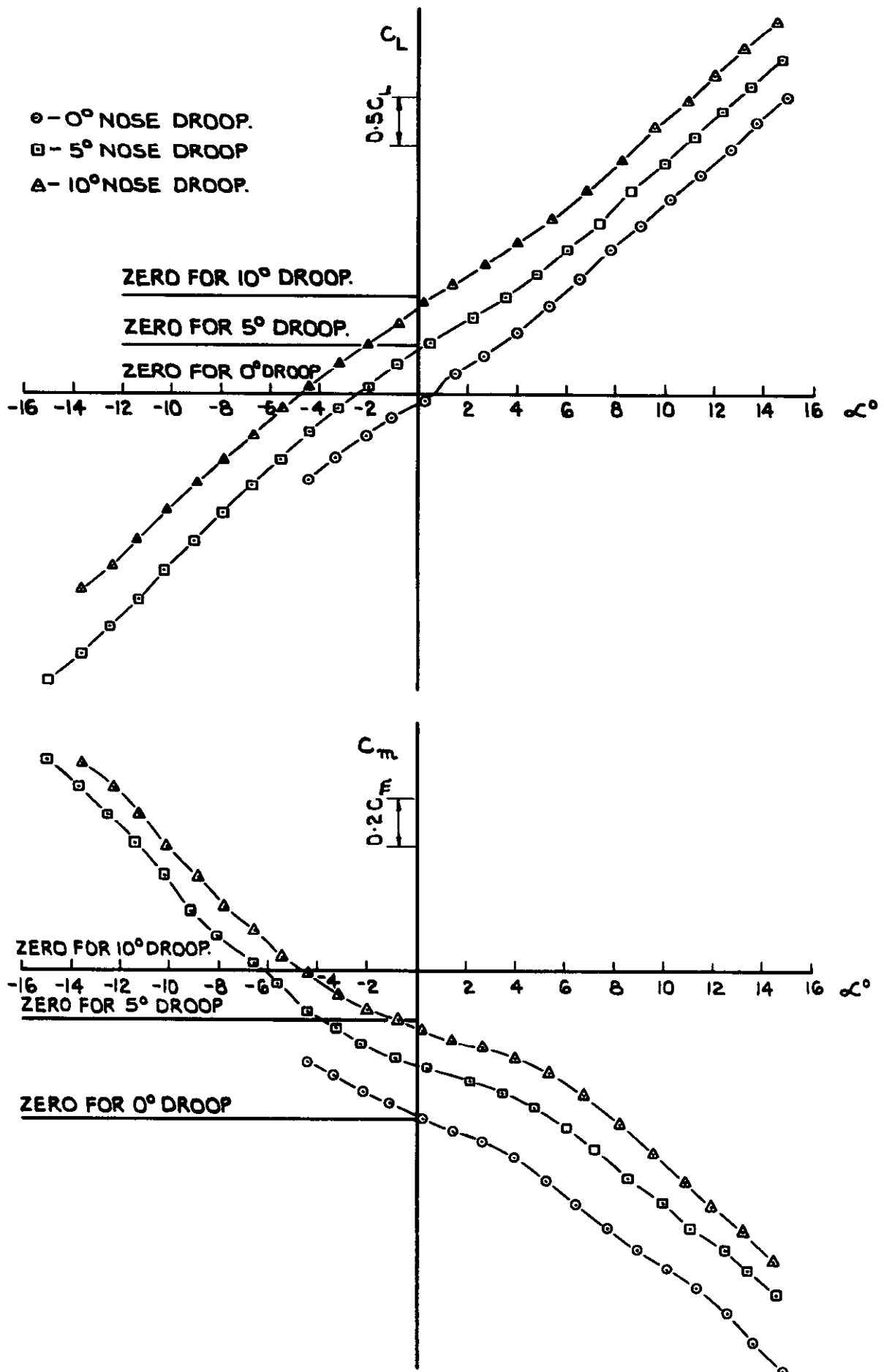
FIG.19. LIFT & PITCHING MOMENT AT M= 2·19, OF
DROOPED NOSE DUCTS, h/l=0·5

$\odot - 0°$ NOSE DROOP
$\square - 5°$ NOSE DROOP
$\triangle - 10°$ NOSE DROOP.

ZERO FOR 10° DROOP

ZERO FOR 5° DROOP

ZERO FOR 0° DROOP

C_L

$0.5 C_L$

-16 -14 -12 -10 -8 -6 -4 -2 2 4 6 8 10 12 14 16 $\alpha°$

C_m

$0.2 C_m$

ZERO FOR 10° DROOP

ZERO FOR 5° DROOP

ZERO FOR 0° DROOP

-16 -14 -12 -10 -8 -6 -4 -2 2 4 6 8 10 12 14 16 $\alpha°$
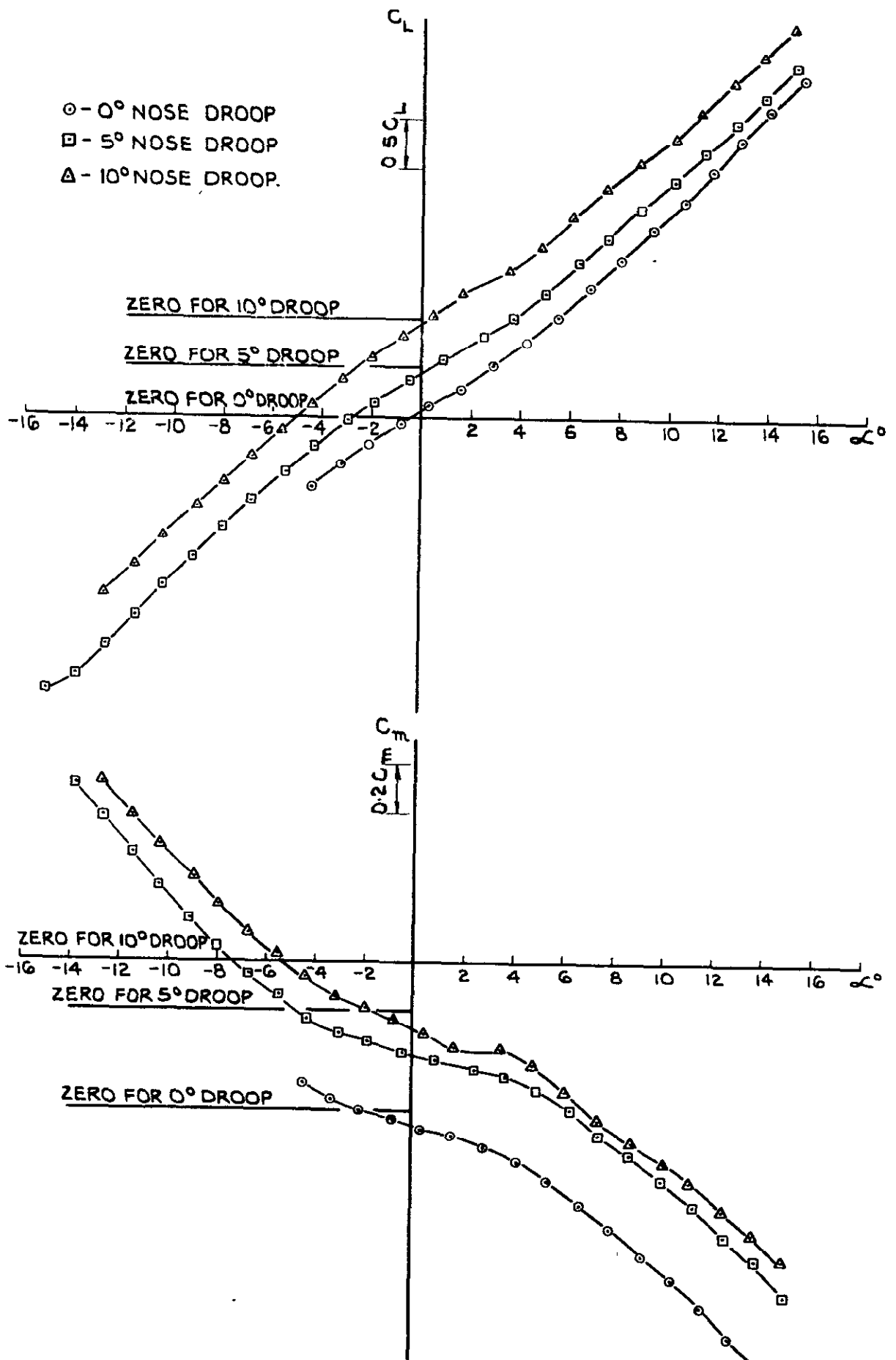
FIG 20. LIFT & PITCHING MOMENT AT M = 2·02, OF
DROOPED NOSE DUCTS, $h/\ell = 0.5$
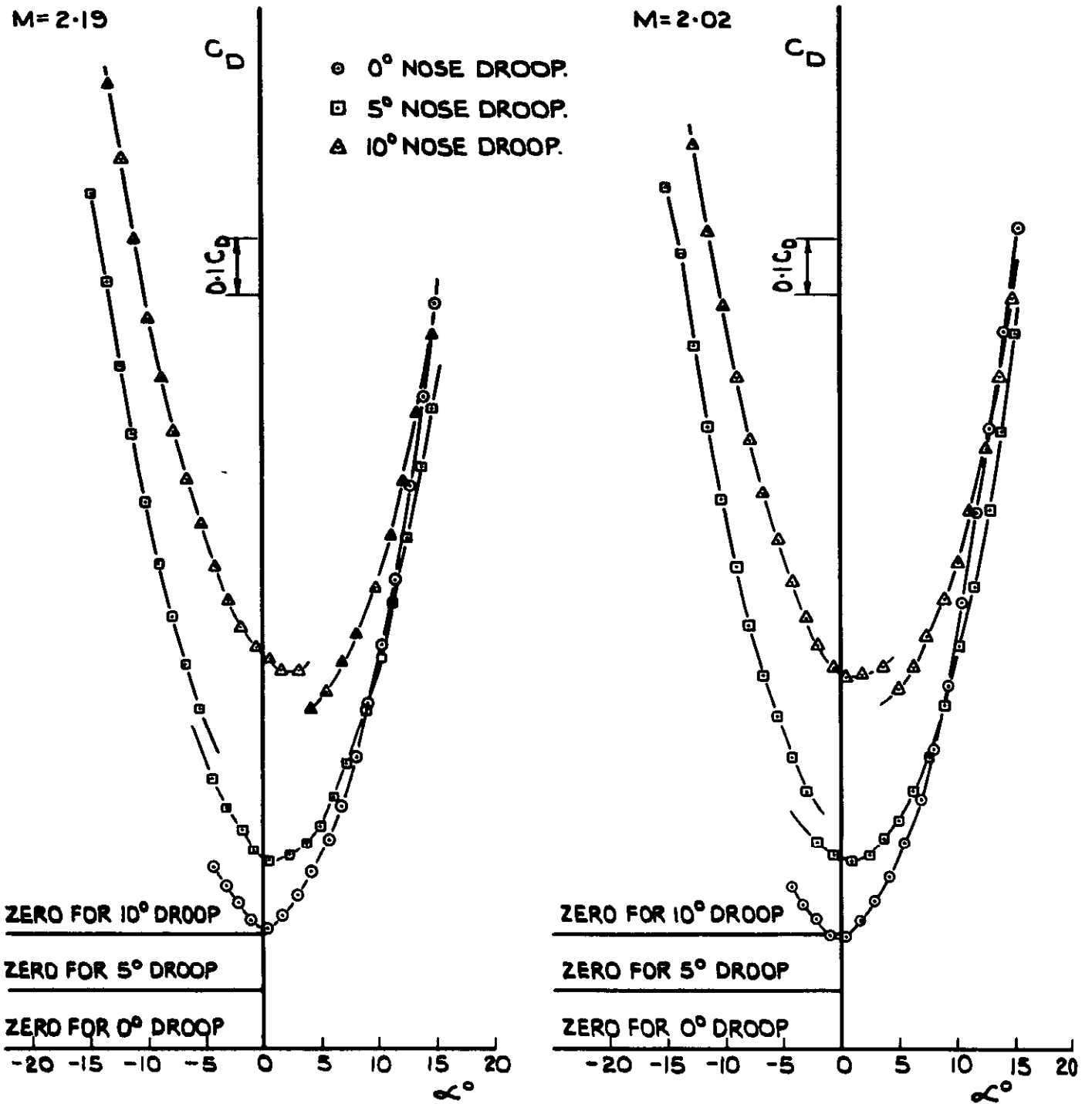
FIG. 2I. DRAG OF DROOPED NOSE DUCTS, $h/l = 0.5$

NOSE DROOP OF 0°
NOSE DROOP OF 5°
NOSE DROOP OF 10°
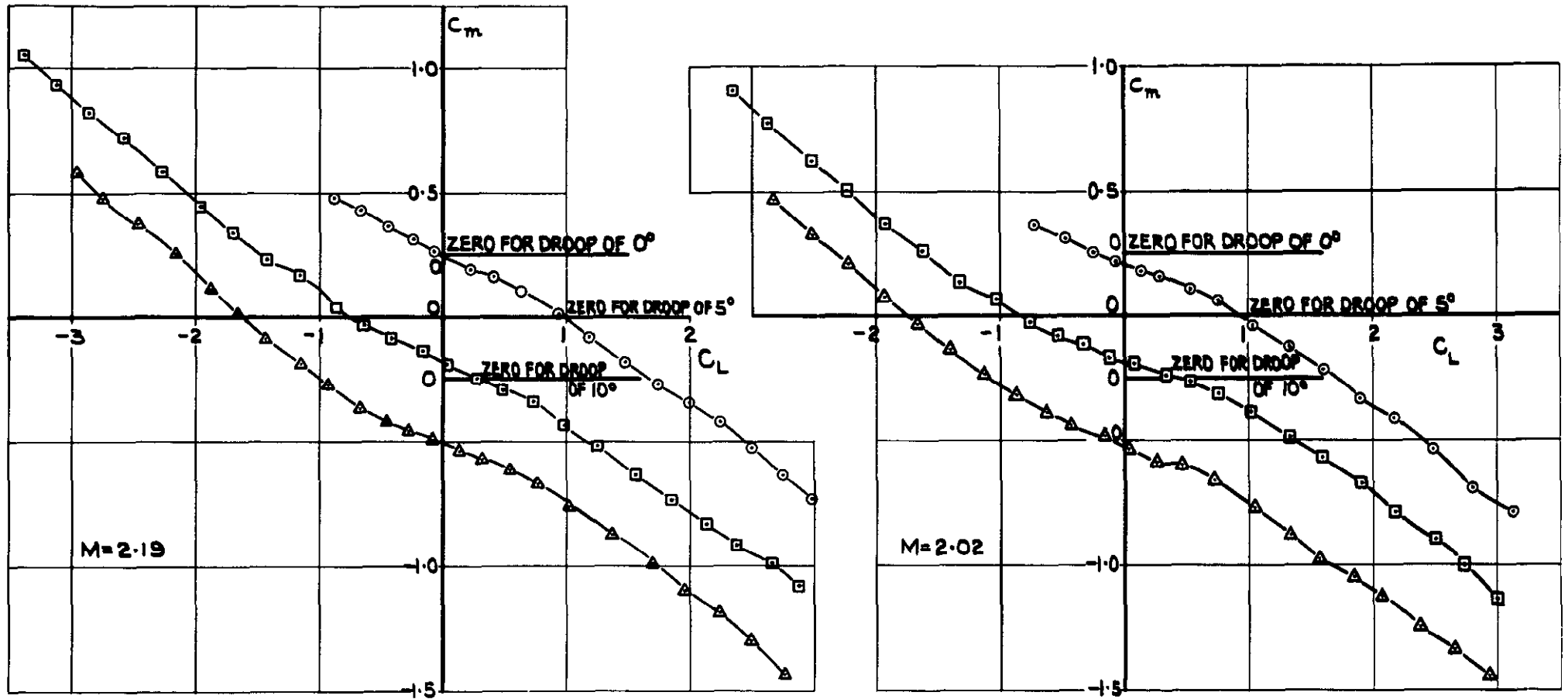
FIG. 22. $C_m \sim C_L$ FOR DROOPED NOSE DUCTS $h/\ell = 0.5$
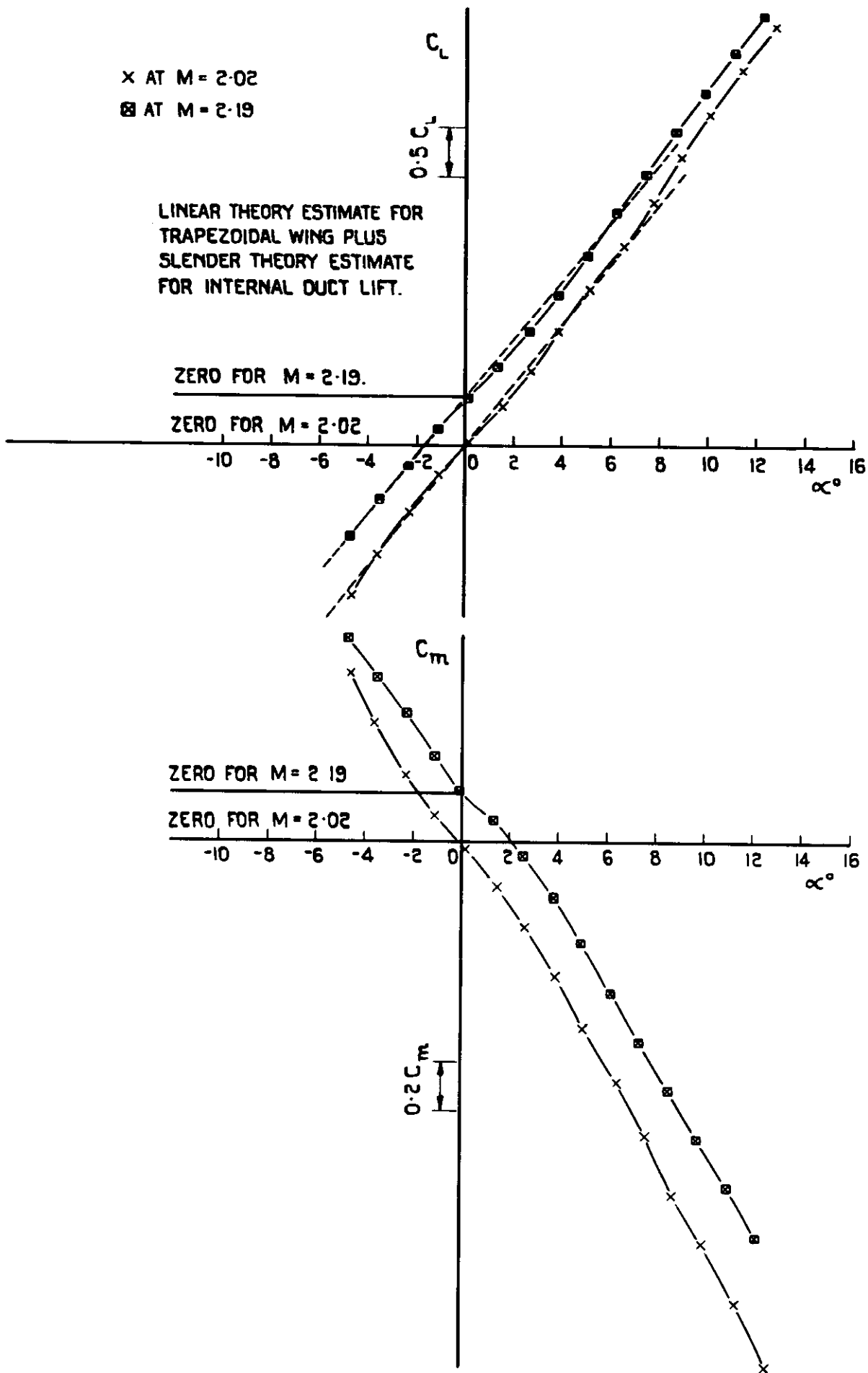
FIG. 23. LIFT & PITCHING MOMENT, AT M=2·19 AND M=2·02, OF WINGED DUCT.
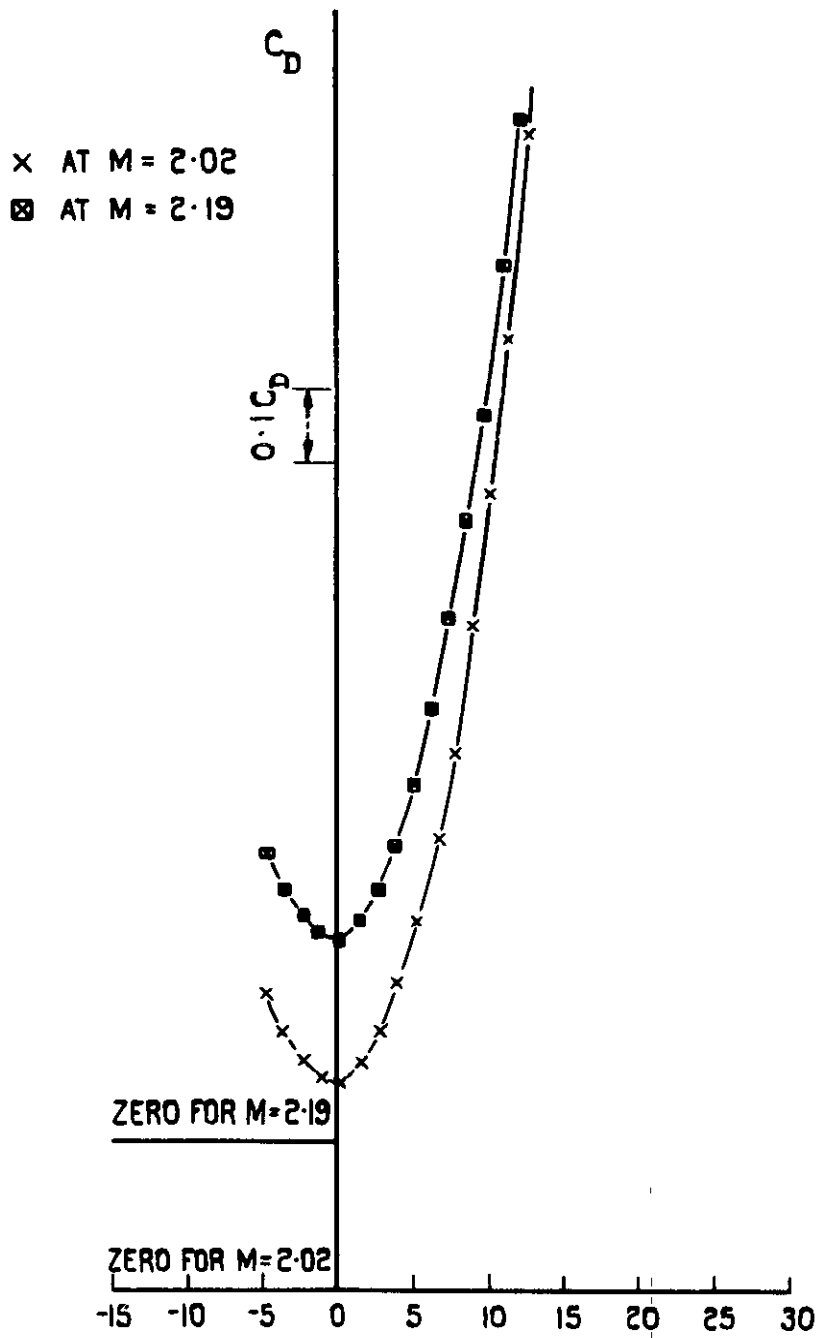
FIG.24. DRAG OF WINGED DUCT AT M=2·19 AND M=2·02.
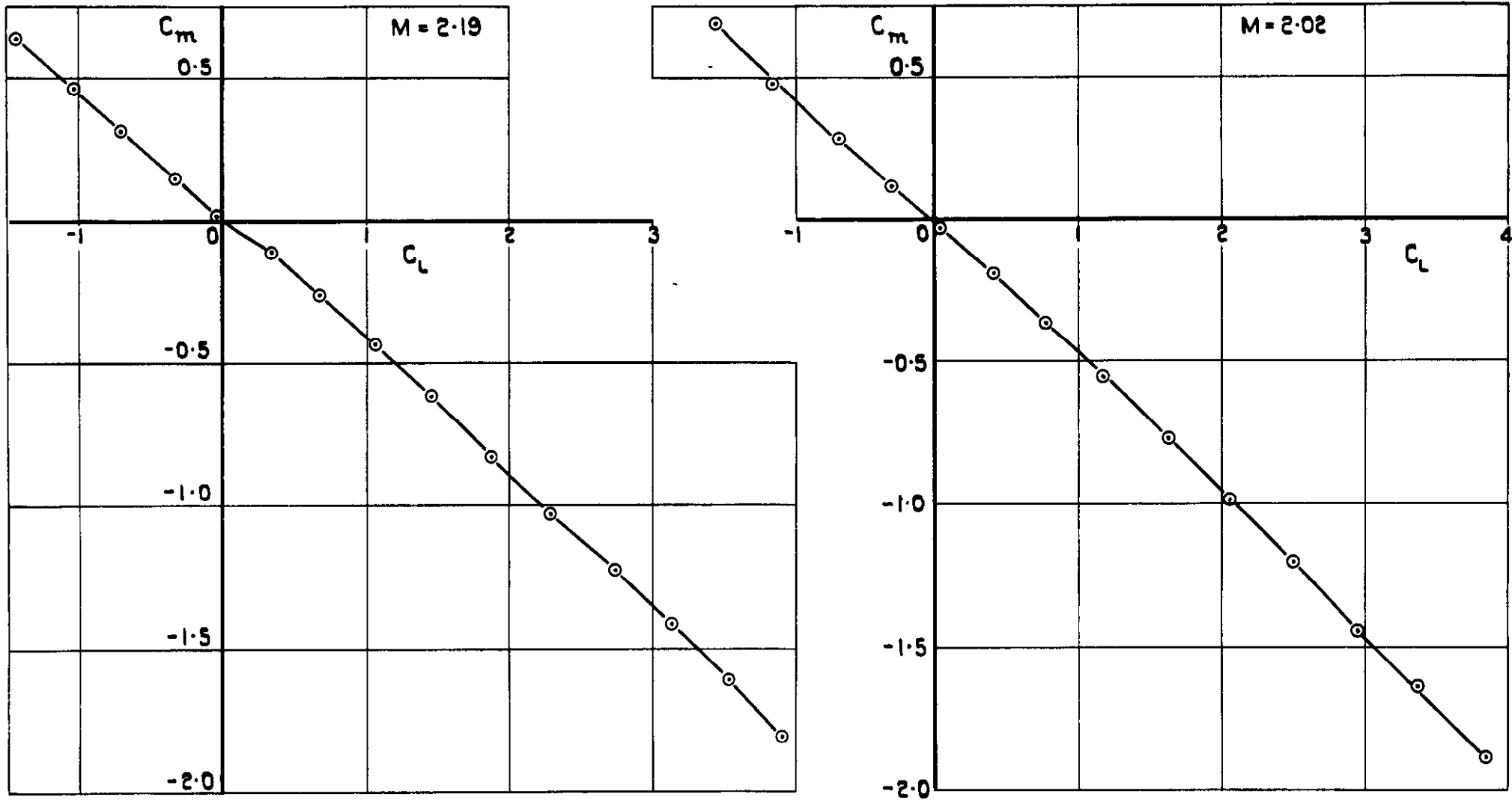
FIG. 25. $C_m \sim C_L$ FOR WINGED DUCTS.
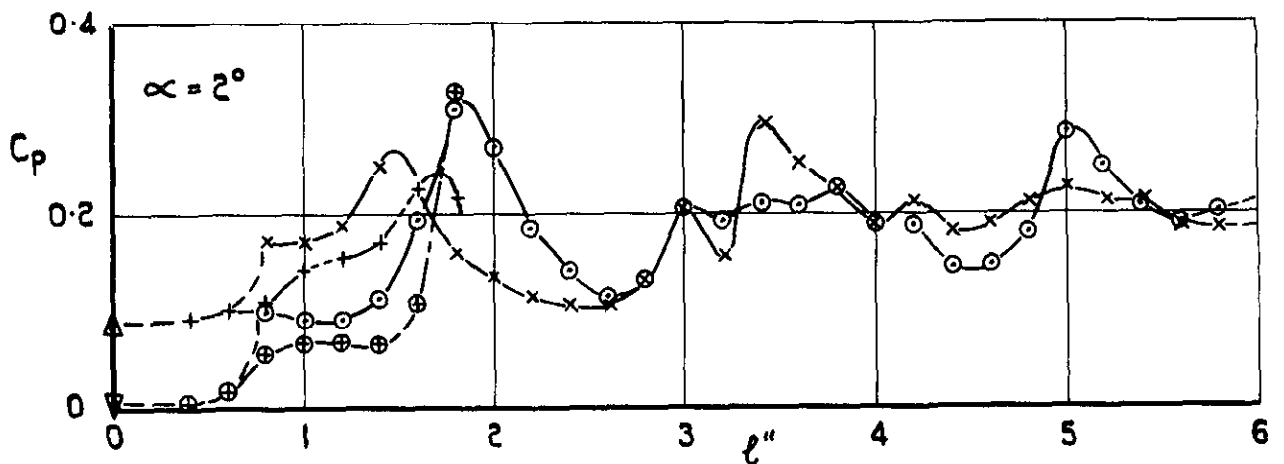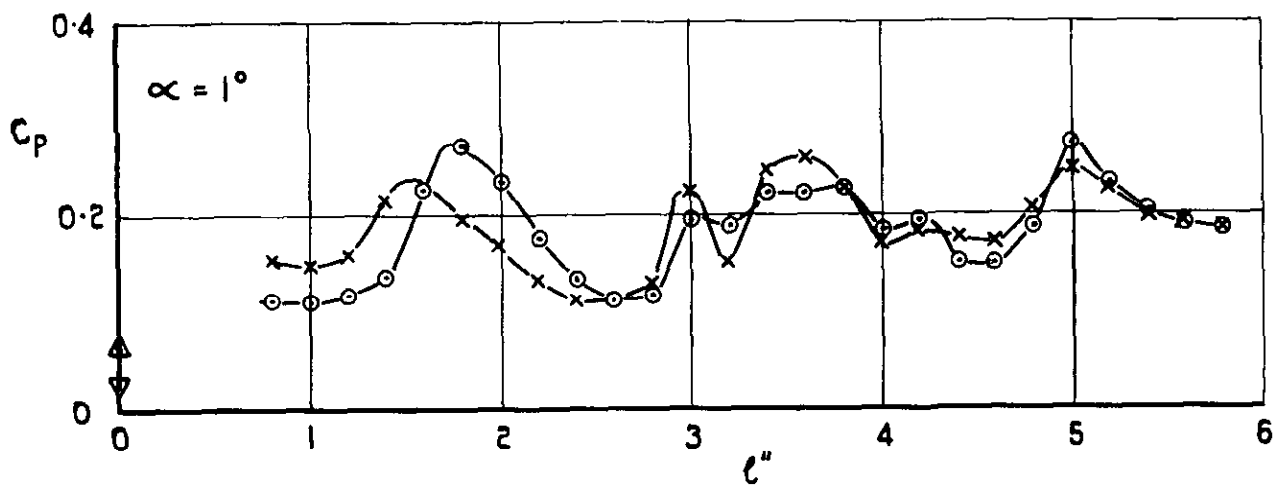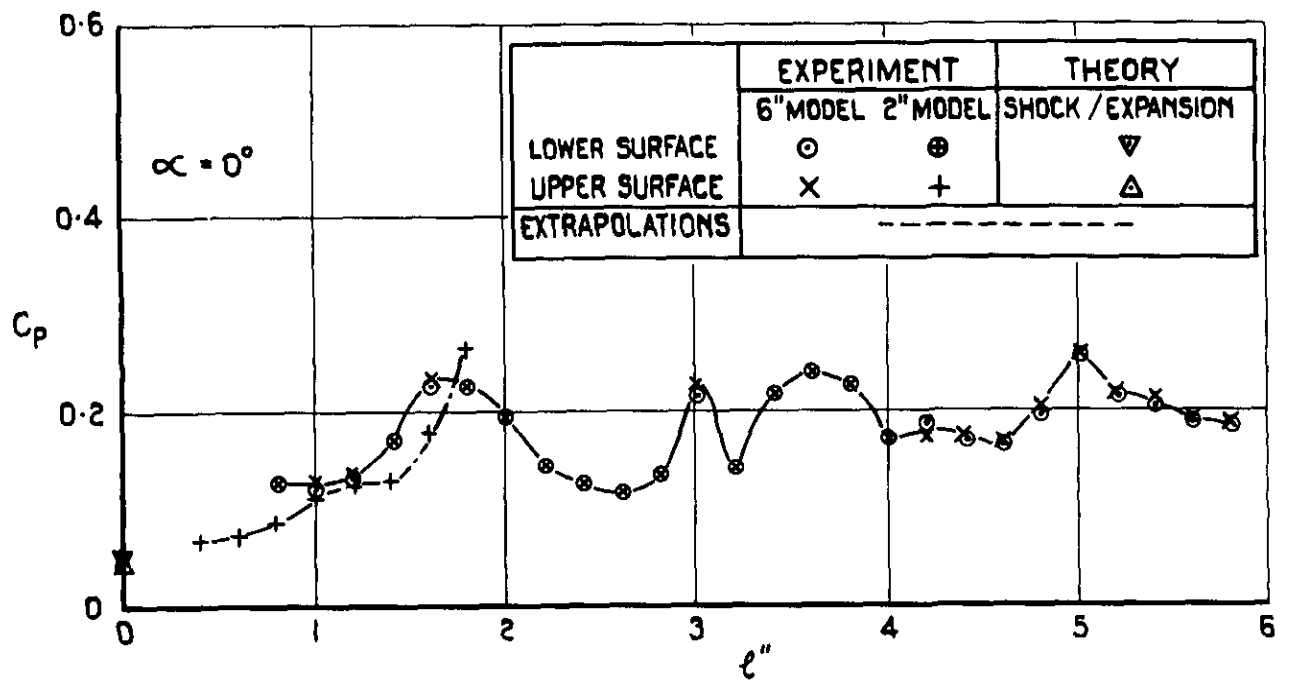
FIG 26. INTERNAL PRESSURE ON THE ₵ OF RECTANGULAR DUCTS,
$h/l = 0.75$, M=2.19.
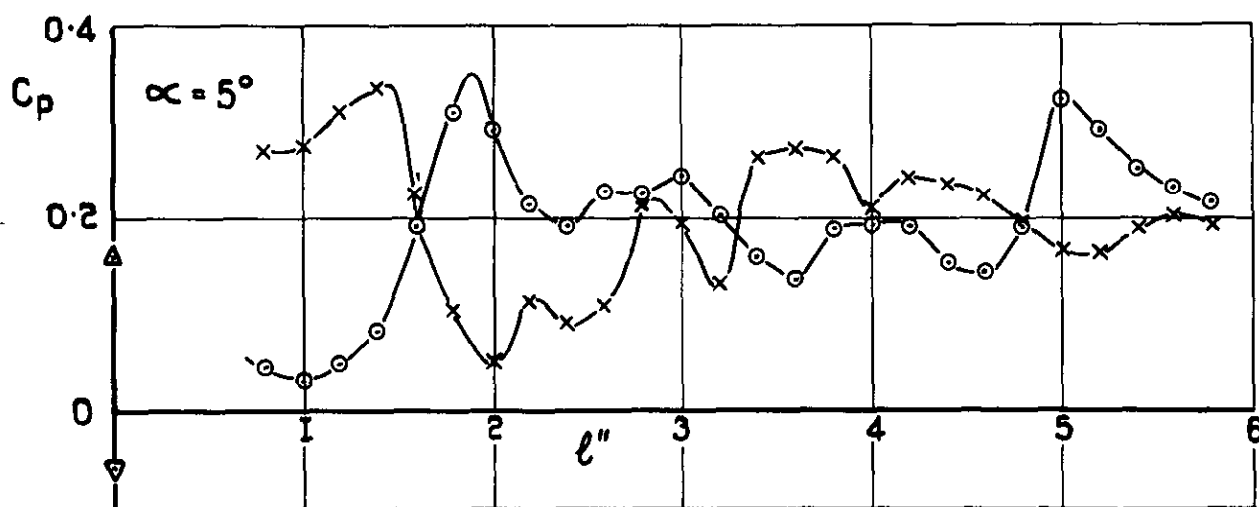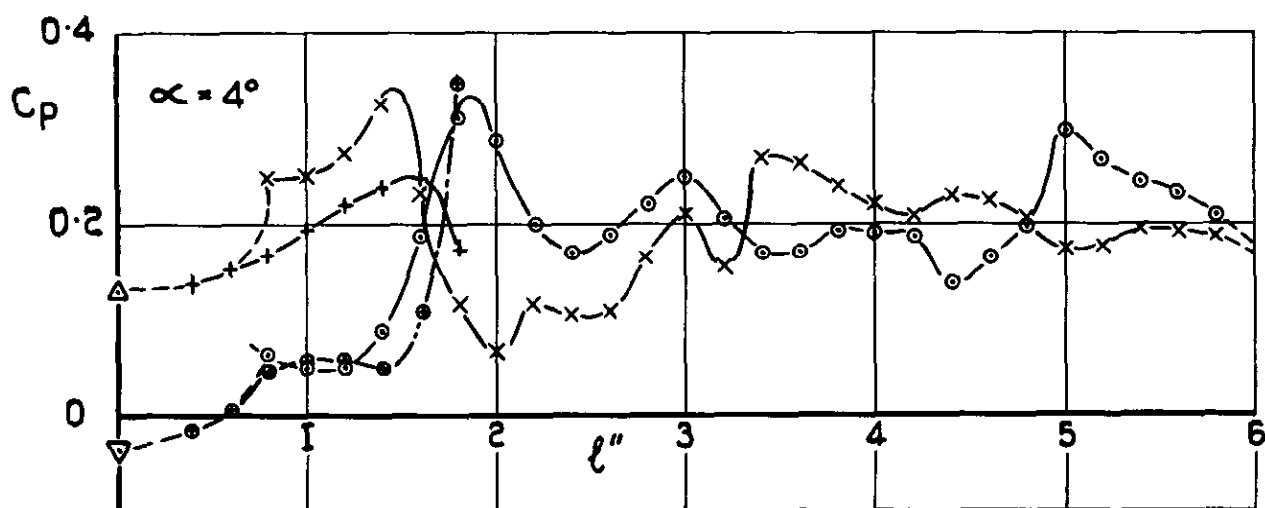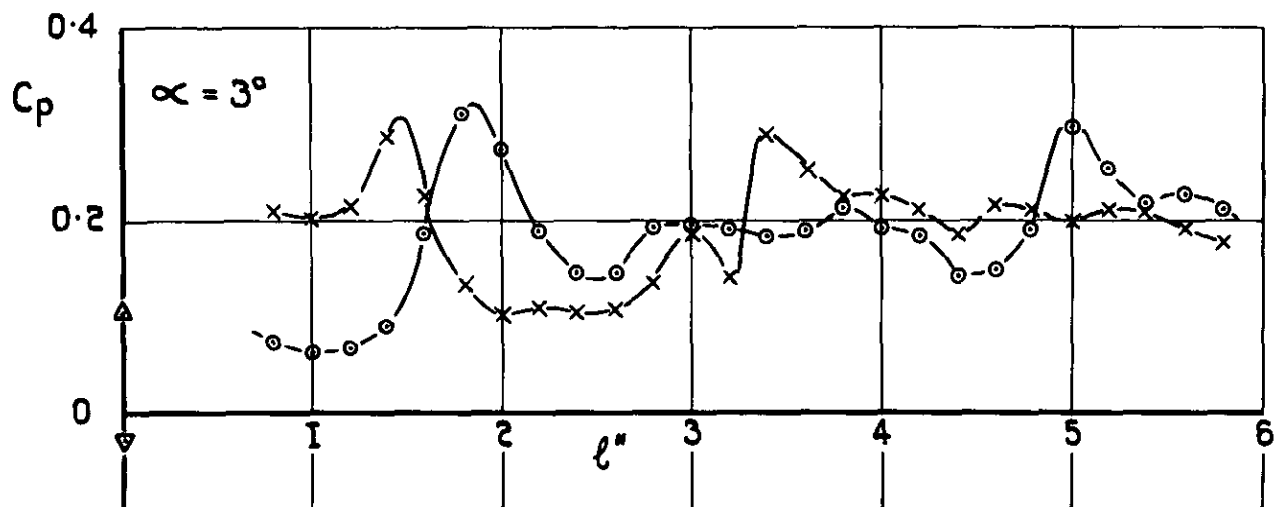
FIG.26.(CONTD) INTERNAL PRESSURE ON THE ℄ OF
RECTANGULAR DUCTS, h/l = 0·75, M=2·19
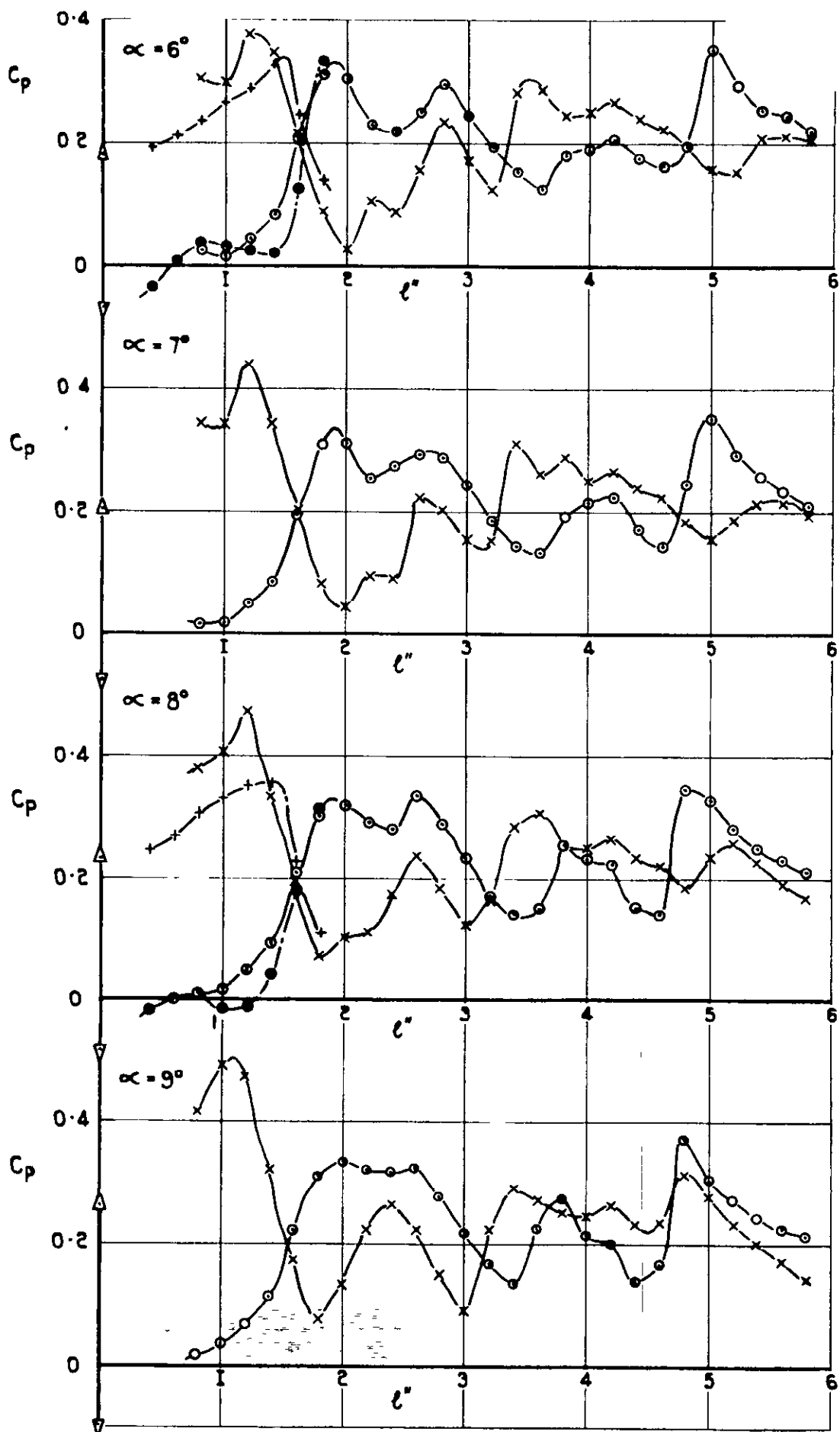
FIG. 26.(CONT'D) INTERNAL PRESSURE ON THE ℄ OF RECTANGULAR DUCTS, h/t = 0·75, M = 2·19.
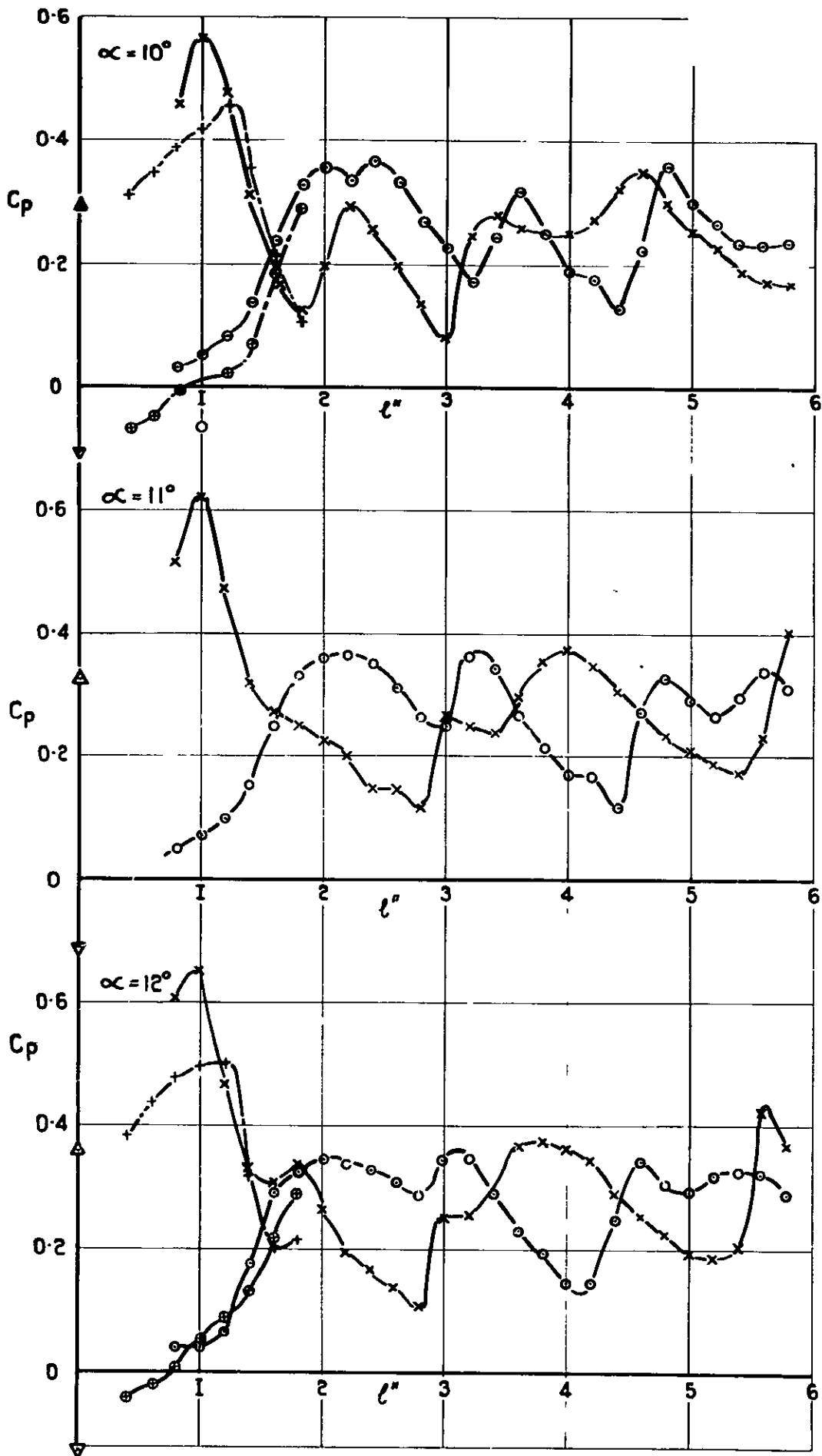
FIG. 26. (CONCL'D.) INTERNAL PRESSURE ON THE ₵ OF
RECTANGULAR DUCTS, h/l = 0·75, M = 2·19.
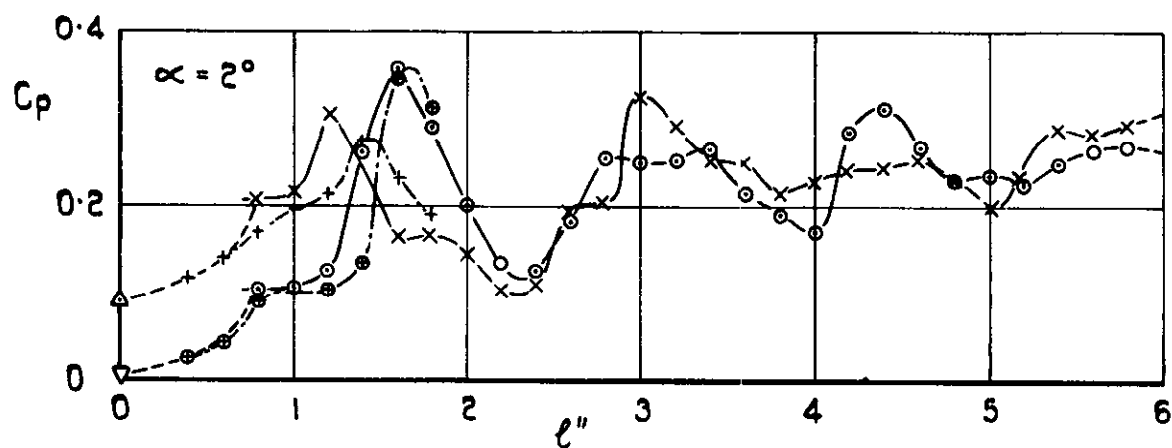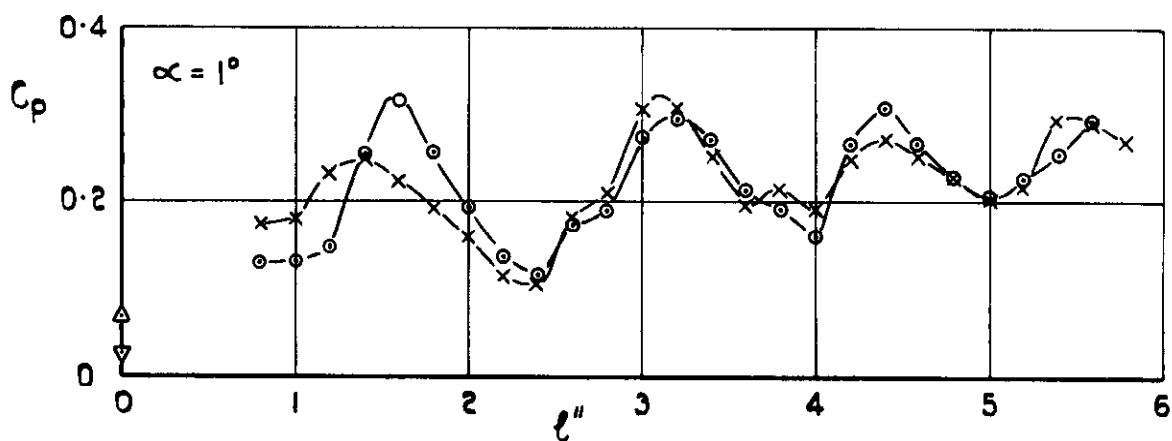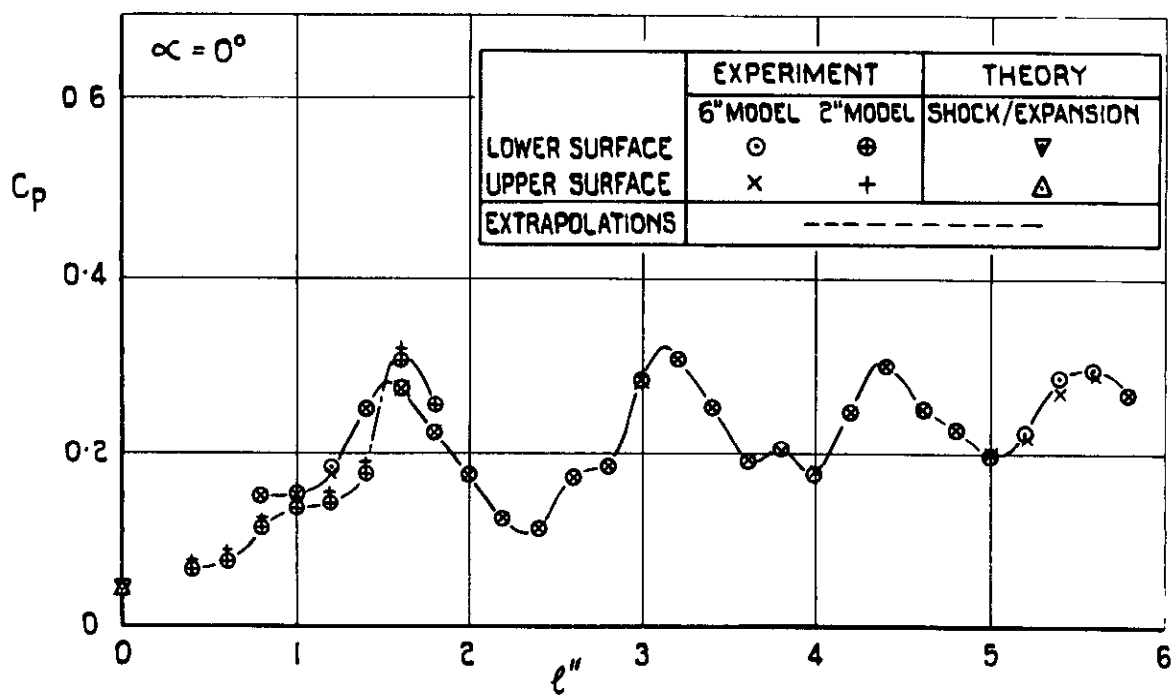
FIG.27 INTERNAL PRESSURE ON THE ₵ OF RECTANGULAR DUCTS, h/ℓ = O·75, M=2 02.
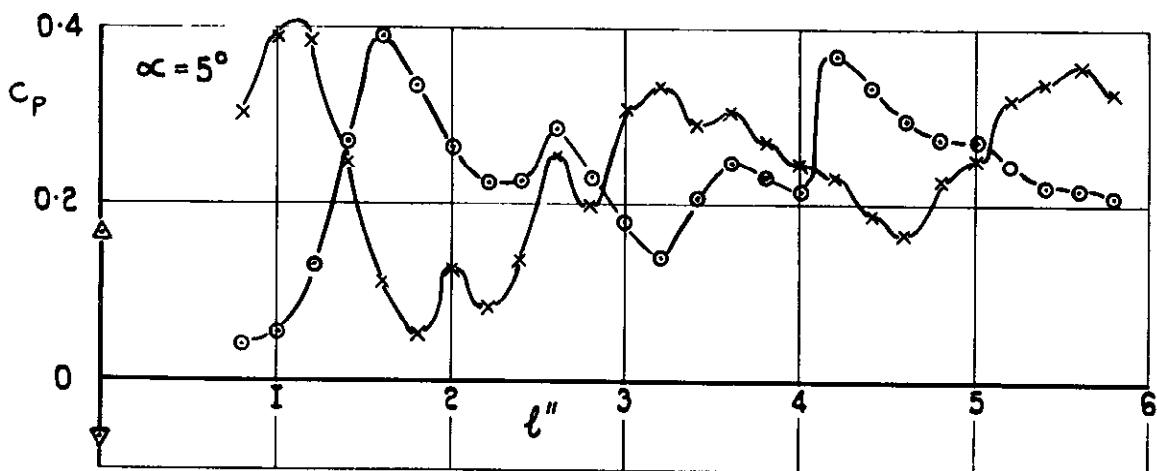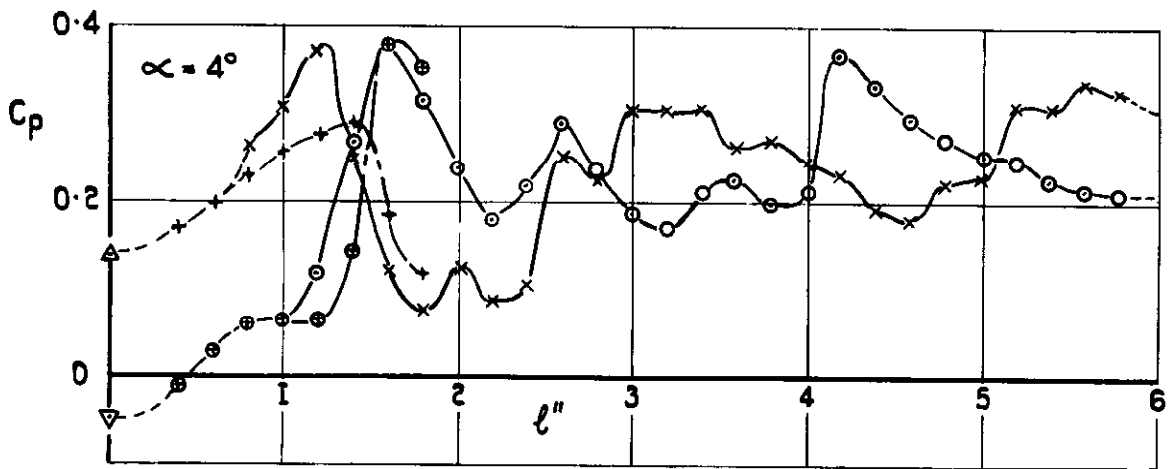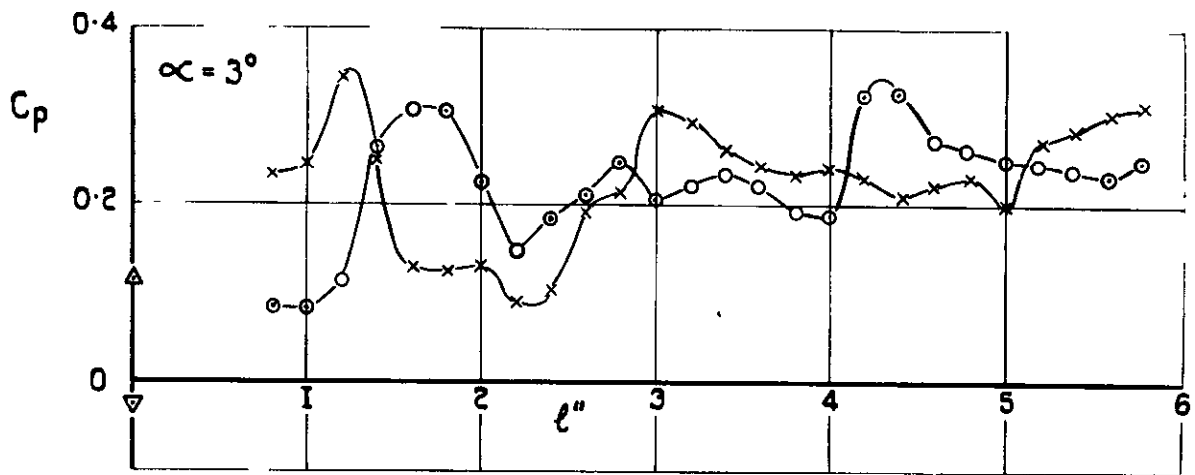
FIG. 27 (CONT'D) INTERNAL PRESSURE ON THE ₵ OF RECTANGULAR DUCTS, $h/\ell = 0.75$, M = 2.02
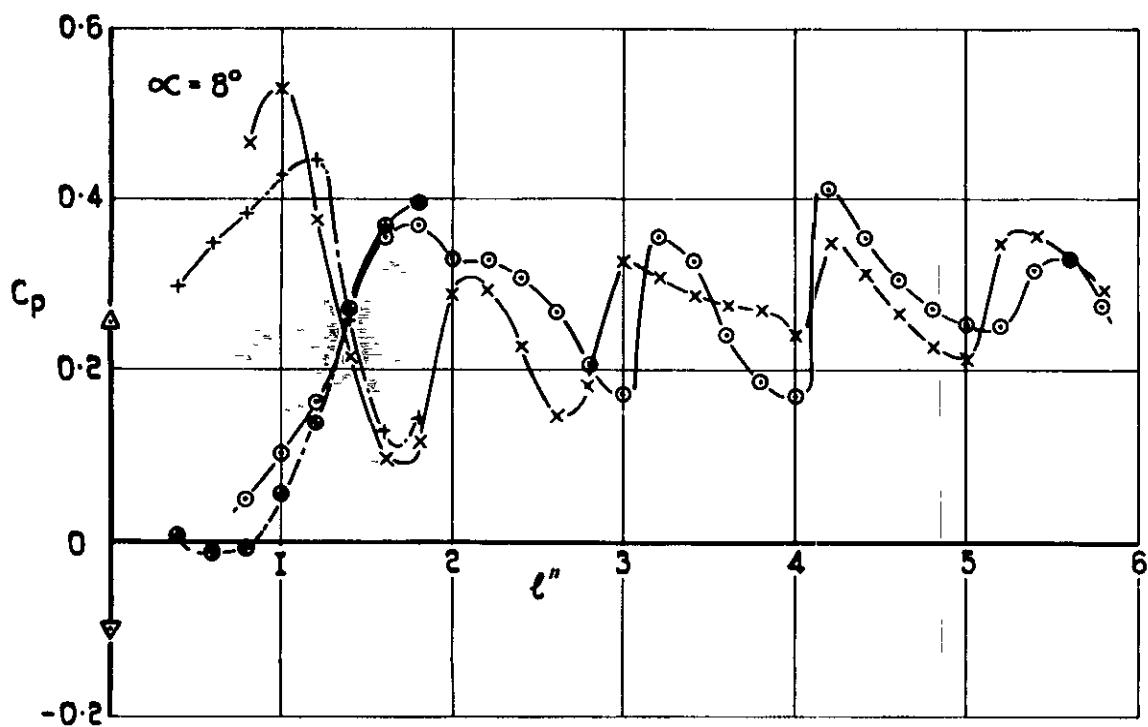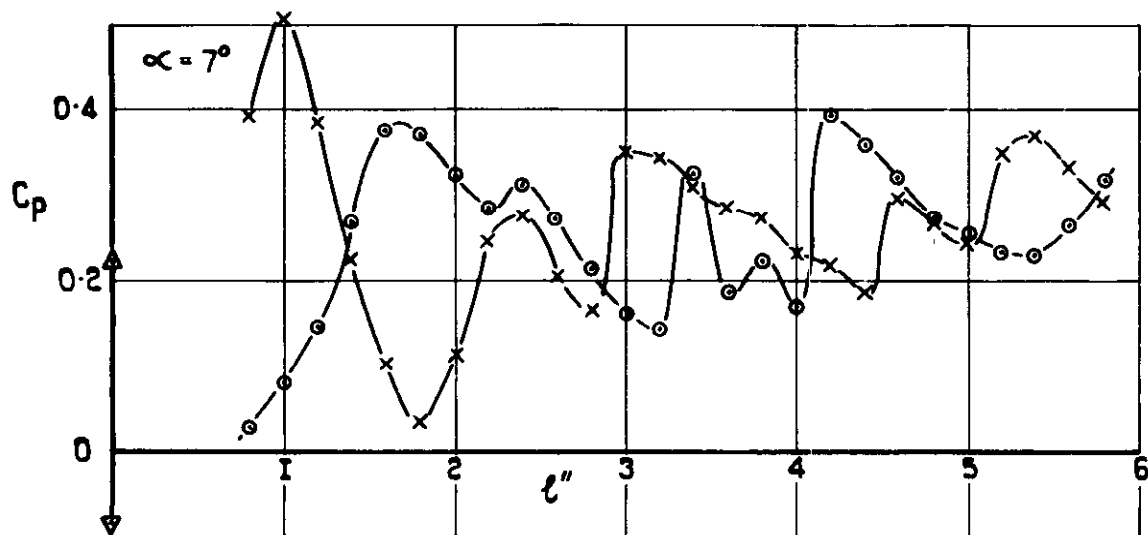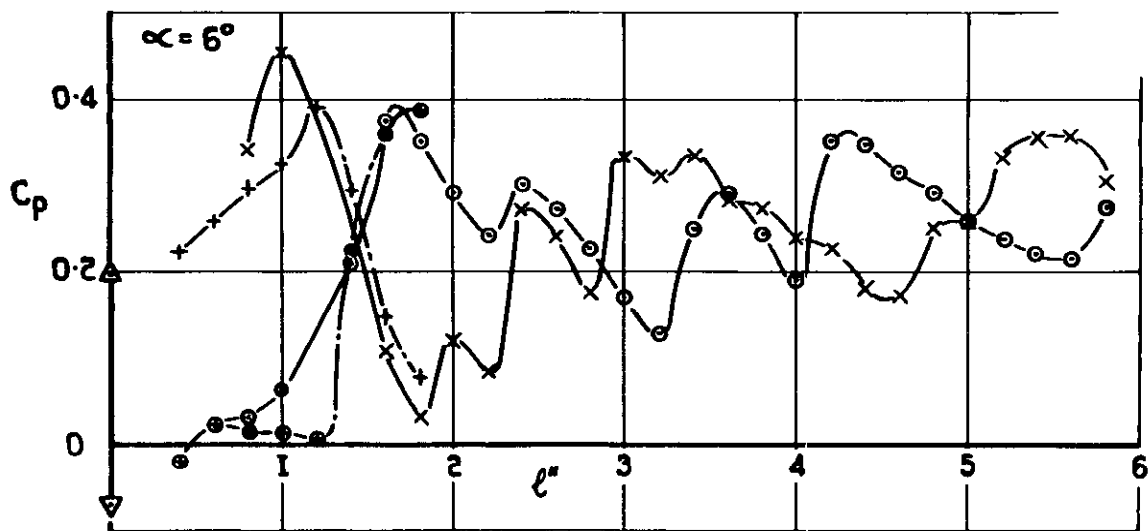
FIG.27(CONTD)INTERNAL PRESSURE ON THE ₵ OF RECTANGULAR DUCTS, $h/\ell = 0.75, M = 2.02$
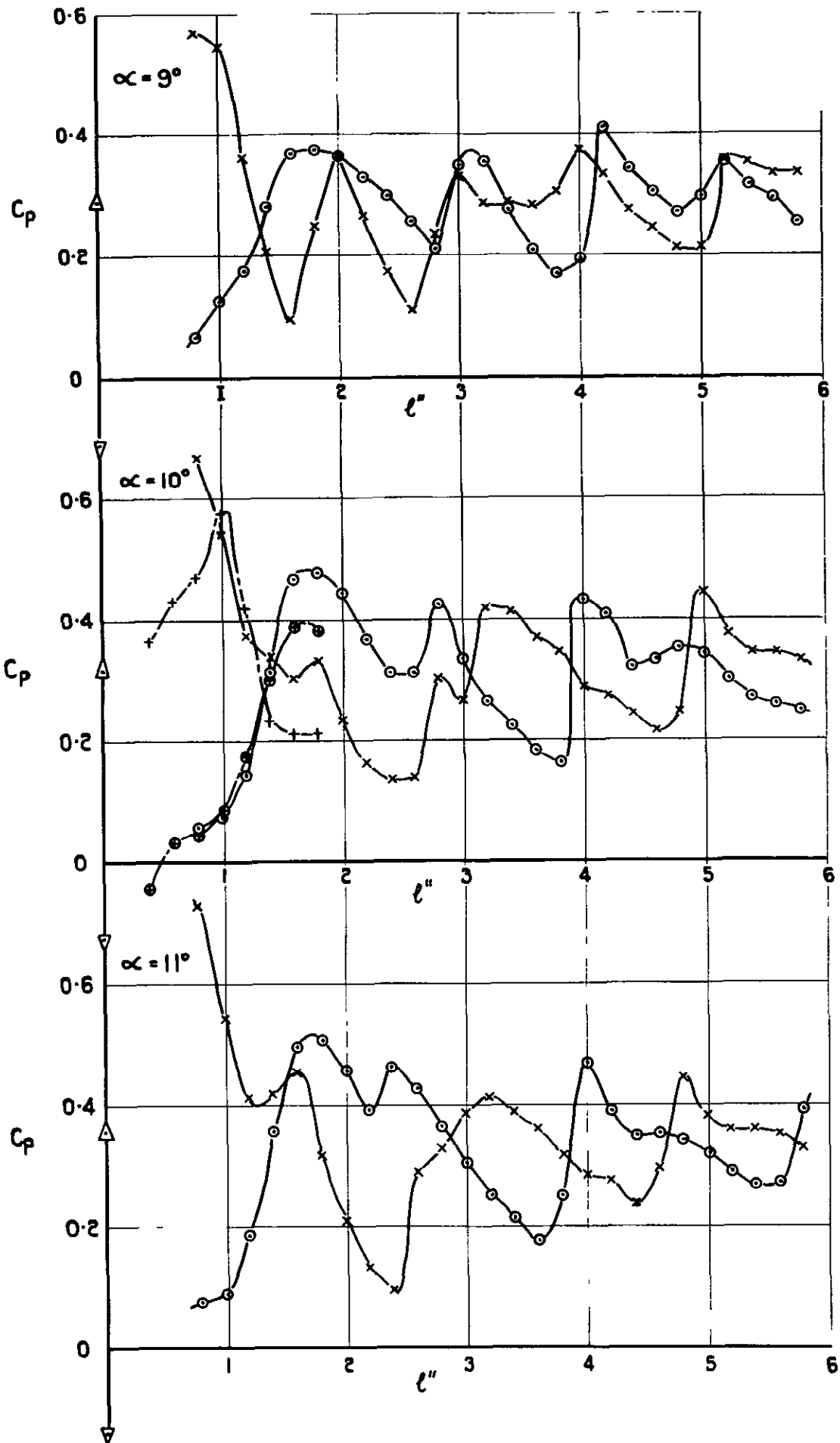
FIG. 27. (CONCL'D) INTERNAL PRESSURE ON THE $\mathcal{C}$ OF RECTANGULAR DUCTS, $h/\ell = 0.75$, M = 2.02.
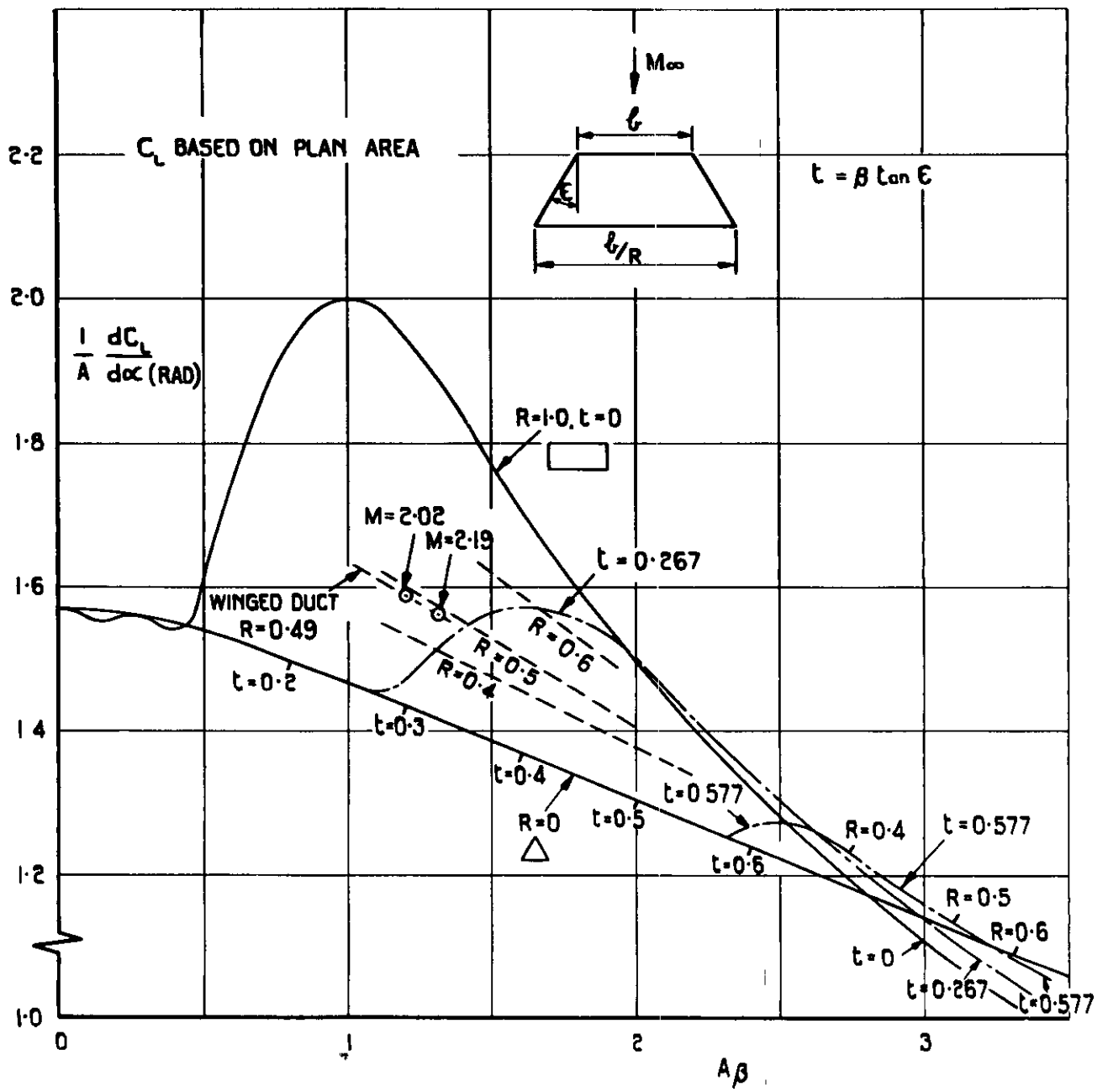
FIG.28. LINEAR THEORY LIFT OF TRAPEZOIDAL WINGS.
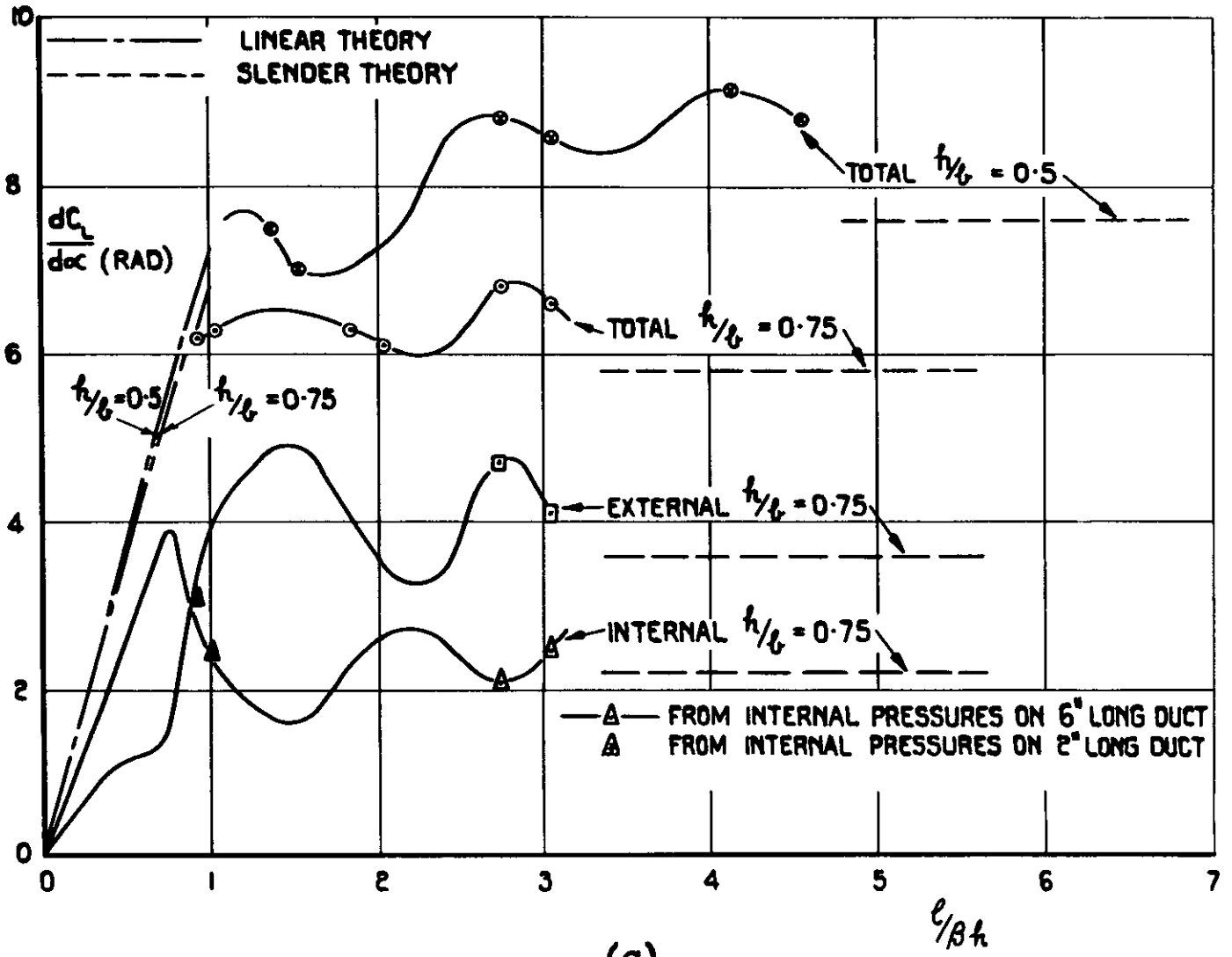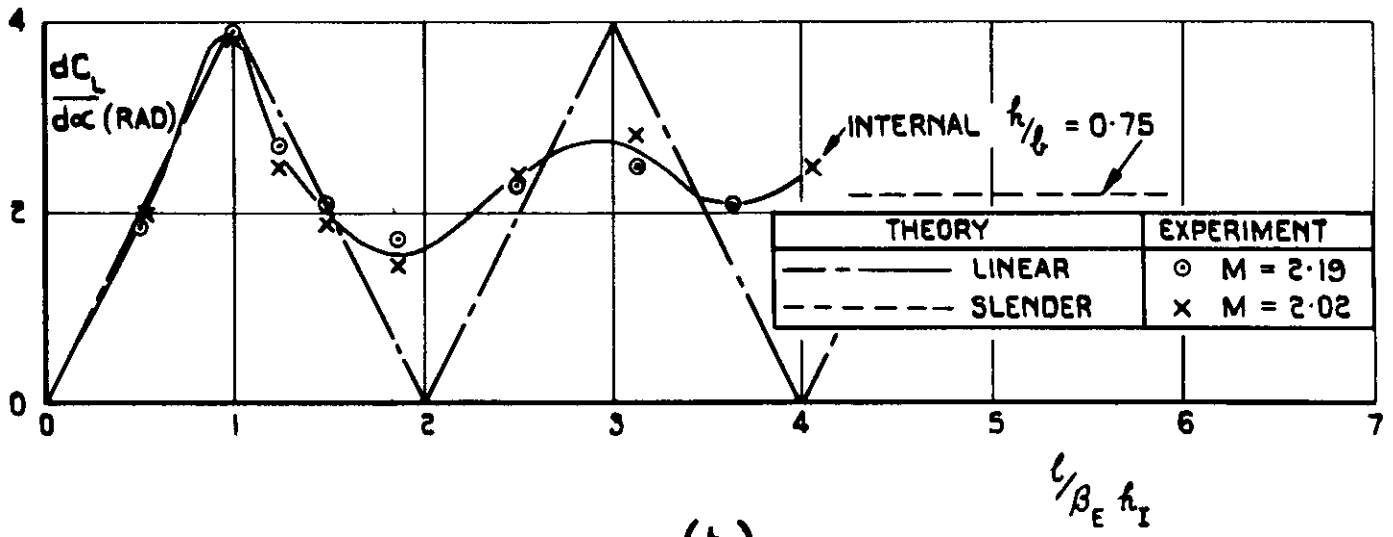
FIG. 29. INITIAL LIFT CURVE SLOPE OF RECTANGULAR DUCTS.
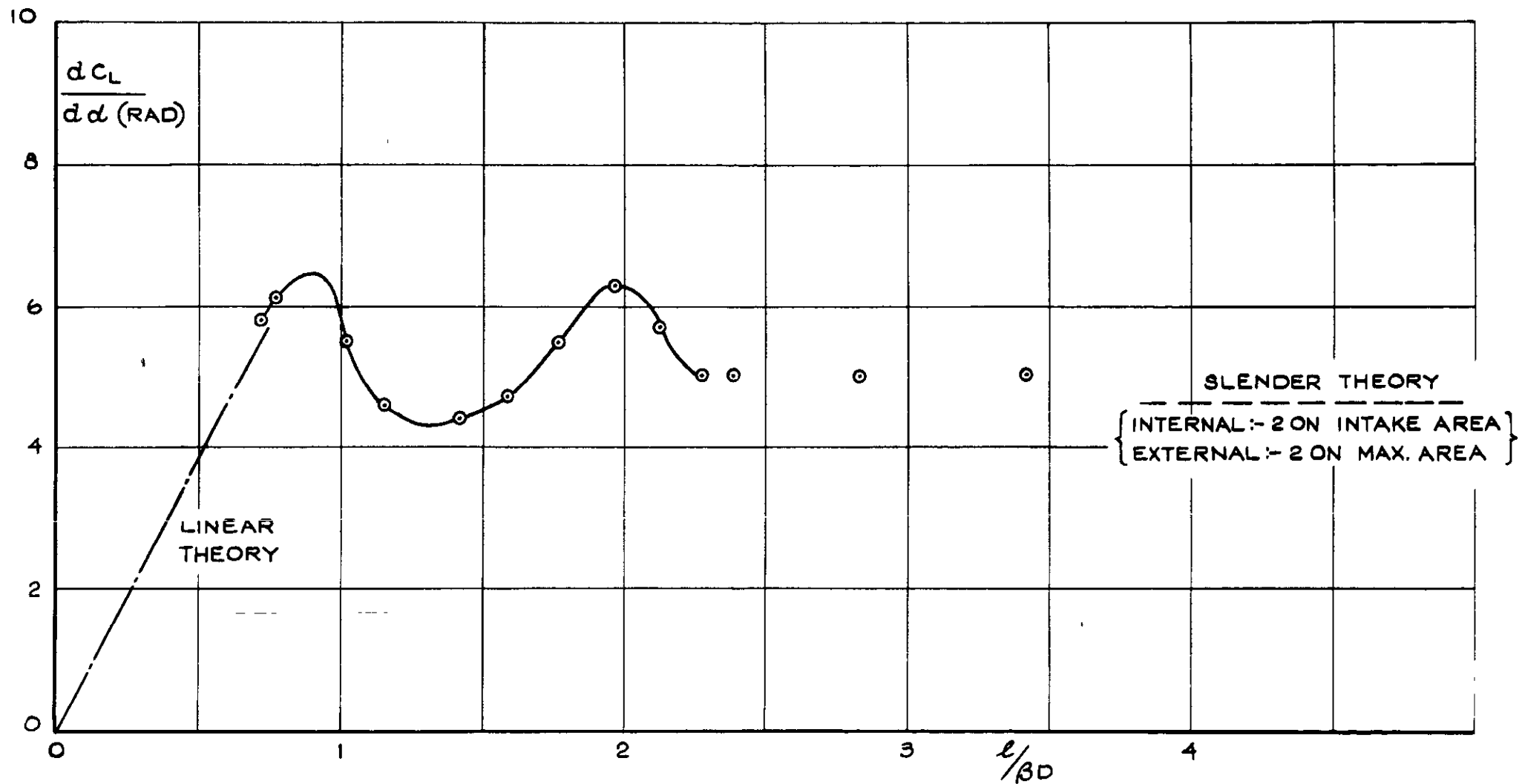
FIG. 30. INITIAL LIFT CURVE SLOPE OF CIRCULAR DUCTS.
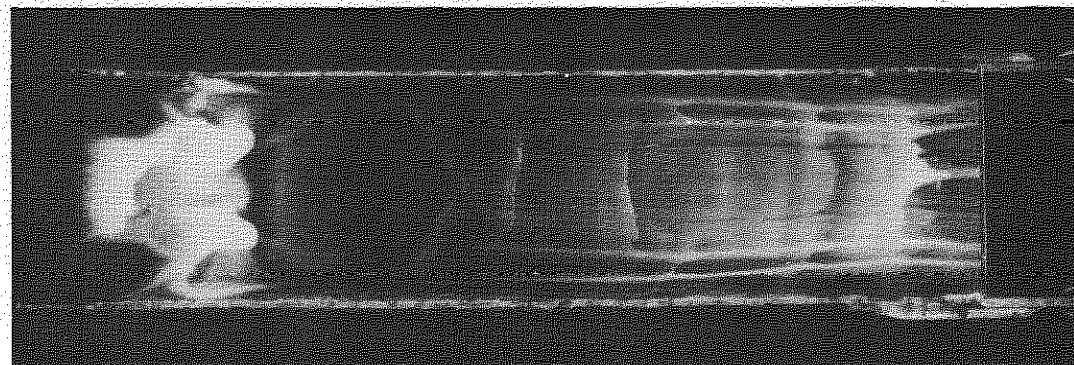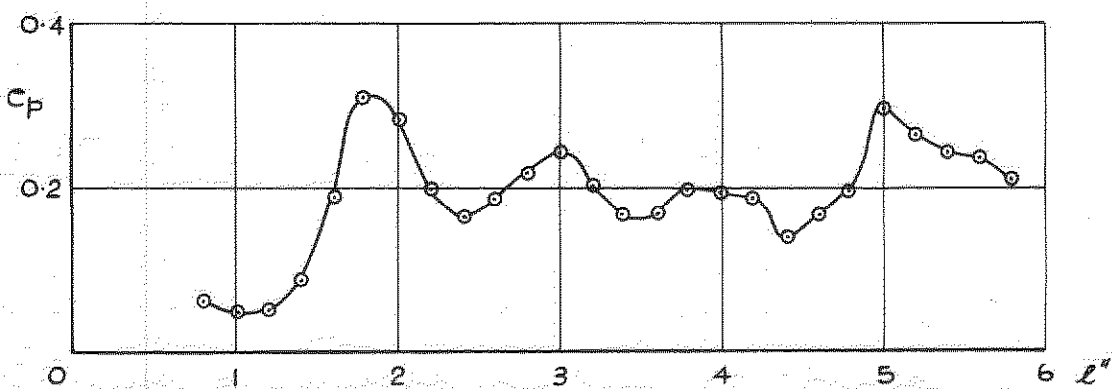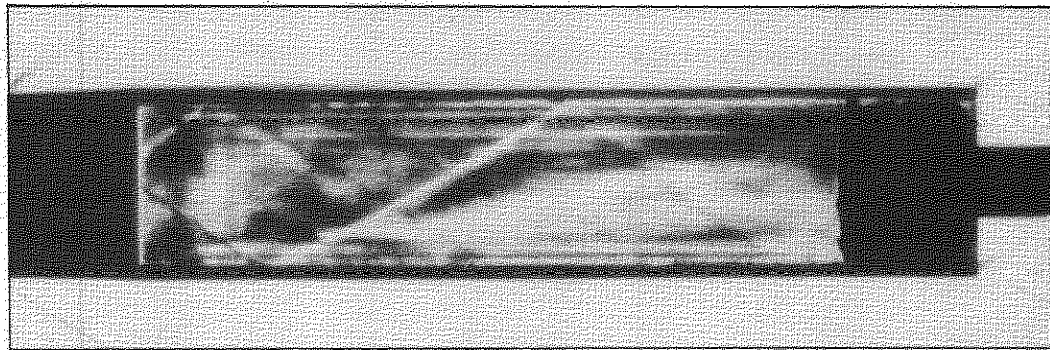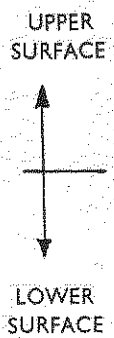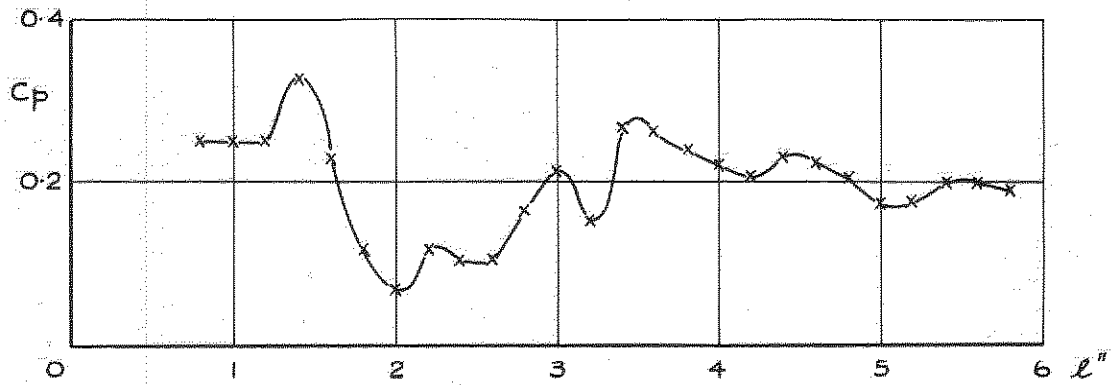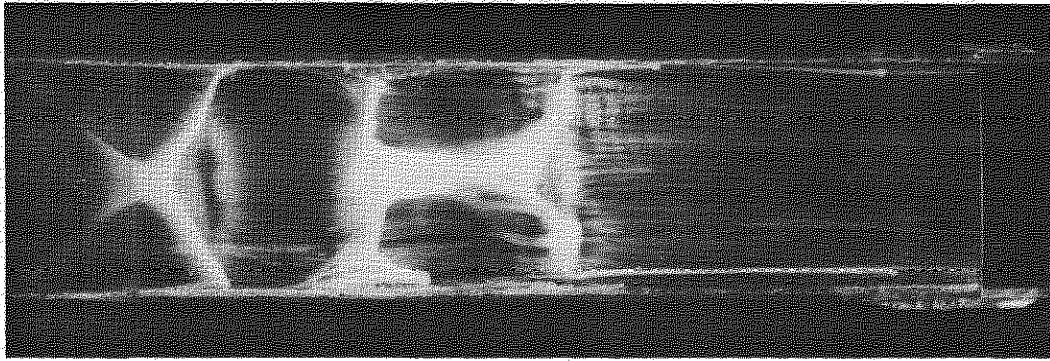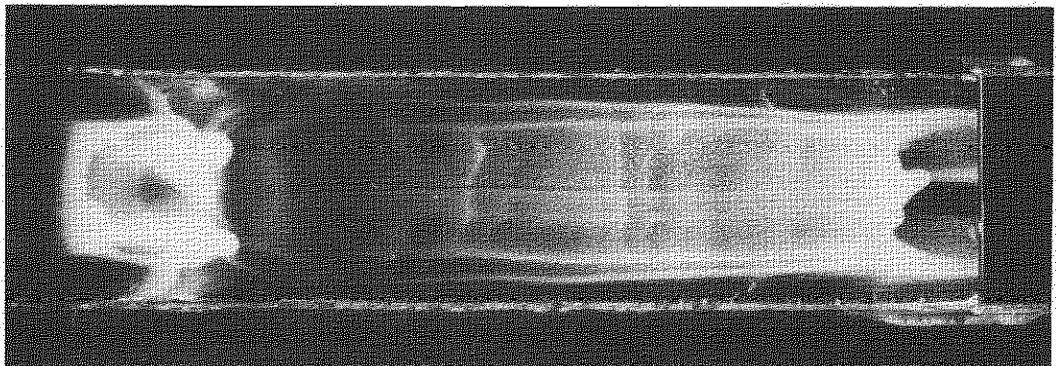
FIG.37 Cont'd. INTERNAL FLOW AT $\alpha = 4°$; M = 2.19, h/h = 0.75
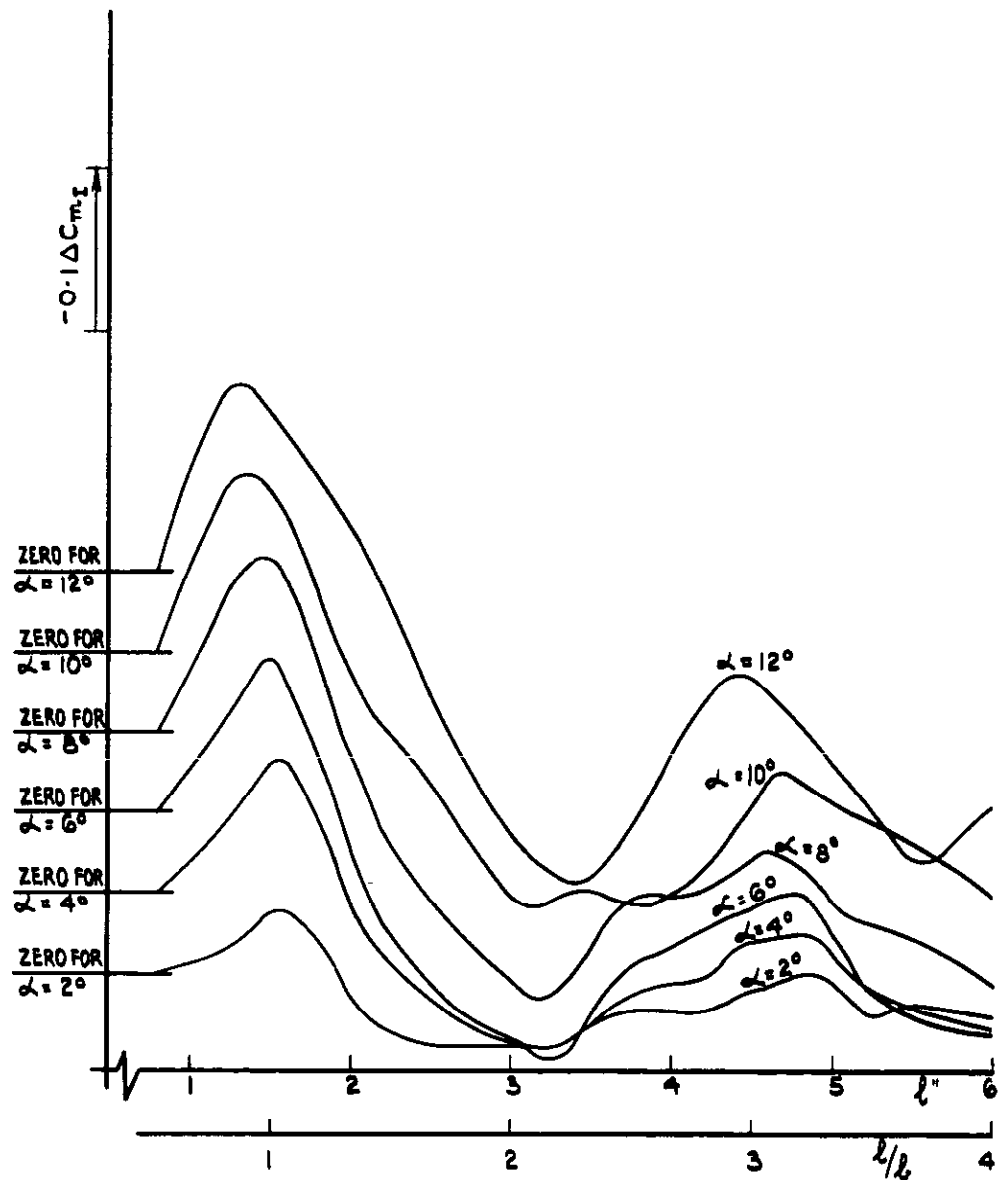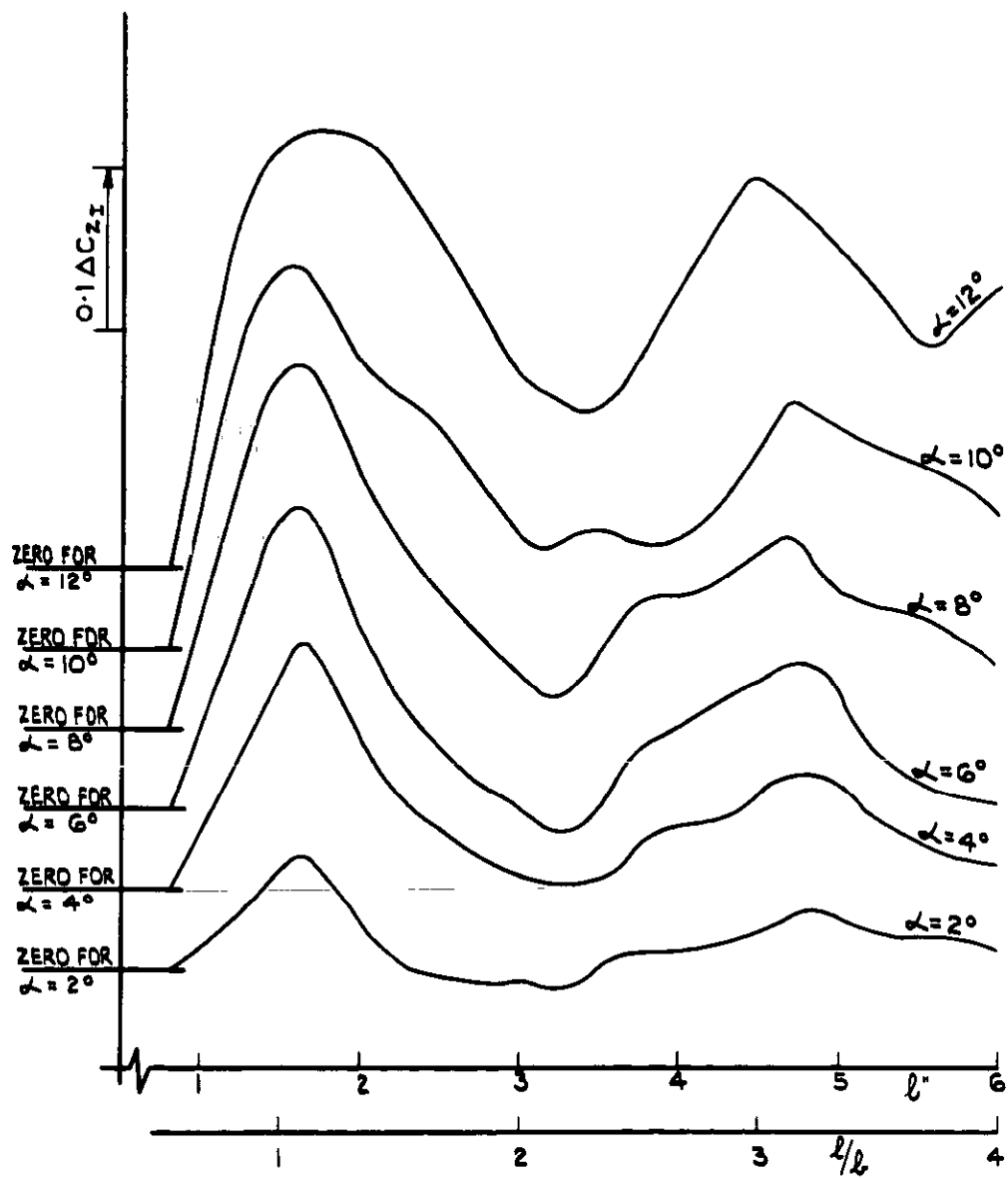
FIG. 32. INTERNAL LIFT & PITCHING MOMENT INCREMENT WITH DUCT LENGTH
$M = 2.19$, $h/\ell = 0.75$
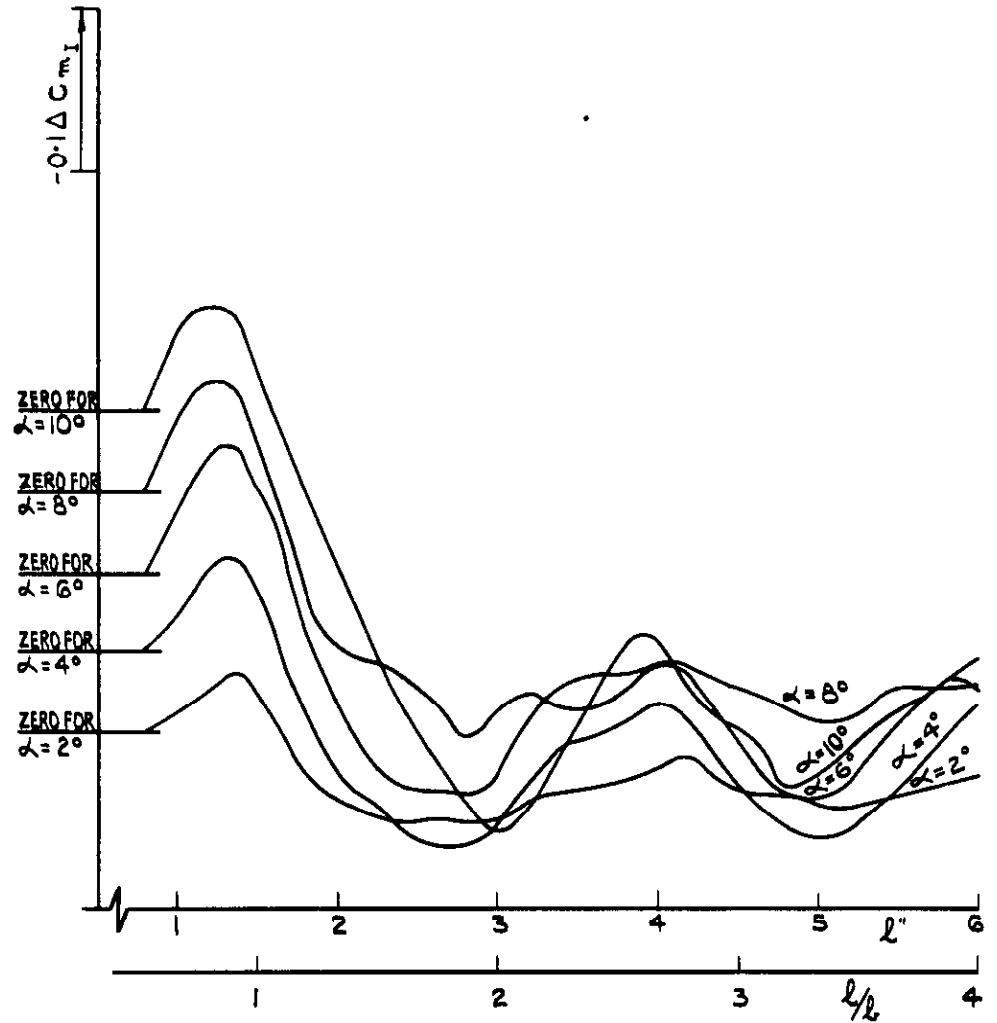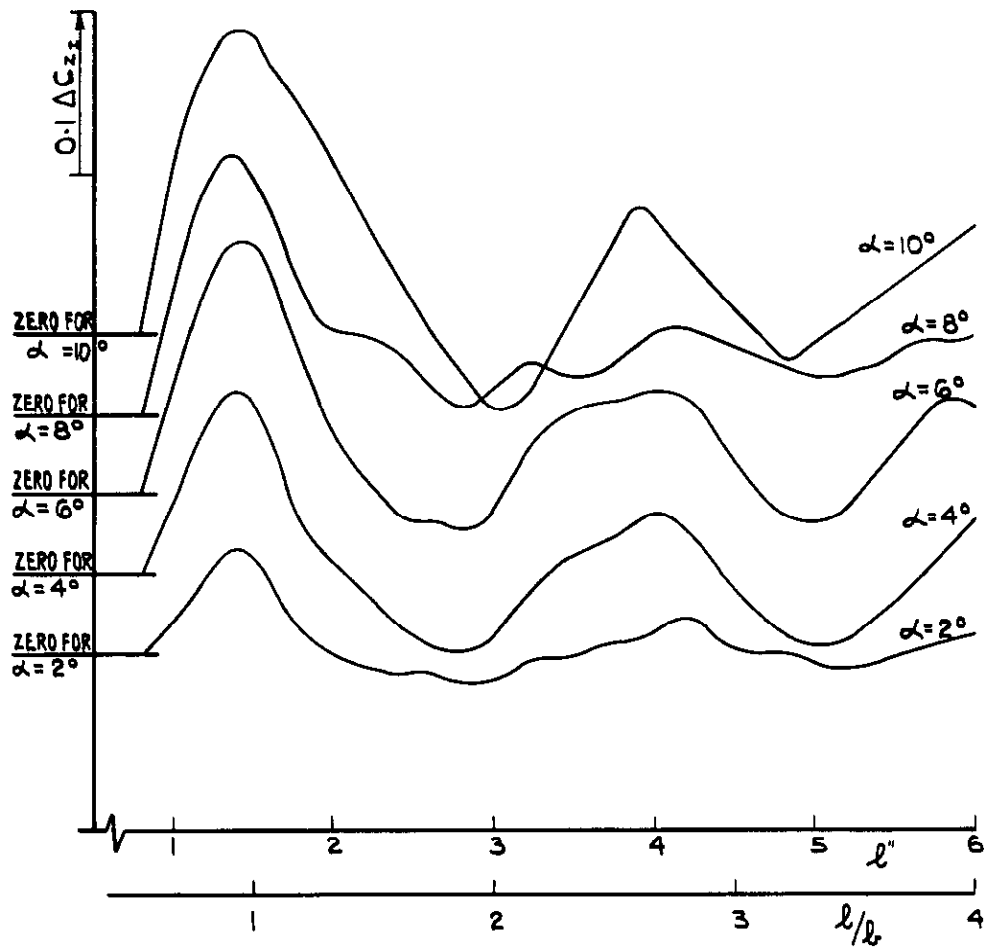
FIG. 33. INTERNAL LIFT & PITCHING MOMENT INCREMENT WITH DUCT LENGTH.

$M = 2 \cdot 02$ $\frac{h}{l} = 0.75$
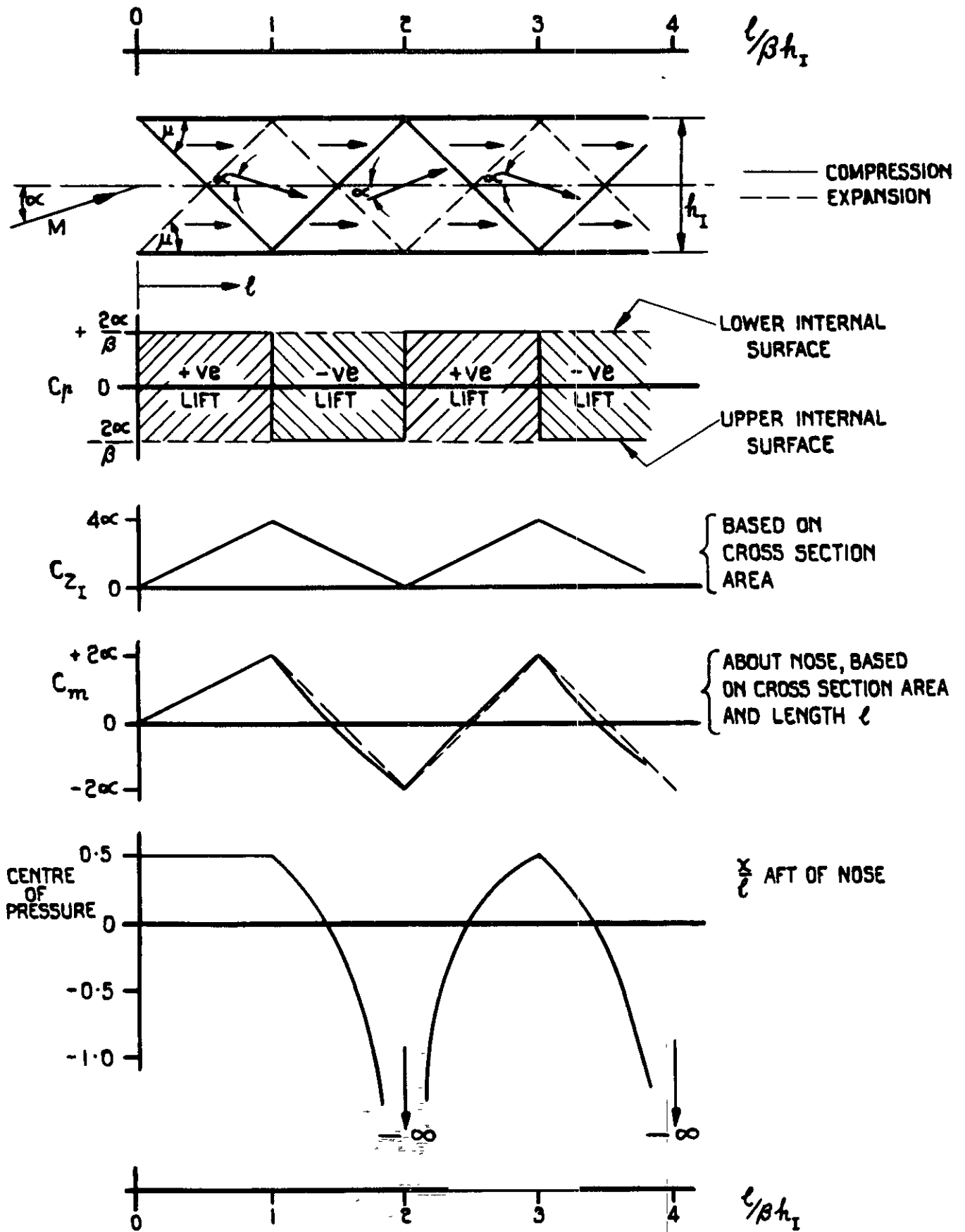
FIG. 34.   SIMPLIFIED LINEAR THEORY FOR THE INTERNAL FLOW

OF RECTANGULAR DUCTS.
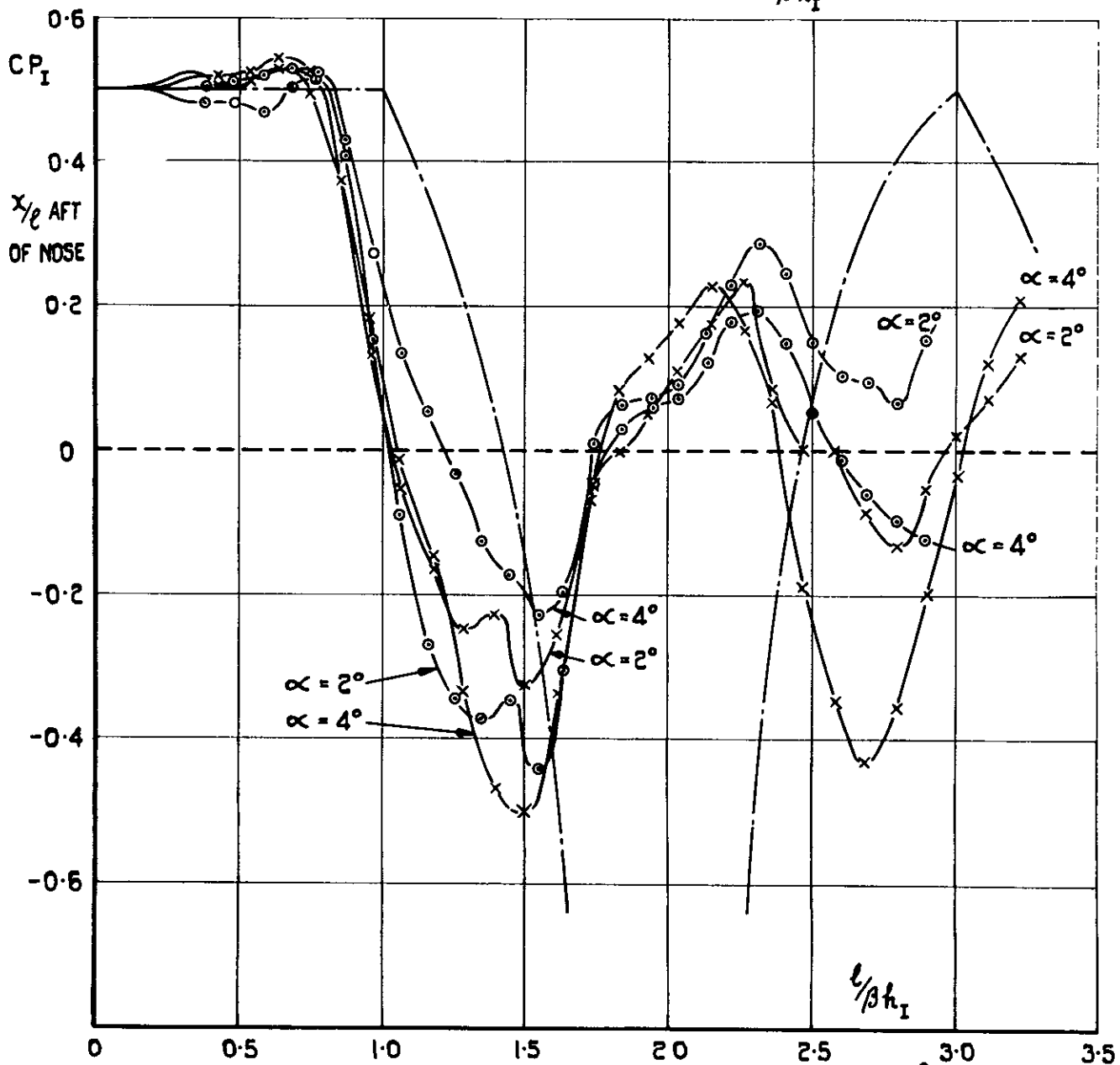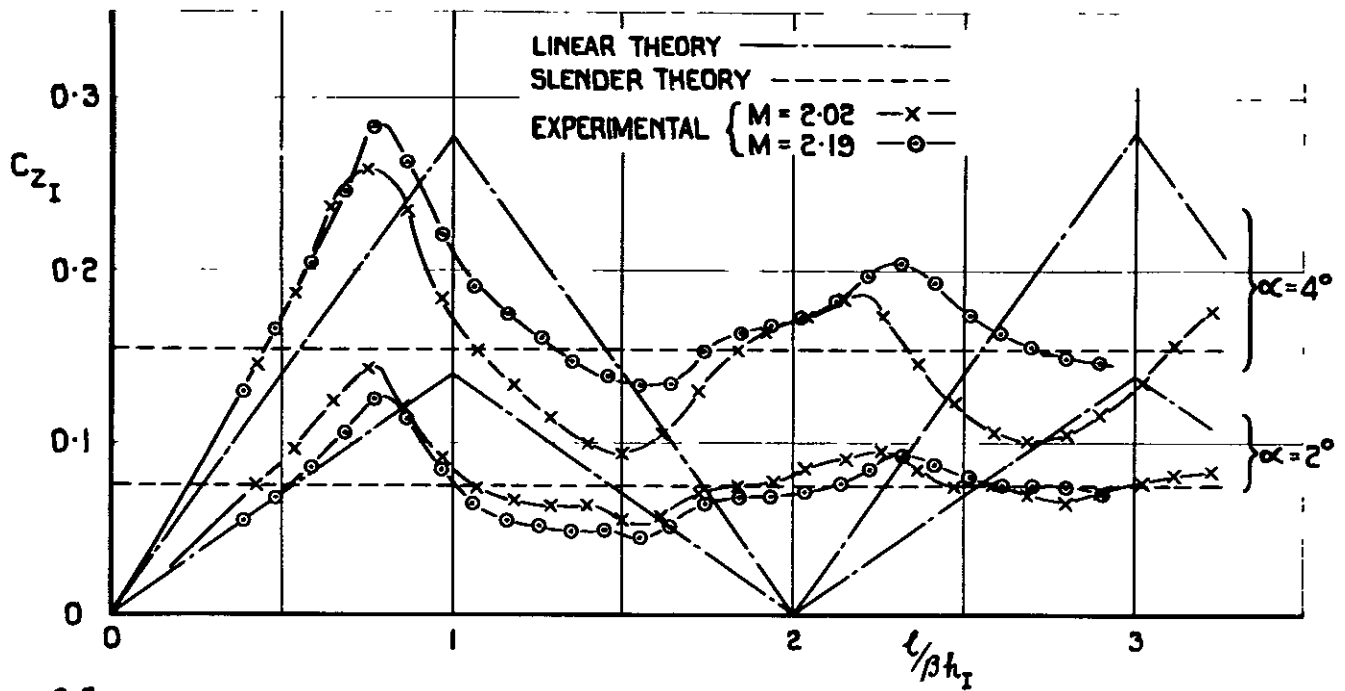
FIG 35   INTERNAL LIFT & CENTRE OF PRESSURE OF RECTANGULAR DUCT, $h/\ell = 0.75$.
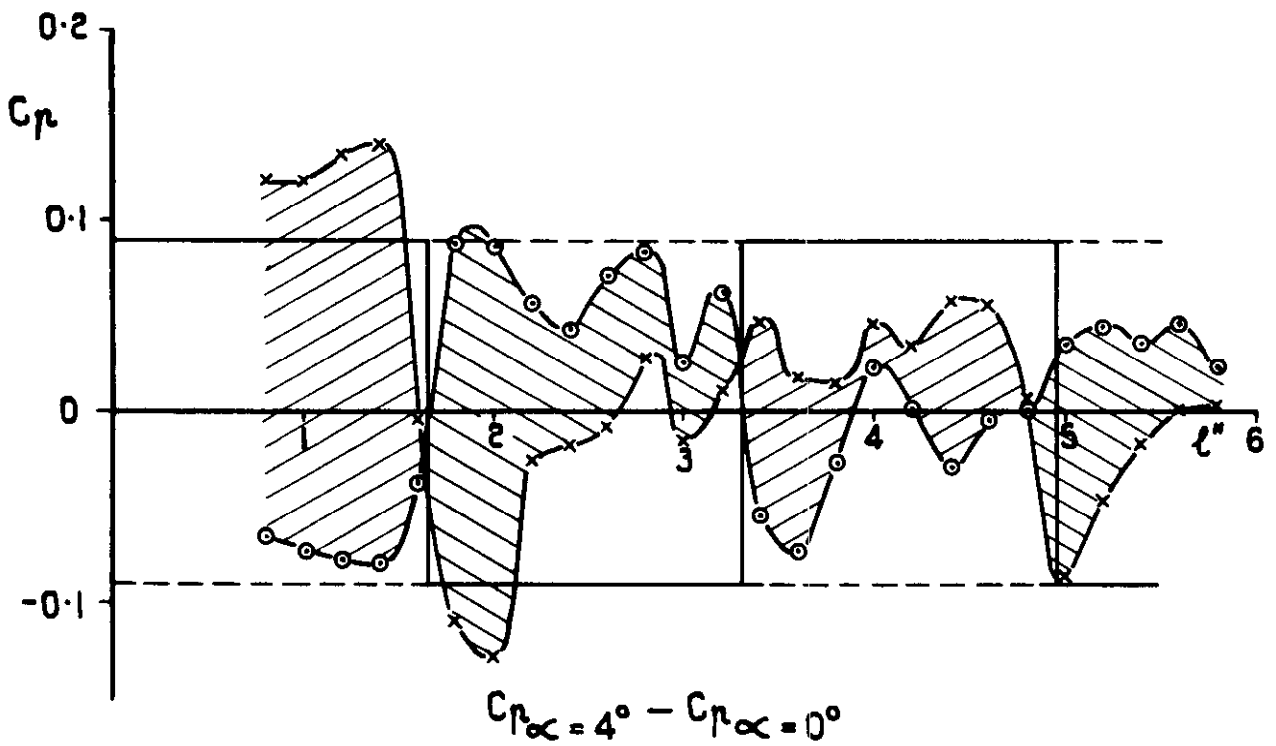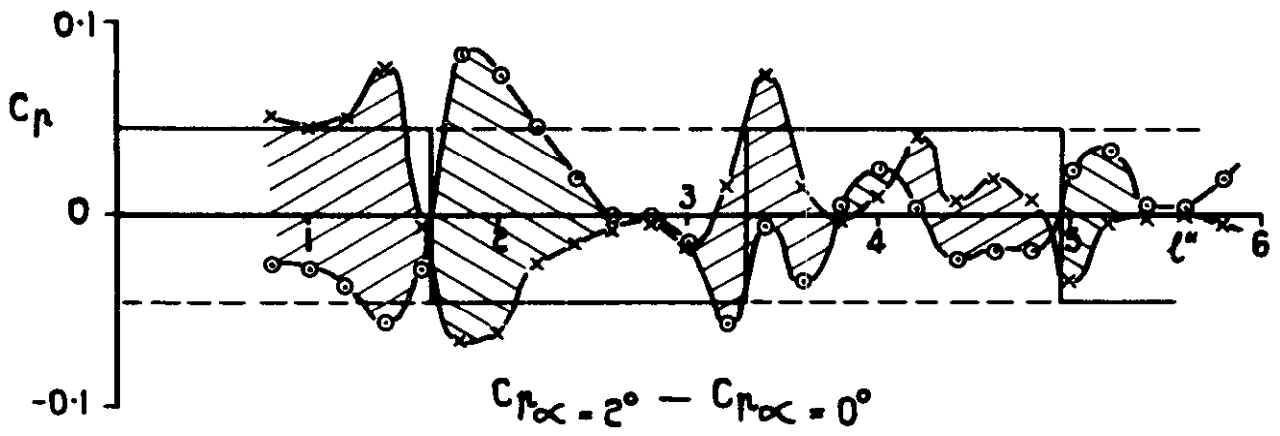
THEORY				
——————— UPPER SURFACE				
— — — — LOWER SURFACE				
$C_p / \alpha°$	ℓ''	h''	M	β
0·0225	1·65	1·06	1·85	1·55
FOR THE VALUE OF 'ℓ' FROM THE EXPERIMENTAL PLOTS OF C_p AND THE MINIMUM INTERNAL HEIGHT OF THE DUCT				

EXPERIMENT	
× UPPER SURFACE	
⊙ LOWER SURFACE	
▨	+ ve LIFT
▨	– ve LIFT

FIG. 36 INCREMENT IN INTERNAL C_p DUE TO INCIDENCE COMPARED WITH LINEAR THEORY AT M=2·19, h/ℓ = 0·75.
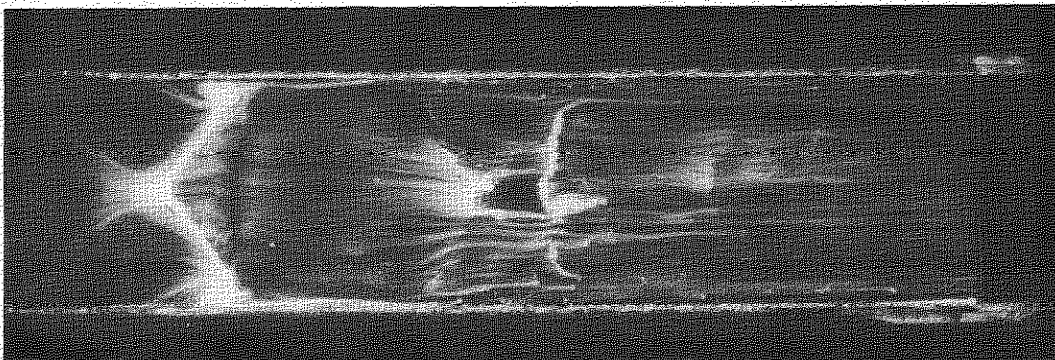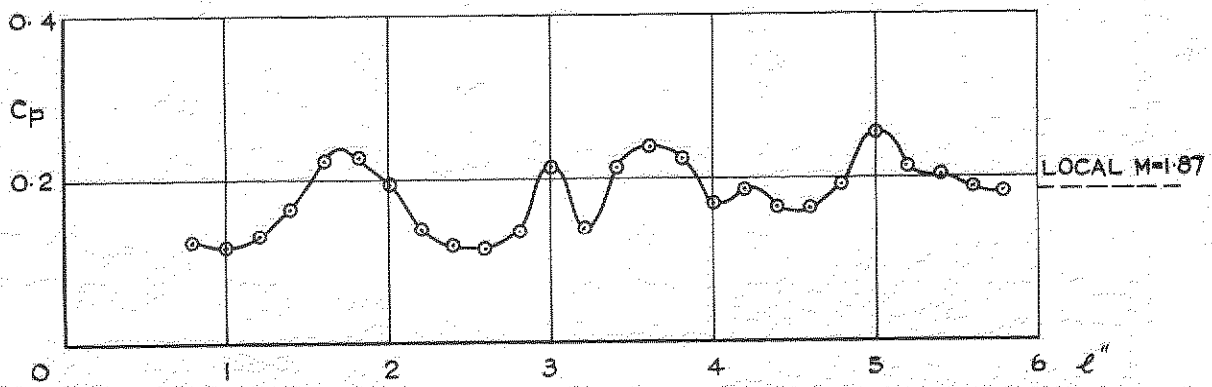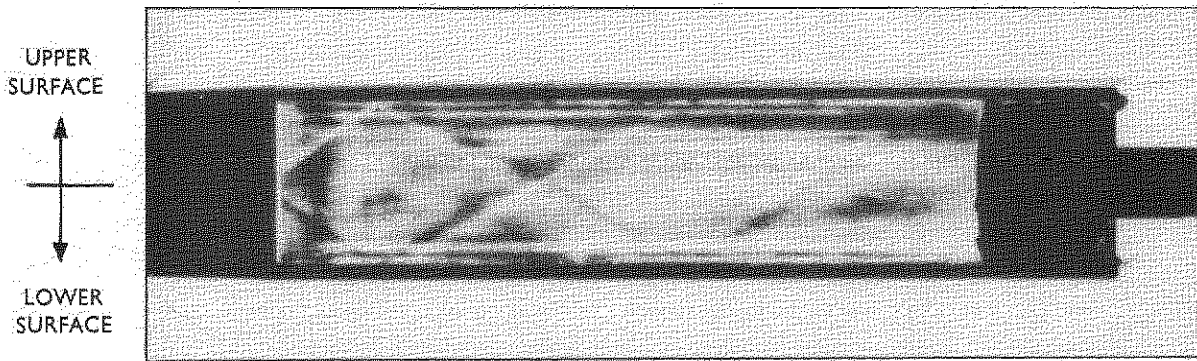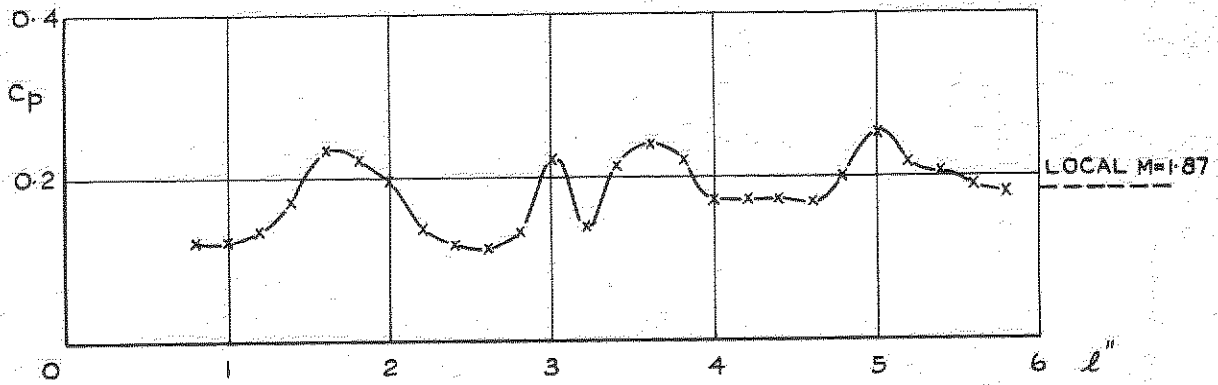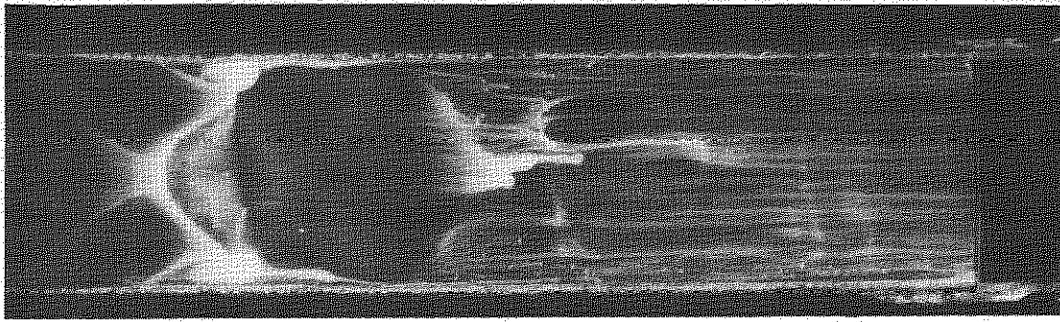
FIG.37 INTERNAL FLOW AT $\alpha = 0$; M = 2.19, h/b = 0.75
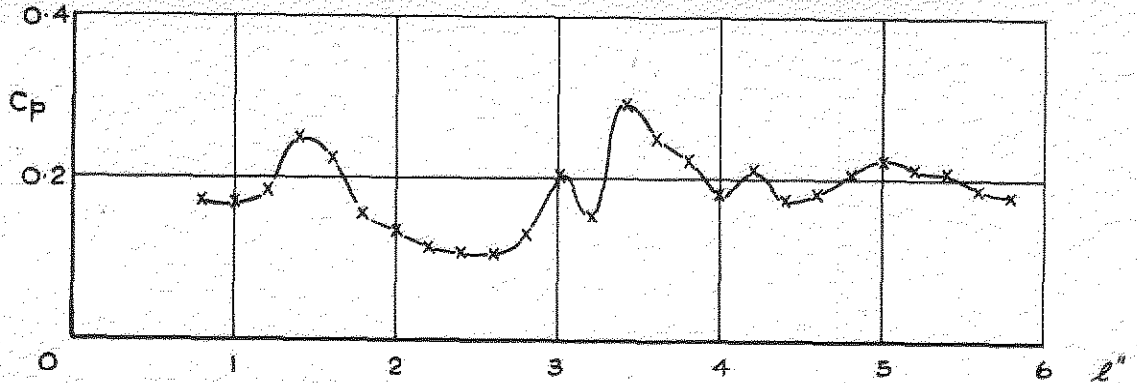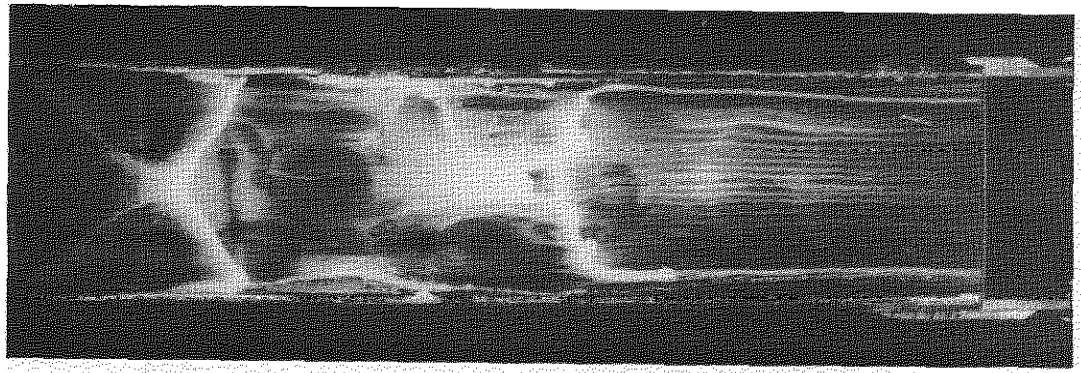
UPPER
SURFACE
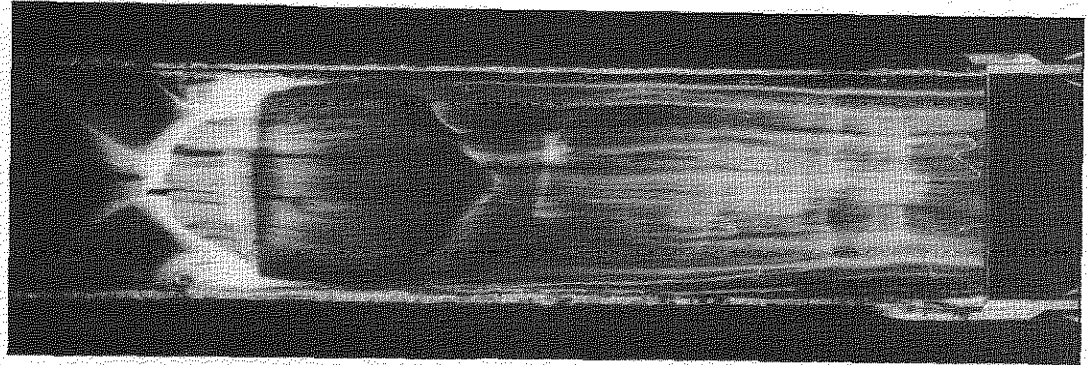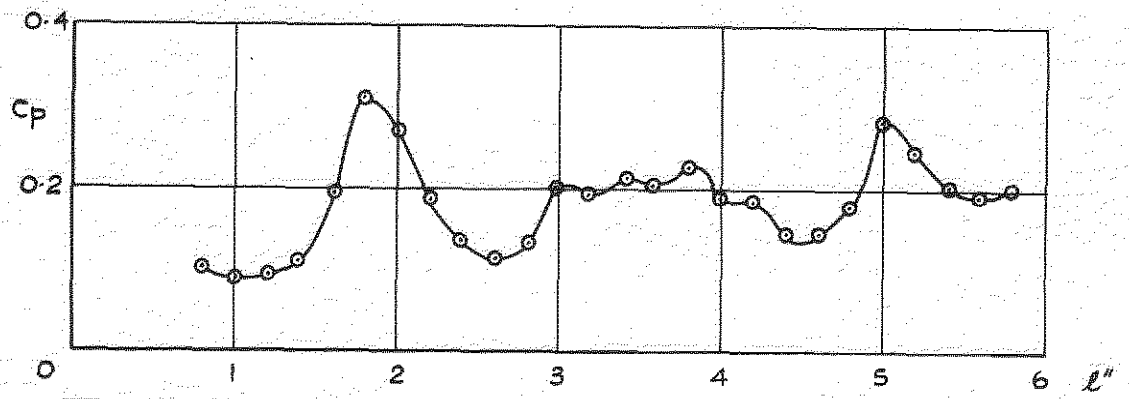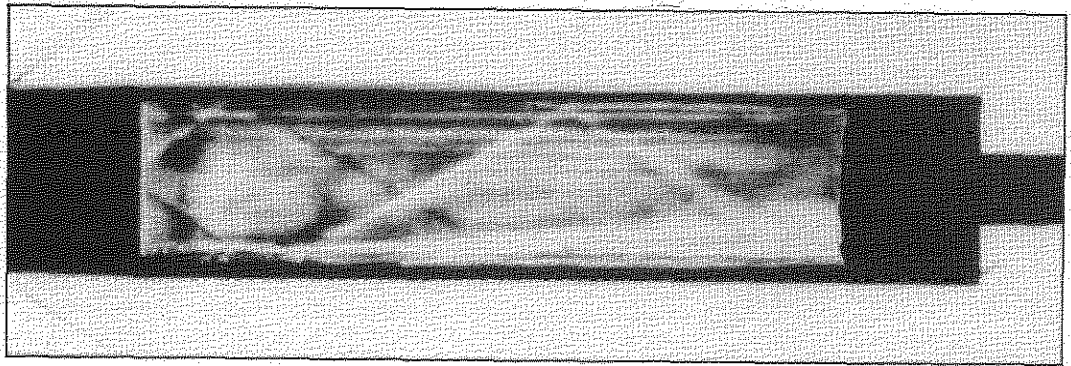
LOWER
SURFACE

FIG. 37 Cont'd. INTERNAL FLOW AT $\alpha = 2°$; M = 2·19, h/b = 0·75

UPPER
SURFACE

LOWER
SURFACE
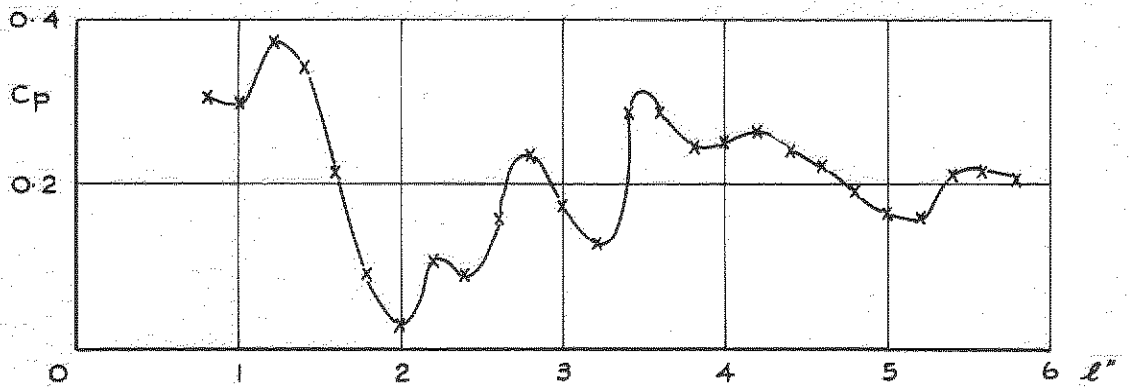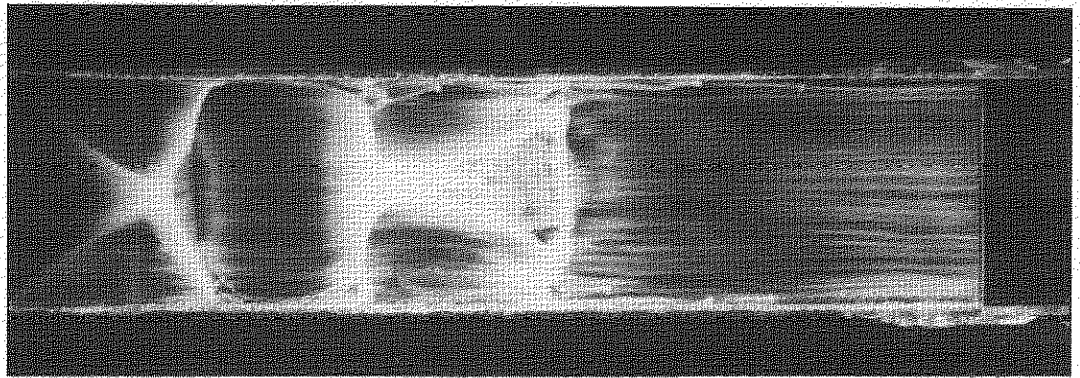
FIG.37 Cont'd. INTERNAL FLOW AT $\alpha = 4°$; M = 2·19, h/h = 0·75
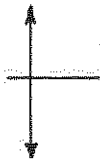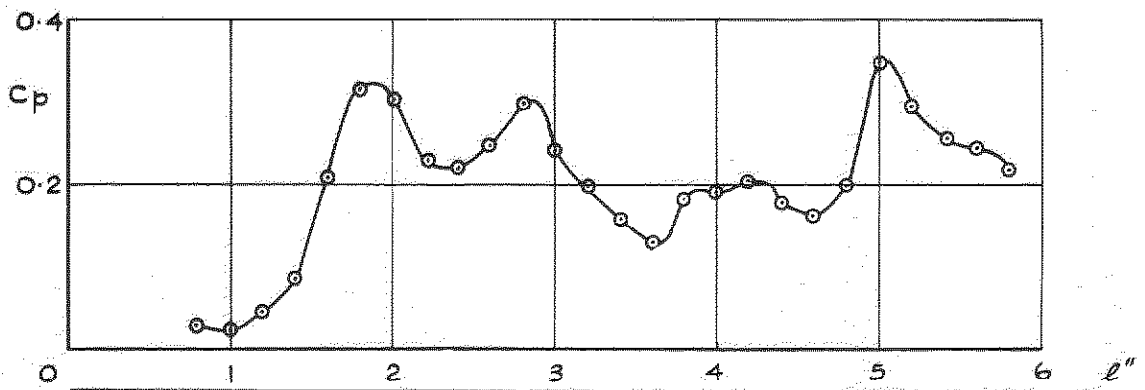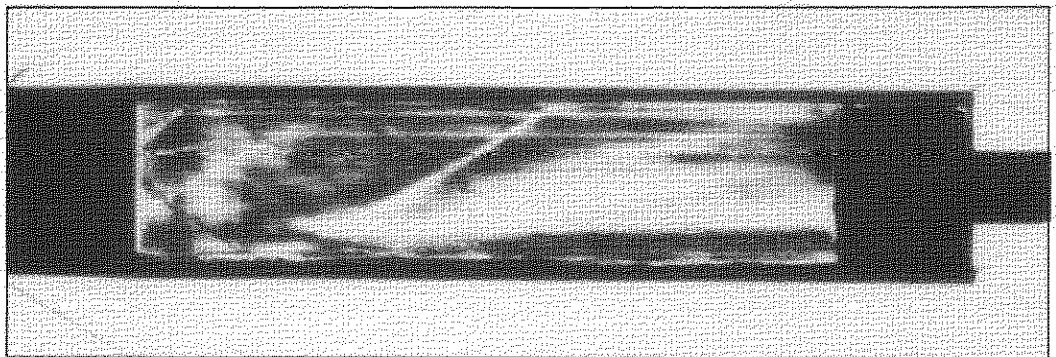
FIG.37 Concl'd.   INTERNAL FLOW AT $\alpha = 6°$; $M = 2.19$, $h/b = 0.75$
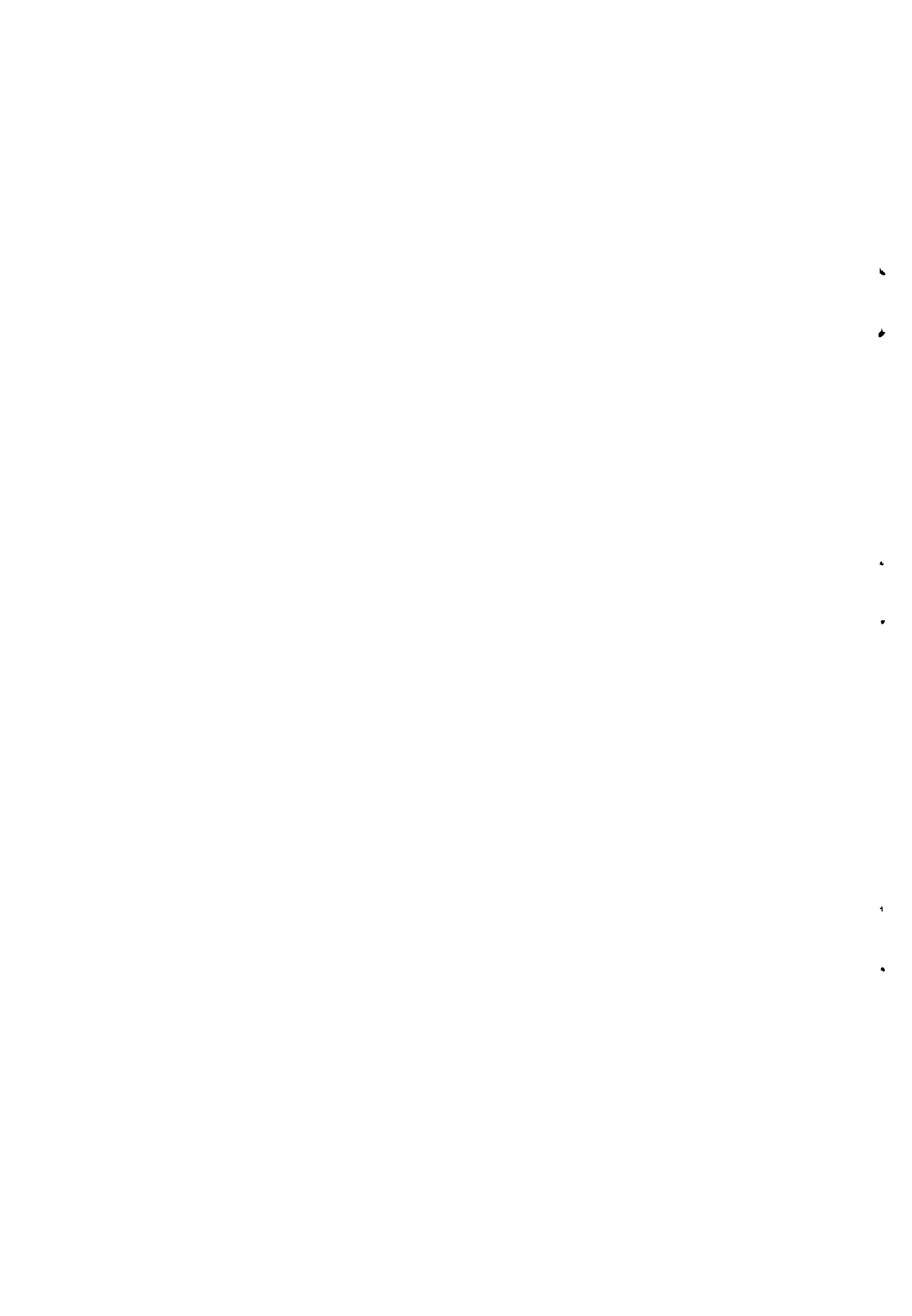
A.R.C. C.P. No.768

533.6.013.13 :
533.697.3 :
629.13.012.12

SUPERSONIC WIND TUNNEL MEASUREMENTS OF THE LOADS AND
INTERNAL PRESSURE DISTRIBUTIONS ON DUCTS AT INCIDENCE.
Cook, P.H. February 1964.

An attempt has been made to find a method of estimating the external
lift of full scale engine nacelles and the internal lift of rectangular cross
section ducts used to represent engine nacelles on wind tunnel models.

The results for the total lift curve slope of circular cross section
ducts look promising in that an adequate collapse of the experimental data
has been achieved. For the rectangular ducts, the internal lift at low
incidence may be predictable if the internal flow Mach number is known, and
the available results for total lift suggest a similar collapse to that
achieved for the circular ducts. The experimental data for the rectangular
ducts are limited and will be supplemented later by a further series of
models.